Parametric Heat Exchanger Sizing Model for Early Aircraft Design Phases

Eyrn Scarlet Sagala

A Thesis
in
The Department
of
Mechanical, Industrial and Aerospace Engineering

Presented in Partial Fulfillment of the Requirements
for the Degree of
Master of Applied Science (Mechanical Engineering) at
Concordia University
Montréal, Québec, Canada

August 2025

CONCORDIA UNIVERSITY
School of Graduate Studies

This is to certify that the thesis prepared

By: **Eyrn Scarlet Sagala**
Entitled: **Parametric Heat Exchanger Sizing Model for Early Aircraft Design Phases**

and submitted in partial fulfillment of the requirements for the degree of

Master of Applied Science (Mechanical Engineering)

complies with the regulations of this University and meets the accepted standards with respect to originality and quality.

Signed by the Final Examining Committee:

_____ Chair
Dr. Moussa Tembely

_____ External Examiner
Dr. Michel L. Trudeau

_____ Examiner
Dr. Moussa Tembely

_____ Supervisor
Dr. Susan Liscouët-Hanke

Approved by   _____
                Muthukumaran Packirisamy, Chair
                Department of Mechanical, Industrial and Aerospace Engineering

_____ 2025   _____
                                Mourad Debbabi, Dean
                                Gina Cody School of Engineering and Computer Science

Abstract

Parametric Heat Exchanger Sizing Model for Early Aircraft Design Phases

Eyrn Scarlet Sagala

The aviation industry aims to reduce its environmental impact, and alternative propulsion architectures, including hydrogen-based, hybrid-electric, or all-electric systems, are seen as promising pathways. However, these novel designs have raised new requirements and feasibility questions regarding thermal management. Electric Propulsion Aircraft (EPA) and Hybrid-Electric Propulsion Aircraft (HEPA) fundamentally change the Thermal Management System (TMS) landscape by relocating heat loads from the nacelle to inside the fuselage. Consequently, new design and development methods for TMSs are necessary, beginning at the component level. These systems are typically comprise of Heat Exchanger (HX)s, headers, distributors, pumps, pipes, ducts, valves, and nozzles. Heat exchangers serve as the core component, facilitating heat transfer between materials. This thesis presents research on the development and validation of a parametric sizing methodology for heat exchangers intended for early aircraft design phases within a Multidisciplinary Design Analysis and Optimization (MDAO) framework, i.e., for cryogenic heat transfer. The method is based on physical equations, combined with validated empirical relationships for heat exchanger design with iterative solver algorithms for sizing purposes. Since design problems typically involve multiple variables and possible solutions, the methodology employs constraint-based optimization techniques alongside a weighted sum solution selection method. The methodology is validated experimentally by comparing its results with a commercial heat exchanger, and cross-validated with a cryogenic HX. The research examines an all-electric hydrogen fuel cell aircraft architecture with a 7.6 MW propulsion system. Results show that the methodology successfully characterizes heat exchanger performance across multiple operating conditions. The study reveals that idealized assumptions overestimate system cooling potential by approximately 10%, with pressure losses reducing liquid hydrogen cooling capacity by 60 kW and single-stage expansion further decreasing it by 38 kW. This methodology advances aircraft design by providing a parametric framework for evaluating TMS requirements and feasibility during conceptual design. It enables more precise assessment of hydrogen-based propulsion systems integration challenges while supporting the development of efficient, sustainable aviation technologies.

Acknowledgments

This thesis represents not only countless hours of work, research, coding, plant watering, recoding, presentation preparation, meetings, and writing, but also a significant milestone in my academic journey. This achievement would not have been possible without the remarkable individuals who supported me along the way.

First and foremost, I wish to express my profound gratitude to my supervisor and mentor, Prof. Susan Liscouët-Hanke, whose expertise, guidance, patience, and unwavering support were instrumental throughout my research. Your insightful feedback consistently challenged me to refine my ideas and elevate the quality of my work. Your belief in my capabilities, especially during challenging phases of this research, gave me the confidence to persevere.

I would also like to extend my sincere gratitude to Prof. Jonathan Liscouët for his valuable support throughout my academic journey. His encouragement and guidance were instrumental in my decision to pursue this MASc degree.

I am deeply indebted to the Gina Cody School of Engineering faculty members and staff for creating an environment conducive to academic growth and exploration. Special thanks to the members of my thesis committee for their valuable feedback and constructive criticism, which significantly enhanced the depth and rigor of this work.

This research was enriched by the expertise of industry and academic partners from the CRIAQ EAP project. I extend my sincere thanks to Prof. Frédéric Sirois for sharing his valuable technical expertise on cryogenic systems.

I extend my sincere appreciation to my colleagues and fellow researchers at the Aircraft Systems Lab, the High Reliability Aerospace Design Lab, and my Space Concordia team for the stimulating discussions, collaborative problem-solving sessions, and Exploding Kittens game sessions that fostered camaraderie and made this academic journey enriching. Particularly, I must acknowledge Gala Licheva and Dr. Musavir Bashir, whose diverse perspectives and technical expertise significantly enhanced the quality and depth of this thesis.

I owe an immeasurable debt of gratitude to Nicole, Athena, Nessie, and the Gonzales and Calmera families for their unconditional love, understanding, and support throughout my studies. This achievement is as much yours as it is mine.

Finally, to my friends who provided much-needed distractions, emotional support, and encouragement – thank you for being my pillars of strength. Your unwavering belief in my abilities helped me navigate the complexities of this academic pursuit.

Contents

List of Figures

List of Tables

Nomenclature

$P_{downstream}$ power required downstream (kW)
η efficiency

Capitals

A	$[m^2]$	area
C^*		heat capacity rate ratio
C	$[W/K]$	heat capacity rate
C_R		heat capacity rate ratio
G	$[kg/m^2s]$	mass velocity
L	$[m]$	length
N		thermal length
NTU		Number of Transfer Units
Nu		Nusselt number
P	$[Pa]$	pressure
Pr		Prandtl number
$\dot{Q}$	$[W]$	heat transfer rate
Q	[J]	heat transfer capacity
T	$[K]$	temperature
U	$[m/s]$	flow velocity
V	$[m^3]$	Volume

Lower Case Letters

b	$[m \cdot K]$	Wien's displacement constant ($\approx 2.898e-3 \; mK$)
b_{fin}	[mm]	plate-gap
c_p	$[kJ/kgK]$	specific heat
c_{th}	$[J/K]$	thermal mass
c_v	$[J/kgK]$	constant volume specific heat capacity
d_h	$[mm]$	hydraulic diameter
f_D		Darcy-Weisbach friction factor
f_f		Fanning friction factor
h	[mm]	passage height
j		thermal surface performance parameter
j_{factor}		flow area goodness factor
k_t	$[W/mK]$	thermal conductivity
l	[mm]	fin (strip) length
$\dot{m}$	$[kg/s]$	mass flow

n		number of energy carriers
q	$[W/m^2]$	heat flux
s	$[mm]$	fin spacing
t	$[mm]$	separation plate thickness
t_{fin}	$[mm]$	fin thickness
t_s	$[mm]$	splitter plate thickness
$\overline{v}$	$[m/s]$	average molecular velocity

Symbols

α	$[W/m^2K]$	overall heat transfer coefficient
α_{fin}		fin spacing to passage height ratio
β	$[°]$	chevron angle
$\Delta\overline{T}$	$[K]$	log-mean temperature difference
ΔP	$[kPa]$	pressure loss
δ_{fin}		fin thickness to fin length ratio
η_0		surface effectiveness
γ		specific heat ratio
γ_{fin}		fin thickness to fin spacing ratio
λ	$[m]$	wavelength
μ	$[Pa \cdot s]$	dynamic viscosity
∇T	$[K/m]$	temperature gradient
ρ	$[kg/m^3]$	density
σ	$[\%]$	porosity
ε		effectiveness

Subscripts

abs	absolute
pk	peak
atm	atmospheric
cd	collisions distance
c	cold
$cphe$	corrugated plate heat exchanger
$cryo$	cryogenic
cs	cross-sectional area
el	electron
fin	fin
g	gas
h	hot
in	inlet
max	maximum
min	minimum
out	outlet
$pfhe$	plate fin heat exchanger
ph	phonon

sf	surface area
tot	total
w	wall

List of Acronyms

ε-NTU	Effectiveness-NTU
AC	Air Conditioning
AEA	All-Electric Aircraft
ARP	Aerospace Recommended Practice
ATAG	Air Transport Action Group
BMS	Battery Management System
CAD	Computer Aided Design
CARs	Canadian Aviation Regulations
CFD	Computational Fluid Dynamics
CGH_2	Cryogenic Gaseous Hydrogen
CHE	Compact Heat Exchanger
CPACS	Common Parametric Aircraft Configuration Schema
CPHE	Corrugated Plate Heat Exchanger
CRIAQ	Consortium for Research and Innovation in Aerospace in Québec
DOE	Design of Experiments
EAP	Exploration and modeling of Alternative Propulsion technologies for business jets
ECS	Environmental Control System
EES	Engineering Equation Solver
EOS	Equations of State
EPA	Electric Propulsion Aircraft
FC	Fuel Cell
FDM	Finite Difference Method
FEA	Finite Element Analysis
FEM	Finite Element Method
H_2	Hydrogen
He	Helium
HEA	Hybrid Electric Aircraft
HEP	Hybrid-Electric Propulsion
HEPA	Hybrid-Electric Propulsion Aircraft
HTSC	High-Temperature Superconducting Cables
HVAC	heating, ventilation, and air conditioning
HX	Heat Exchanger
ICAO	International Civil Aviation Organization
IPTMS	Integrated Power and Thermal Management Systems
ISA	International Standard Atmospheric

LH$_2$	Liquid Hydrogen
LINMAP	Linear Programming Technique for Multidimensional Analysis of Preference
LMTD	Log-Mean Temperature Difference
LNG	Liquefied Natural Gas
MDAO	Multidisciplinary Design Analysis and Optimization
MEA	More Electric Aircraft
MINLP	Mixed Integer Nonlinear Programming
MLI	Multi-Layer Insulation
MNN	M-Nearest Neighbors
N$_2$	Nitrogen
NASA	National Aeronautics and Space Administration
NIST	National Institute for Standards and Technology
NLBGS	Nonlinear Block Gauss-Seidel
NSGA-II	Non-dominated Sorting Genetic Algorithm II
NTU	Number of Transfer Units
OSF	Offset-Strip Fin
p-H$_2$	Parahydrogen
PCHE	Printed Circuit Heat Exchanger
PEMFC	Proton-Exchange Membrane Fuel Cell
PFHE	Plate-Fin Heat Exchanger
PHE	Plate Heat Exchanger
PMS	Power Management System
PPHE	Perforated Plate Heat Exchanger
RCE	Remote Component Environment
REFPROP	Reference Fluid Thermodynamic and Transport Properties Database
SAE	Society of Automotive Engineers
SCM	Superconducting Motor
SLM	Selective Laser Melting
SOC	State of Charge
SOH	State of Health
TC	Transport Canada
TMS	Thermal Management System
TOPSIS	Technique for Order of Preference by Similarity to Ideal Solution
TRL	Technology Readiness Level
WIPS	Wing Ice Protection System
XDSM	eXtended Design Structure Matrix

Chapter 1

Introduction

D URING the October 2022 International Civil Aviation Organization (ICAO) Assembly, a landmark decision established a "net-zero carbon emissions by 2050" global aspirational goal for international aviation, aligning with the Paris Agreement's temperature objectives [1]. Furthermore, recent advancements in Hydrogen (H_2) and electric motor technologies have motivated both industry and academic stakeholders to investigate alternative propulsion systems as potential pathways toward environmentally sustainable and energy-efficient air transportation [2]. According to the Air Transport Action Group (ATAG) Waypoint 2050 project report [3], these technologies are projected to enable fully hybrid-electric and H_2-powered aircraft to become commercially feasible between 2035 and 2040. Thus, there are viable pathways to net-zero carbon emissions, which is particularly significant considering that aviation's fuel burn accounted for 2.05% of all human-induced CO_2 emissions in 2023 [4].

Similarly, in alignment with ICAO's goal, the Québec government mandated the Consortium for Research and Innovation in Aerospace in Québec (CRIAQ) to increase the competitiveness of Quebec's aerospace sector by stimulating technological innovation and corporate commitment through collaborative research and development [5]. The Exploration and modeling of Alternative Propulsion technologies for business jets (EAP) project, which "aims to identify promising alternative propulsion technologies to reduce the environmental impact of business aircraft while maintaining the aircraft's performance criteria" [6], is one such collaboration. It brings together academic and industry partners to quantify the real benefits and challenges of new propulsion systems. This thesis is one of several within the academic component of the EAP project.

1.1   Background and Motivation

In conventional turbo-engine technologies, combustion exhaust gases are directly released into the atmosphere, eliminating the need for complex Thermal Management System (TMS)s. In contrast, alternative propulsion systems increasingly house high-powered electronics that must be actively cooled. Some of these heat sources are relocated to inside the nacelles outside of the airflow or within the fuselage, creating new thermal management challenges. Figure 1.1 highlights the main heat sources and sinks of a conventional aircraft. Focusing on the nacelle, it can be seen that there is a 4:1 ratio of heat sources to heat sinks, with the power unit being the most significant heat source and the ambient air the optimal heat sink. Once the power unit is electrified, it is no longer possible to directly eject the hot fuel/air mixture to the ambient air, as the combustion process is replaced by batteries or fuel cells.
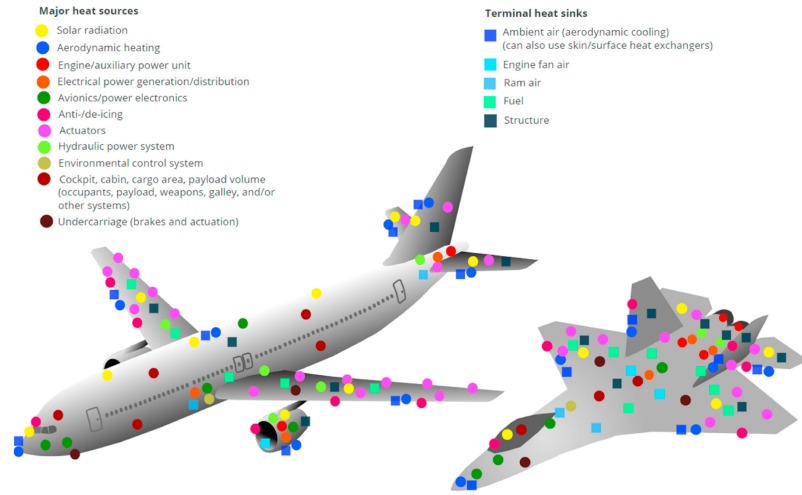
Figure 1.1: Location of the main heat sources and sinks as discussed by Vanheerden et al. [7].

The ZeroAvia ZA2000 and ZA600 H_2 powertrains, presented in figures 1.2 and 1.3 [8], demonstrate the importance of thermal management, as evidenced by the extensive integration of Heat Exchanger (HX)s and liquid cooling throughout the systems.

Conventional aircraft propulsion systems deliver four types of power: mechanical, hydraulic, pneumatic, and electric. A portion of the generated power serves various aircraft systems such as: pumps (hydraulic/mechanical), actuation systems (pneumatic), Environmental Control System (ECS) (pneumatic), Wing Ice Protection System (WIPS) (pneumatic), and avionics (electric) [9]. For example, for Hybrid-Electric Propulsion Aircraft (HEPA) or those using a turbo generator, there remains a compression device to provide the ECS with the necessary pneumatic power, but when Electric Propulsion Aircraft (EPA) are considered, a replacement compression unit is required

Another consideration for proposed architectures for novel EPA and HEPA using batteries or Fuel Cell (FC)s as energy sources is their placement within the aircraft. In some aircraft configurations, they are placed inside the fuselage due to their projected size, adding new space and thermal management requirements. Furthermore, batteries have stringent thermal requirements; lithium-ion batteries, for instance, must operate within a narrow temperature range of 15°C to 35°C and are considered the least energy-efficient electric drive train components [10].
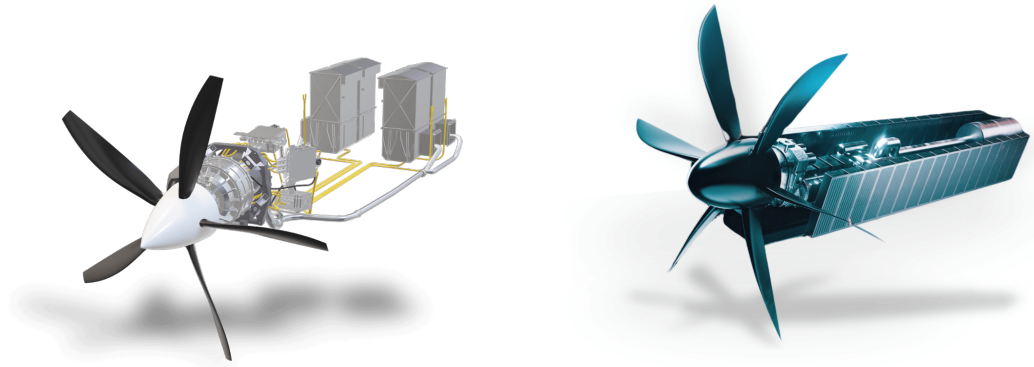
Figure 1.3: Render of the ZeroAvia ZA2000 electric powertrain.

Figure 1.2: Render of the ZeroAvia ZA600 electric powertrain.

With regard to H_2 FCs, which are becoming the preferred power source for electric motors in smaller aircraft [11], H_2's lower energy density compared to conventional fuels, as shown in figure 1.4, will most likely lead to significant modifications to fuel storage systems. Despite its higher specific energy, H_2 requires a larger storage space than current fuels and must be maintained at cryogenic temperatures to maximize volumetric efficiency, which introduces new fuel heating challenges. As noted by the National Aeronautics and Space Administration (NASA), All-Electric Aircraft (AEA) power systems convert approximately 20% of their energy into heat, requiring robust cooling mechanisms, which present an additional engineering challenge [12]. To dissipate the electric power systems' heat, the newly required TMS adds more weight and requires extra energy, reducing the aircraft's efficiency.
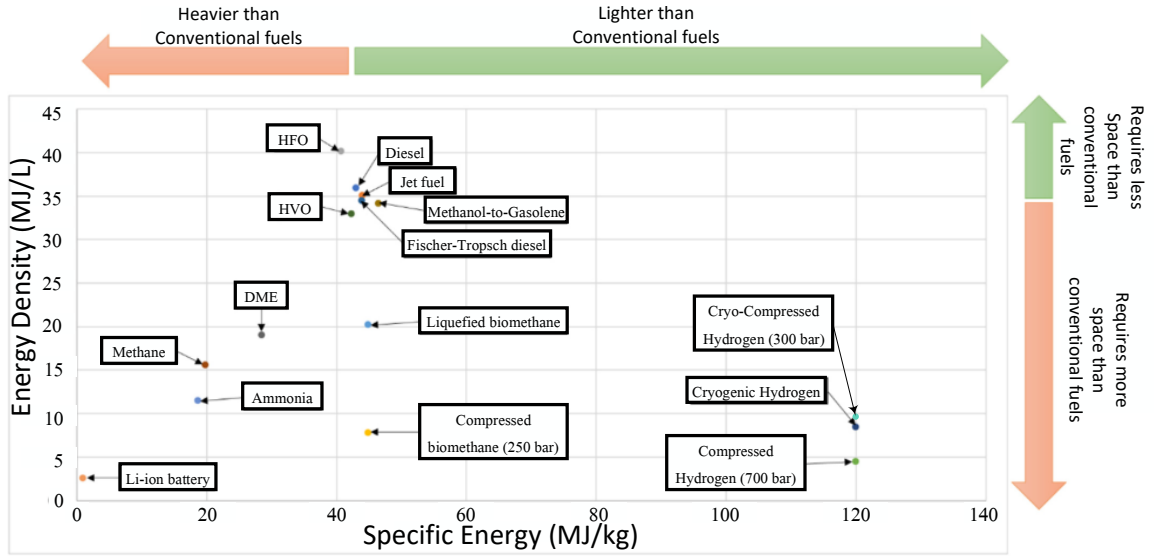
Figure 1.4: Comparison of energy density with respect to specific energy for different fuels [13].

Thus, although electric propulsion system components are more energy efficient than their combustion-based counterparts, as outlined in table 1.1, current designs suffer from both lower volumetric and gravimetric efficiencies. This not only drives novel architectures toward more optimal space and weight utilization, but also toward more integrated systems to maintain current aircraft performance standards in range and payload capacity.

Table 1.1: Efficiency range for various propulsion system components.

Component	Efficiency Range
Fuel Cell[1]	98.5 - 99.5
Battery[2]	90.0 - 95.0
Gearbox[1]	98.5 - 99.5
Electric motor[3]	70.0 - 96.5
Superconducting electric motor[1]	98.0 - 99.9
High Temperature Superconducting Cables[1]	99.9 - 99.99
Cold Power DC/AC Converter[1]	99.0 - 99.8
Cold Power DC/DC Converter[1]	98.0 - 99.0
Turbine efficiency[4]	45.0 - 84.0

[1] Source: [14]
[2] Source: [10]
[3] Source: [15]
[4] Source: [16]

This new landscape is pushing aircraft manufacturers to develop new design tools to address feasibility questions. Since approximately 80% of a new aircraft's development costs and 70% of the life cycle costs are determined during the conceptual design phase [17], new design tools have

become the primary focus of current research efforts. Conventionally, system-level designs are developed during the preliminary design phase, while the conceptual design phase focuses on aircraft initial sizing, cost estimation, performance analysis, stability assessment, and regulatory compliance evaluation, as outlined in [16]. With the increasing thermal management feasibility and efficiency concerns for novel EPA, it is becoming critical to begin evaluating the thermal requirements during the conceptual design phase to initiate the TMS sizing as early as possible.

1.1.1 Cryogenic Heat Exchanger Design

A discussion of cryogenic HX design serves as a necessary foundation to understanding the unique challenges and considerations in designing TMSs for cryogenic applications. Cryogenic temperatures, defined as those below 123 K (-150°C), introduce complex thermophysical behaviors that significantly deviate from conventional ambient temperature assumptions [18]. The transport properties of materials exhibit dramatic non-linear variations within the cryogenic temperature range, invalidating the constant property analysis typically employed in standard heat transfer calculations. These variations affect thermal conductivity, specific heat capacity, and viscosity, which are fundamental parameters that govern HX performance and sizing.

The thermodynamic critical pressure for many cryogenic fluids is considerably lower than that of conventional fluids, resulting in more frequent occurrences of near-critical and supercritical convective heat transfer in cryogenic systems. At the thermodynamic critical point, both specific heat capacity and thermal expansion coefficient approach infinity, while most other fluid properties undergo substantial changes as temperature and pressure fluctuate around this point. These rapid variations present challenges in correlating heat transfer and pressure drop data, necessitating specialized analytical approaches.

An examination of these phenomena provides context for subsequent discussions of HX design methodologies applicable to novel aircraft propulsion systems utilizing cryogenic fluids. For large concept exploration spaces, it is more time-consuming to employ Computer Aided Design (CAD) software and solve complex Navier-Stokes equations using Computational Fluid Dynamics (CFD) algorithms to account for transfer properties variability than using scaling or empirical modeling techniques. As conventional empirical relationships for heat transfer and HX sizing remain valid at cryogenic temperatures, these relationships can still be used to quickly evaluate and develop feasible designs [18].

Furthermore, cryogenic HX design faces four primary challenges: variable material properties, thermal insulation requirements, near-critical-point convection phenomena, and radiation heat transfer effects[1]. Of these, both material property variations and near-critical-point convection behavior must be carefully incorporated into HX sizing calculations.

While constant property analysis may be valid for many ambient temperature applications, it is often inaccurate when applied to cryogenic heat transfer problems. Specific heat (c_p) is one such property, as it depends on the material state (solid, liquid, or gaseous). Different heat transfer mechanisms dominate the heat transfer process depending on the state.

For example, comparing the properties of Liquid Hydrogen (LH$_2$) at 6 and 20 bar produces the graph shown in figure 1.5, which illustrates significant variations in specific heat values across the cryogenic temperature range for constant pressure. This demonstrates that conventional assumptions, such as near-constant or linear specific heat relationships, cannot be applied universally, as their validity depends on the particular temperature range being examined.

---

[1]Thermal insulation requirements and radiation heat transfer effects are discussed in Appendix A.
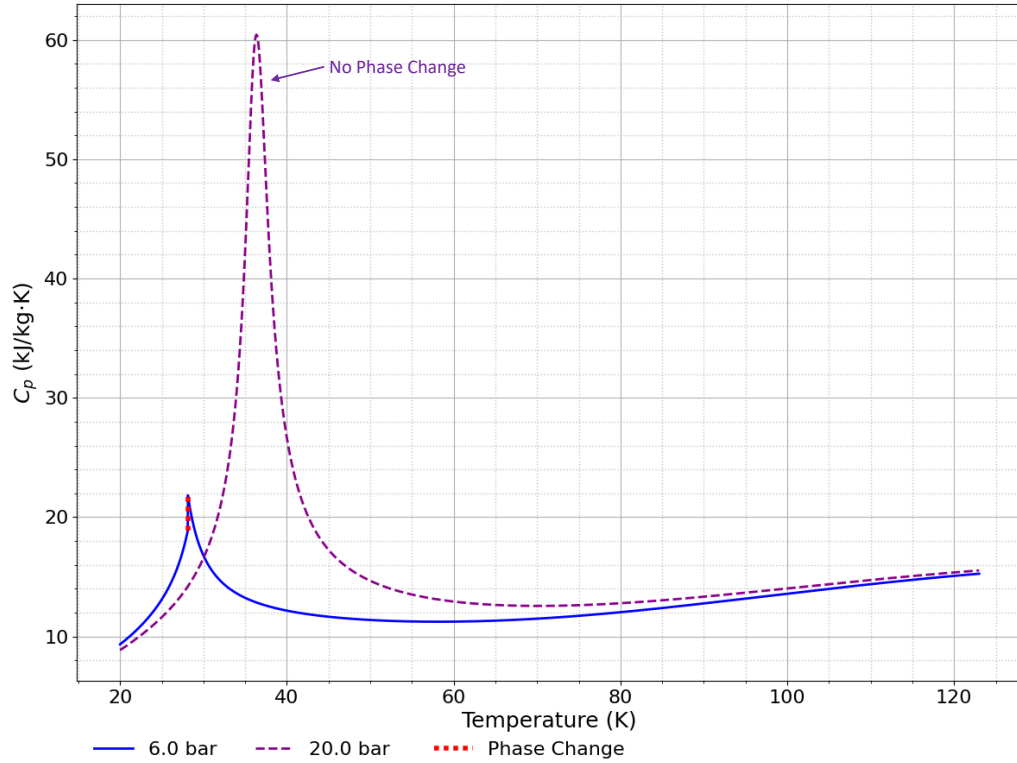
Figure 1.5: Specific heat of H_2 at cryogenic temperatures with constant pressure starting from LH_2 at 6 and 20 bar using Coolprop [19] for fluid transfer properties.

This non-linear behavior necessitates a different approach where the HX must either be analyzed in discrete segments, each with locally valid thermophysical properties, or through the careful selection of representative mean physical properties. A segmented approach can enable designers to account for the non-linear property variations while maintaining computational efficiency, resulting in more accurate performance predictions and optimized designs for cryogenic heat exchange applications.

1.2 Thesis Scope and Objective

This thesis explores parametric HX sizing for novel aircraft propulsion systems within the EAP project's Multidisciplinary Design Analysis and Optimization (MDAO) framework. The project itself investigates multiple design levels, from aircraft-level studies down to technology-level analyses, including environmental impacts, as illustrated in figure 1.6.

For the aircraft-level TMS studies, a number of system-level changes were identified that affect the models required for system sizing. The HX, arguably the most critical component of an aircraft TMS, was identified as the first component-level model needed for parametric system sizing, considering the cryogenic H_2 architectures to be explored within the project. Additional sizing models for components such as headers, distributors, pumps, pipes, ducts, valves, and nozzles were determined to be necessary for subsequent development phases. Two of the EAP project's FC architecture case studies, illustrated in figure 1.7, serves as the foundation for the methodology and

implementation.

This first sizing process addresses the HX that manages the interface between the cryostat and LH_2 fuel for the H_2 FC. The LH_2 parameters depend on tank properties and pumping requirements, while the interfacing cryogenic fluid must achieve specific heat transfer properties to effectively cool superconducting components like the High-Temperature Superconducting Cables (HTSC) and Superconducting Motor (SCM).
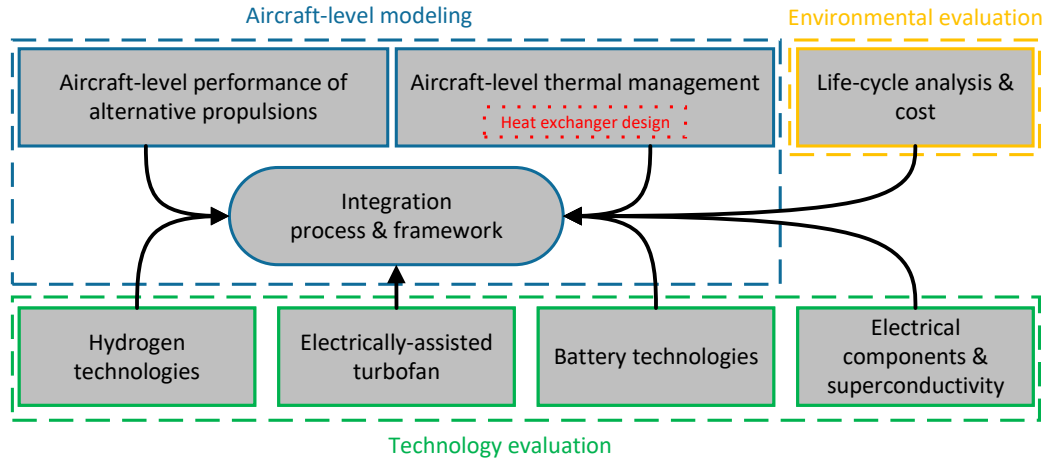
Figure 1.6: EAP project MDAO high-level framework [6].

The second sizing process examines how the exhaust water from the FC can heat the Cryogenic Gaseous Hydrogen (CGH_2) to near the required FC inlet temperature, potentially necessitating multiple heating and cooling loops.

Therefore, the main objectives of this thesis are the following:

(1) investigate and identify appropriate cryogenic HXs technologies for aerospace applications;

(2) develop a parametric methodology for HX sizing during early aircraft design phases;

(3) develop a methodology that addresses heat transfer property variations in materials at cryogenic temperatures;

(4) identify key design parameters that influence HX design for aircraft TMS sizing;

(5) develop a computational tool that facilitates HX sizing in early design phases through systematic parameter variation and integrate it into a MDAO framework.
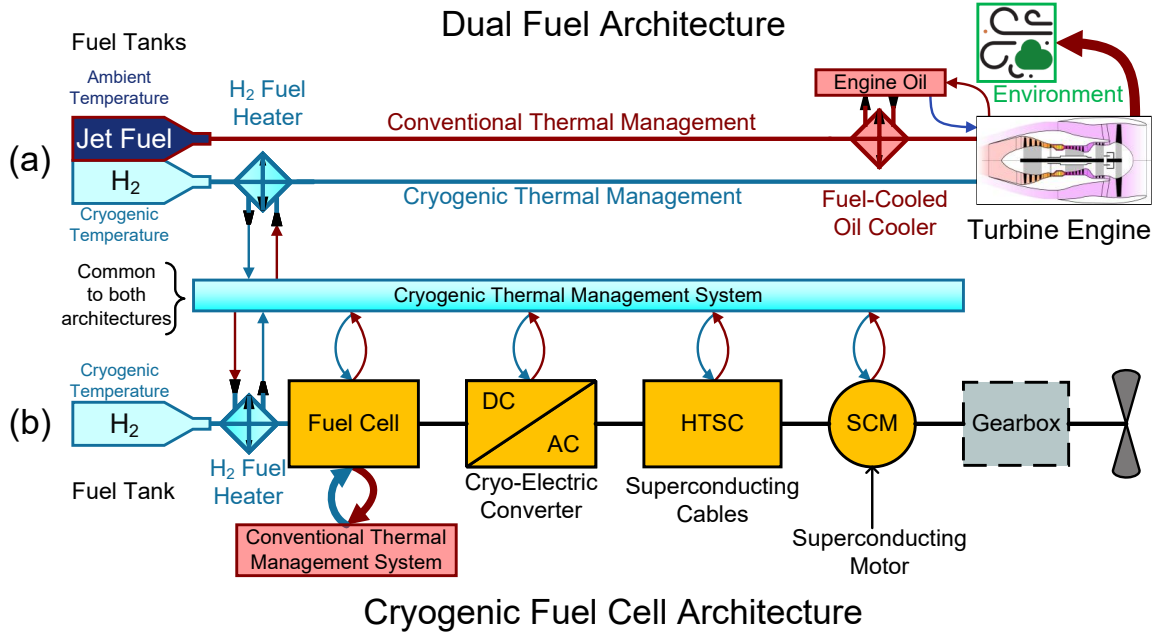
Figure 1.7: EAP project architectures under investigation: (a) HEPA with dual fuel architecture, and (b) EPA with a superconducting cryogenic FC architecture.

1.3 Organization of the Thesis

This thesis is organized into the following chapters:

Chapter 2 provides a literature review covering TMSs, electric aircraft thermal management, and cryogenic HX design. It analyzes the current state-of-the-art at both aircraft and component levels. The chapter examines existing research on HX design methodologies, encompassing traditional and innovative approaches. Special emphasis is placed on HX technologies suitable for cryogenic applications, which are crucial for H_2-powered aircraft. The chapter concludes by identifying research gaps that this thesis addresses.

Chapter 3 presents the methodology for parametric HX sizing, with particular emphasis on addressing the challenges of variable material properties at cryogenic temperatures. The chapter outlines the theoretical foundations and analytical approaches employed in the research, providing a comprehensive explanation of all relevant thermodynamic relationships.

Chapter 4 presents the implementation of the methodology through a computational tool developed for HX sizing. It details the algorithms, data structures, and user interface of this tool, explaining how it enables systematic parameter variation.

Chapter 5 presents an analysis of the parametric sizing results, examining the influence of various design parameters on HX performance and dimensions. It includes sensitivity analyses that identify the most influential parameters affecting sizing outcomes. The chapter validates the developed methodology through comparison with existing experimental data and theoretical models, demonstrating its accuracy and reliability. It concludes with a discussion of the implications of these findings for future aircraft TMS design.

Chapter 6 explores a cryogenic FC case study starting from a TMS level. It showcases four separate frameworks that can be used with the sizing tool. The chapter evaluates the integration

challenges of the sized HXs within the broader aircraft TMS and analyzes the methodology's scalability for different aircraft sizes and power requirements.

Chapter 7 provides conclusions, summarizes key contributions, and discusses the limitations and future work.

Chapter 2

Literature Review

S INCE the advent of aircraft electrification, More Electric Aircraft (MEA) designs, like the Boeing 787 Dreamliner, have introduced new thermal management challenges by replacing conventional systems with electric alternatives, for example, the pneumatic system [20]. For novel EPA and HEPA architectures, these challenges are increasing in complexity and raising questions about TMS requirements. As heat sources shift from nacelles to inside the fuselage, new system designs and requirements become necessary. This section first examines the design challenges from an aircraft-level perspective, showing how electric architectures reshape TMSs and their design requirements. It then explores current component-level research, focusing on HXs, before discussing identified research gaps.

2.1   Aircraft-Level Thermal Management Systems

As outlined in chapter 1, numerous changes occur when novel aircraft electric propulsion systems replace conventional turbo engine systems. Kim et al. [21] have determined that megawatt-class turbo-electric aircraft are infeasible at the current technological level due to the TMS challenges. In the same line of investigation, Van Heerden et al. [7] created a framework to classify current aerospace thermal management practices across civil, commercial, and military applications. They divide TMS components into five categories: heat sources, heat acquisition, thermal transport, heat rejection, and terminal heat sinks (shown in figure 2.1). While their research details the current state-of-the-art, they emphasize that thermal management challenges are increasingly constraining aircraft performance and efficiency improvements. It also highlights ongoing efforts to enhance HX technology through several approaches: innovative geometries, enhanced heat transfer capabilities, advanced manufacturing techniques, skin/surface HXs, cold plates, passive heat transport components, and improved design methodologies. On the last point, the authors emphasize that computational methods require improvements to allow designers to explore broader geometric design spaces for HXs and develop better integration approaches between HX designs and the overall thermal transport system.

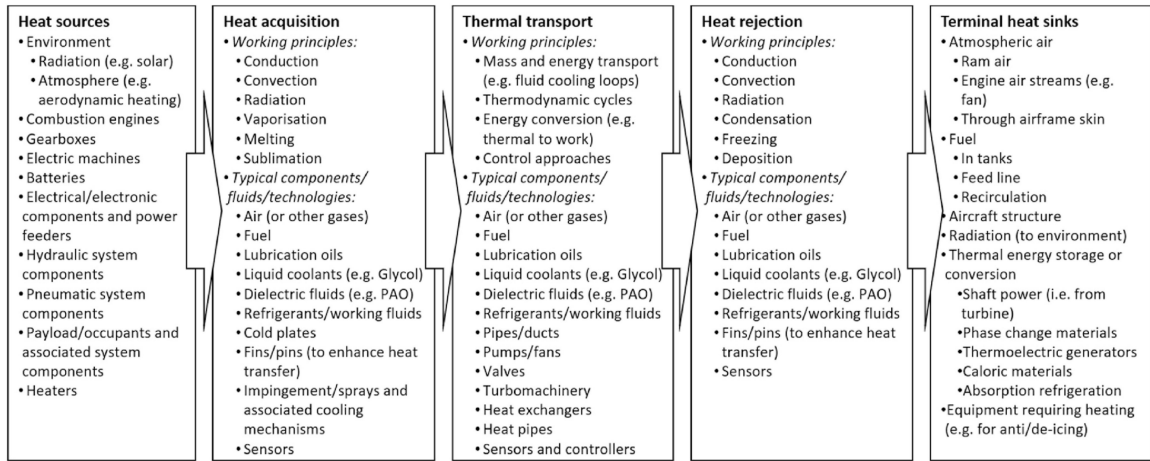| Heat sources	Heat acquisition	Thermal transport	Heat rejection	Terminal heat sinks
• Environment	• *Working principles:*	• *Working principles:*	• *Working principles:*	• Atmospheric air
• Radiation (e.g. solar)	• Conduction	• Mass and energy transport	• Conduction	• Ram air
• Atmosphere (e.g. aerodynamic heating)	• Convection	(e.g. fluid cooling loops)	• Convection	• Engine air streams (e.g. fan)
• Combustion engines	• Radiation	• Thermodynamic cycles	• Radiation	• Through airframe skin
• Gearboxes	• Vaporisation	• Energy conversion (e.g. thermal to work)	• Condensation	• Fuel
• Electric machines	• Melting	• Control approaches	• Freezing	• In tanks
• Batteries	• Sublimation	• *Typical components/ fluids/technologies:*	• Deposition	• Feed line
• Electrical/electronic components and power feeders	• *Typical components/ fluids/technologies:*	• Air (or other gases)	• *Typical components/ fluids/technologies:*	• Recirculation
• Hydraulic system components	• Air (or other gases)	• Fuel	• Air (or other gases)	• Aircraft structure
• Pneumatic system components	• Fuel	• Lubrication oils	• Fuel	• Radiation (to environment)
• Payload/occupants and associated system components	• Lubrication oils	• Liquid coolants (e.g. Glycol)	• Lubrication oils	• Thermal energy storage or conversion
• Heaters	• Liquid coolants (e.g. Glycol)	• Dielectric fluids (e.g. PAO)	• Liquid coolants (e.g. Glycol)	• Shaft power (i.e. from turbine)
	• Dielectric fluids (e.g. PAO)	• Refrigerants/working fluids	• Dielectric fluids (e.g. PAO)	• Phase change materials
	• Refrigerants/working fluids	• Pipes/ducts	• Refrigerants/working fluids	• Thermoelectric generators
	• Cold plates	• Pumps/fans	• Fins/pins (to enhance heat transfer)	• Caloric materials
	• Fins/pins (to enhance heat transfer)	• Valves	• Sensors	• Absorption refrigeration
	• Impingement/sprays and associated cooling mechanisms	• Turbomachinery		• Equipment requiring heating (e.g. for anti/de-icing)
	• Sensors	• Heat exchangers		
		• Heat pipes		
		• Sensors and controllers		

Figure 2.1: Elements of a generic aircraft TMS. The arrows indicate the flow of thermal energy [7].

Additionally, studies by Coutinho et al. [22] and Yu et al. [23] highlighted that atmospheric heat dissipation is reduced during subsonic flight, and this issue is worsened by the increasing use of composite materials rather than heat-conductive metallic structures. Therefore, changes are needed, and researchers are investigating various conceptual architectures for both battery-powered and fuel cell aircraft.

2.1.1 Electric Aircraft Thermal Management Research

Starting with battery electric aircraft architectures, the battery TMS represents one of the most critical subsystems of the Power Management System (PMS). As current high-power density batteries have strict operating temperature ranges: between 0°C and 40°C according to Tarhan et al. [24], between 0°C and 35°C as reported by Cyrille et al. [25], or even more narrowly between 15°C and 35°C as noted by Kellermann et al. [10]. Failure to maintain the battery cells within the optimal temperature range could reduce the battery system's lifespan or worse, risk thermal run-away, a condition to which certain lithium-ion cells are particularly susceptible, potentially leading to catastrophic failure.

As mentioned in section 1.1, batteries are not the only components generating heat in MEA or AEA. Indeed, a paper by Jansen et al. [26] emphasizes the relationship between electrical components' efficiencies and heat generation while discussing ongoing investments to improve the Technology Readiness Level (TRL) of lightweight, high-efficiency, high-powered electrical systems. The authors identify several areas requiring assessment, with thermal management at the top of the list. They note that these assessments must occur at each conceptualization stage to ensure the integrated solution is achievable, cost-effective, and fits within volume and weight constraints.

This integrated solution requirement is becoming a key driver for stakeholders to investigate new design and development methods [7], as conventional design methods are proving inadequate for electric architectures [20]. Ouyang et al. [20] investigate the current state-of-the-art of Integrated Power and Thermal Management Systems (IPTMS) design and argue that these systems could overcome the existing roadblocks. In new AEA and HEPA architectures, the PMS and TMS are interdependent. They determined that managing energy in either domain separately limits optimization because power management must account for the TMS's consumption for optimal battery use throughout the flight. The authors conclude that:

- TMS designs must integrate with other systems;

- varying power requirements during flight affect component efficiencies, making heat loads calculated using efficiency-based methods inaccurate;

- for accurate TMS-PMS assessment, experiment-based and physics-based modeling should be used;

- IPTMS offer optimized integrated designs for power management;

- IPTMS reduce thermal requirements and energy consumption; and

- IPTMS combined with the correct modeling methods enables modular designs for more optimized aircraft.

Building upon the integrated system approach, Rheaume et al. [27][28] propose innovative configurations for HEPA TMSs. They investigate the weight and fuel consumption impact of a commercial Hybrid Electric Aircraft (HEA) TMS. Their methodology leverages different flight phases to calculate heat loads, which then determine the appropriate dimensions for air-oil coolers, fuel-oil coolers, and ram-coolant coolers.

The first paper [27] establishes a baseline TMS design for a parallel hybrid electric commercial aircraft with a battery as an energy storage system. The Hybrid-Electric Propulsion (HEP) system includes a low spool motor with its drive, propulsion batteries, and supplementary batteries for TMS loads during takeoff and climb. The system manages heat from bearings, the fan drive, and the accessory gearbox. Using their proprietary modeling software under International Standard Atmospheric (ISA) temperature +15°C (hot day) conditions, the researchers found the minimal fuel consumption solution. Their results show that the HEPA's TMS increases fuel consumption by 3.4% during takeoff, climb, and cruise.

The updated design from [28] implements separate cooling loops for motor drive and batteries, resulting in reduced component weight and fuel consumption. This reduction is due to the higher operating temperature of the motor drive and the colder air available at the altitude where the battery HX was sized. These findings highlight the importance of integrated design strategies for HEPA.

2.1.2 Hydrogen & Cyrogenic Aircraft Thermal Management Research

Cryogenic architectures present another set of challenges and are being investigated to reduce heat losses from electrical components. For example, a paper by Sumption et al. [29] looks into cryogenic motors, generators, and power transmission and their efficiencies. The authors conclude that, with cryogenic components, it is possible to reduce the size and weight of the electrical parts and increase their efficiency, hence reducing their heat losses.

Yet, it does come at the cost of requiring either a cryogenic cooling apparatus or a cryogenic coolant onboard, such as helium or hydrogen, not to mention the hydrogen storage complications as highlighted in a paper by Licheva and Liscouët-Hanke [30]. Sumption et al. evaluated the two configurations shown in figure 2.2, and found that only superconductors could give reductions of mass, volume, or loss for the cryocooled case. However, for the liquid cryogen case, both cryoconductors and superconductors could show mass, volume, and loss reductions.

Hartmann et al. [14] investigated a concept similar to case (b) of figure 2.2 by proposing an integrated superconducting cryogenic fuel cell propulsion system that uses cryogenic hydrogen fuel to cool the electrical components, as shown in figure 2.3. They explore three different 2035 scenarios,
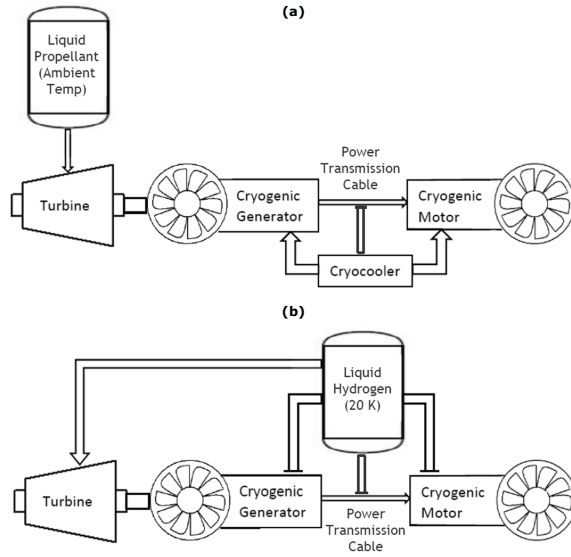
Figure 2.2: Cryogenic configurations studied by Sumption et al. [29]; (a) cryogenic generator, motor, and power transmission line cooled by cryocooler, and (b) generator/motor/transmission line heat rejected to (cryogenic) liquid propellant.

baseline, conservative, and optimistic, with varying component efficiencies drawn from literature to determine the architecture's feasibility and the fuel cell's optimal working point for gravimetric optimization. Their findings show that in the optimistic scenario, the hydrogen provides sufficient cryogenic cooling capacity to maintain proper conditions for all components. However, in the baseline scenario, the DC/DC converter exceeds the defined temperature limit of 110 K, an arbitrarily chosen limit.
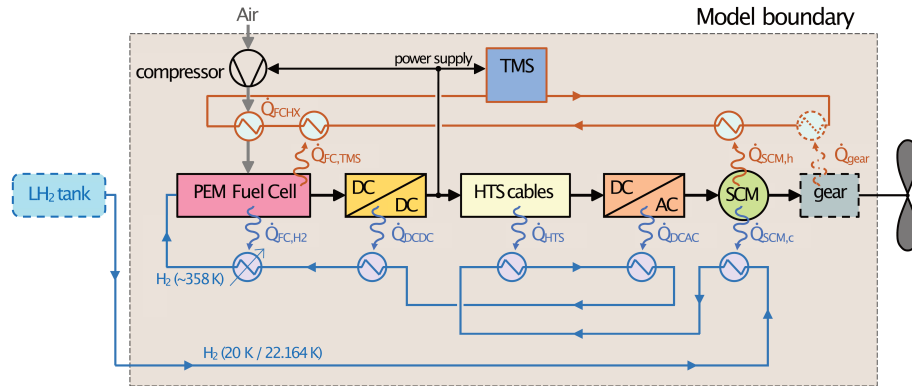
Figure 2.3: System arrangement featuring a Proton-Exchange Membrane Fuel Cell (PEMFC), HTSC, and a SCM, along with the cooling system design, TMS, and fuel cell compressor [14].

13

2.1.3 Cryogenic Heat Exchangers in Aerospace

According to Barron and Nellis [18], common cryogenic HXs include tubular HXs, Giauque-Hampson HXs[1], Plate-Fin Heat Exchanger (PFHE)s, Perforated Plate Heat Exchanger (PPHE)s, and Sintered Metal Powder Exchangers. The latter are primarily used for the lowest temperature cryogenic applications, as highlighted by Nakagawa et al. [31], who investigated the thermal and structural properties of sinters made from fine silver powder for ultra-low-temperature cooling[2]. Other cryogenic applications for such HXs are for He^4/He^3 dilution refrigerators or miniature Joule-Thomson refrigerators [18]. Additionally, the Giauque-Hampson exchanger represents a more volumetrically efficient variant of tubular HXs.

Figure 2.4 compares the performance of the most compact cryogenic HX types based on aerospace requirements from literature such as Sundén and Fu [32], and HX design books such as Hesselgreaves et al. [33], Barron et al. [18], and the latest edition of Kays and London [34]. The comparison uses the PFHE as a baseline since it is the primary HX used in aircraft design, as documented in both Society of Automotive Engineers (SAE) Aerospace Recommended Practice (ARP) 85 [3] [35] and SAE ARP [4] [36]. The figure shows that there are three types of Plate Heat Exchanger (PHE)s within the comparison, which highlights their advantageous ratio of total heat transfer-to-volume as compared to other types of exchangers. Also, to support figure 2.4, the typical features taken from [32] are listed in table 2.1.

Table 2.1: Typical features of aerospace HXs as highlighted by [32].

Feature	Reasoning
Compact	Compact Heat Exchanger (CHE)s are mainly used due to the space constraints for heat transfer systems in the aerospace industry.
Lightweight	Lightweight materials such as aluminum alloy and metal foam are preferable as weight directly impacts aircraft performance, safety, and efficiency.
High temperature and pressure resistance	In certain cases, materials used in aircraft HXs must maintain their structural integrity when exposed to high temperature differentials and pressures from turbine engines, hydraulic systems, and future cryogenic systems.
High effectiveness and minimum pressure loss	Heat-exchanging surfaces and flow paths should be designed to maximize thermal conductance while minimizing pressure loss because it impacts cooling capacity, reduces operational efficiency, and increases performance degradation, system instability, weight, and size.

---

[1]Also known as coil-wound HXs.
[2]This is defined in [31] as temperatures at or below 10 mK.
[3]Recommended practices for Air Conditioning (AC) systems.
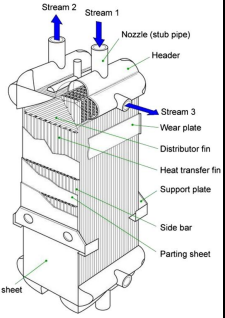[4]Recommended practices for bleed air systems.

14

		Plate-Fin	Giauque–Hampson	Printed Circuit	Perforated Plate
Legend					
Better	✓				
Less	✗				
Equal	≈				
Compactness		Baseline	✗	✓	✓
Cryogenic		Baseline	≈	≈	≈
Lightweight		Baseline	≈	≈	≈
Geometrically Flexible		Baseline	✗	≈	≈
Low Power		Baseline	≈	✗	✗
Phase Change		Baseline	✗	≈	✗
Other Considerations		• Startup cooling process and shutdown warming process necessary due to thermal stresses	• High material costs • More complex maintenance • Few manufacturers & complex	• Startup and shutdown needed	• Less risk of leaks but risk of blocks • Highest thermal effectiveness • High cost

Figure 2.4: Comparison of possible cryogenic HXs for aerospace applications. The PFHE is from [37], the coil-wound HX is from [38], the PPHE is from [39], and Printed Circuit Heat Exchanger (PCHE) is from [40].

2.2 Heat Exchanger Design

HX design is explicitly noted in Section 525.1125 of Transport Canada (TC)'s Canadian Aviation Regulations (CARs) by addressing exhaust systems HXs. The rules ensure compliance with requirements for high-temperature operations, corrosion resistance, inspection access, cooling when exposed to exhaust gases, elimination of stagnant areas when exhaust gases are within, and the installation of a secondary intermediate HX when used in the ECS. Consequently, CARs impose minimal constraints on HX designs.

For aircraft AC systems, the SAE ARP 85 [41] recommends having liquid-cooled HXs designed to prevent structural failures that could cause fuel/coolant leakage into the air supply, which might lead to fire, explosion, toxicity, or noxious odors within the cabin. They should also allow for easy contaminant removal and low-cost internal leak repairs with minimal performance impact.

Research is underway to reduce weight, increase compactness and effectiveness, and improve manufacturing techniques of aerospace HXs [7]. While the previous section highlights some of this work, the most common approach is still to size HXs using conventional assumptions and technologies such as air-oil coolers, fuel-oil coolers, and ram-coolant coolers. Hence, even as researchers investigate novel cryogenic configurations and TMS designs, such as those proposed by Ouyang et al. [20] and Hartmann et al. [14], system sizing typically relies on either scaling existing technologies or remaining at the aircraft-level in terms of energy or exergy analyses. Meanwhile, papers utilizing parametric sizing methods often rely on proprietary software that does not fully describe their process, preferring to maintain their focus on aircraft architecture rather than computational details. Table 2.2 summarizes the papers discussed in section 2.1.

Table 2.2: Aircraft TMS sizing in literature.

Literature	Topic	Sizing Method
Ouyang et al. [20]	Summary of IPTMS research & technology review	Exergy & energy based analysis at architecture/aircraft level
Kellermann et al. [10]	Summary of TMS research & technology	Industry software & effectiveness-NTU
Hartmann et al. [14]	Cryogenic aircraft architecture analysis	Conventional TMS scaling & no cryogenic system sizing
Coutinho et al.[22]	Summary of TMS development for HEPA	Energy based analysis at architecture/aircraft level mostly using ram air or liquid cooling loops
Yu et al. [23]	Analyzes the interaction between powertrain and TMS	No sizing - Energy optimization
Tarhan et al. [24]	Battery Management System (BMS) design for electric aircraft	No sizing - Monitor voltage, temperature, current, State of Charge (SOC), State of Health (SOH)
Cyrille et al. [25]	Summary of battery TMS designs	No sizing - Papers reviewed are detailed designs using CAD software
Jansen et al. [26]	Show one or more viable EAP concepts for narrow-body aircraft	Energy based analysis at architecture/aircraft level
Rheaume et al. [27], [28]	Baseline and optimized TMS designs for a parallel HEA	Multi-design point sizing and optimization of TMS components using a proprietary, object-oriented modeling tool
Sumption et al. [29]	Performance evaluation of electrical conductors, both normal-state and superconducting, at cryogenic temperatures for AEA & MEA	Sizing for electrical components only

While much of the literature on novel aircraft propulsion systems remains focused at the aircraft level, there are papers focused on TMS design and HX configurations. Strumpf and Mirza [42], for instance, developed a microchannel HX in collaboration with Honeywell Aerospace to address size and weight concerns. Their analysis and testing demonstrated notable potential for volume reduction and moderate potential for weight reduction benefits. However, as with many industry collaborations, the specific sizing methodology remains confidential behind proprietary methods, though they do mention using literature analytical correlations for heat transfer and pressure drop through plain rectangular passages.

Aerospace HXs are typically custom-designed for specific aircraft requirements, necessitating a unique design for each application [36], [41]. Aircraft manufacturers commonly outsource the detailed design of these components to specialized firms such as Honeywell, Meggitt PLC, TAT Technologies, and Safran. Therefore, moving away from the aerospace-specific literature, researchers have identified solutions to many of the design challenges through investigations in adjacent fields [7], with relevant findings documented across heating, ventilation, and air conditioning (HVAC),

heat and mass transfer, electronics technology, thermal engineering, and process safety and environmental protection literature.

Arsenyeva et al. [43] proposed an Effectiveness-NTU (ε-NTU) method to design an optimized multi-pass plate-and-frame HX with mixed grouping of plates. They used the number of passes for both streams, the number of plates with different corrugation geometries in each pass, and the plate type and size as design variables. For their method, they developed a mathematical model of algebraic equations in matrix form that is readily obtainable to represent a number of plate packs with co- and counter-current directions of streams.

Their model makes the following assumptions:

- The heat transfer process is stationary.

- No change of phases in streams.

- The number of heat transfer plates is sufficient to disregard the differences in heat transfer conditions for plates at the edges of passes.

- Flow distribution irregularities in collectors can be disregarded.

- The streams are fully mixed[5] in the common sections of the PHE collectors.

The thermal and hydraulic performance of channels between plates with various corrugation geometries is accounted for by using exponents and coefficients in heat transfer and friction factor formulas as model parameters. The PHE heat transfer area was used as an objective function for optimization, as they determined that it also characterizes the PHE cost and need for sophisticated materials in plates and gaskets. The authors conclude that the presented method can be used for statistics when generalizing the correlations for PHEs' thermal and hydraulic performance or for modeling of PHEs when making multiple calculations for HX network design.

In a more recent study, Xu and Smith [44] developed a more computationally efficient method for HX network retrofit design. They proposed a Mixed Integer Nonlinear Programming (MINLP) approach to optimize the design of two-stream multi-pass plate HXs by minimizing the total area of a PHE through selecting optimal plate geometries, chevron angle, and flow arrangement. They incorporate standardized plate sizes from Alfa Laval as parameter models within a deterministic general MINLP global optimization framework[6] for practical applications, which consequently constrains the design space.

2.2.1 Cryogenics

Regarding cryogenic applications, a paper by Popov et al. [37], which reviewed research for HXs for process cooling and renewable energy storage, concludes that accurate simulation and design models for all cryogenic HXs are necessary and that the current shift is toward advanced numerical models. For example, White et al. [46] validate experimentally a numerical modeling technique for PPHEs that accounts for axial conduction, external parasitic heat loads, variable fluid and material properties, and conduction end to end of the HX. The experimental testing demonstrated the ability of their numerical model to accurately predict both the overall performance and

---

[5]In this case, "mixed" does not imply the mixing of streams, but rather describes the condition where fluid mixes freely perpendicular to its main flow direction, creating a more uniform temperature distribution across the flow path.

[6]The authors use the GAMS [45] high-level modeling software's ANTIGONE algorithm.

the internal temperature distribution over a range of geometries and operating conditions. They used a ε-NTU model based on a paper by Nellis et al. [47] which uses a Finite Difference Method (FDM). The governing equations are derived, nondimensionalized, discretized, and solved on an exponentially distributed grid, as shown in figure 2.5.
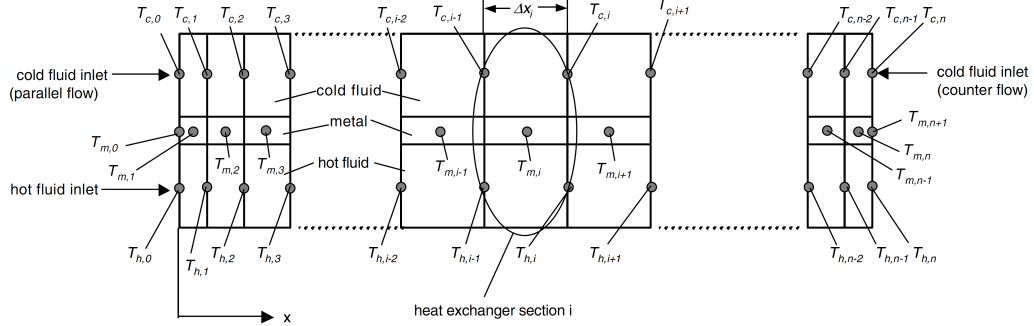
Figure 2.5: Nellis et at. [47] computational grid.

Allahyarzadeh-Bidgoli et al. [48] propose a sizing methodology for multi-stream PFHE for Liquefied Natural Gas (LNG). They established that HX optimization is crucial for improving energy efficiency. Their optimization focuses on five design variables for applied fins: fin type, height, thickness, frequency, and the number of layers in multi-stream PFHE. They incorporate a cost model based on work by Najafi et al. [49] and Mehrpooya et al. [50]. The HX sizing methodology follows empirical correlations from Kays and London [51]. For optimization, they employ the Non-dominated Sorting Genetic Algorithm II (NSGA-II) algorithm [52], which performs effectively for complex processes requiring multiple optimization layers [53].

A paper by Zhu et al. [54], which investigated the design, optimization, and testing of a 2 K cryogenic negative pressure PFHE, also selected to use the NSGA-II. The authors determined that the large changes in thermal properties of the working fluid in the 2 K HX, and the variable conductivity of the 6061 aluminum alloy in the working temperature range, make the assumption of constant physical properties invalid. Therefore, the traditional lumped parameter method is not suitable, and a distributed parameter method was used instead, as shown in figure 2.6, similar to the Nellis et al. [47] approach. The HX was divided into several small heat exchange units, and the temperature, pressure, heat transfer coefficient, friction factor, and other parameters were recorded in each unit.

Figure 2.6: Schematic of distributed parameter method [54].

Finally, an important consideration for cryogenic HXs is fouling during boiling, as experimentally tested by Muller-Steinhagen [55]. His research concluded that fouling can occur during the boiling of cryogenic liquids, even when the liquids are of very high purity. This phenomenon becomes more pronounced with increasing wall superheat and system pressure.

2.2.2 Optimization

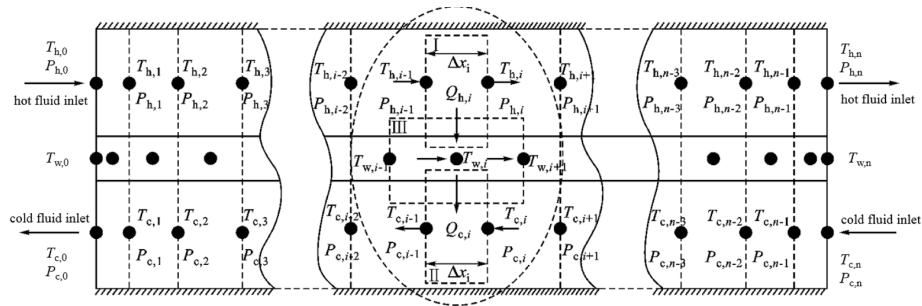A consideration for HX design is determining optimal approaches to balance competing objectives. Raja et al. [56] examine the differences between many-objective and multi-objective approaches to cross-flow PFHE design. They simultaneously pursue four objectives: maximizing effectiveness while minimizing total annual cost, total weight, and entropy generation units, using a multi-objective heat transfer search algorithm. Their analysis employs three decision-making methods: Linear Programming Technique for Multidimensional Analysis of Preference (LINMAP), Technique for Order of Preference by Similarity to Ideal Solution (TOPSIS), and Fuzzy. Using an ε-NTU method, they identified tradeoffs among these objectives, with geometric parameters (cold and hot flow lengths, fin frequency, offset length, and thickness) substantially contributing to conflicting performance requirements. The authors concluded that a many-objective approach produces more realistic designs than a multi-objective one.

2.3 Early Aircraft Design Phases

An important aspect of the proposed methodology involves understanding its intended purpose and position in the design process. This chapter has highlighted research on aircraft TMSs and HX design. However, what remains undetermined is the appropriate level of detail needed in early aircraft design for alternative propulsion systems.

According to Raymer's book on general aviation aircraft design [57], the conceptual design phase primarily determines technical feasibility and establishes the business case. Deliverables such as the initial loft and a "Conceptual Design Evaluation Report" are produced to decide whether to proceed to the preliminary design phase.

The preliminary design phase, as defined by Gudmundsson [16], focuses on confirming the concept's viability by determining whether the idea functions effectively, identifying potential issues, and evaluating possible solutions. This phase encompasses multiple intersecting tasks including detailed geometry development, layout of major load paths, comprehensive component weight estimation, refinement of mission details, thorough pre-maiden performance evaluation, detailed stability and control analysis, assessment of special aerodynamic features, evaluation of certifiability and mission capability, refinement of reproducibility, definition of maintainability parameters (including accessibility for repairs), and preliminary production cost estimation. These elements collectively establish the technical foundation necessary for advancing the design toward implementation.

Based on these tasks, estimating the TMS's weight, geometry, performance, and cost becomes a key deliverable within the "Preliminary Design Evaluation Report." The proposed methodology is especially valuable for novel EPA and HEPA designs where historical data and industry experience are currently lacking in the aerospace sector. It helps demonstrate the feasibility of novel TMSs for conceptual aircraft by providing detailed HX weight, size, and performance specifications. Importantly, feasibility determination should neither require extensive design work nor consume considerable time and resources. From these considerations, the methodology requirements are determined to be:

- Suitable for conceptual and preliminary design phase requirements and level of detail.

- Leverage available inputs to deliver the most accurate sizing estimates while avoiding detailed design work.

- Ensure computational efficiency.

- Ensure compatibility with MDAO frameworks.

2.4   Summary and Gap Analysis

In summary, research is being conducted on thermal management technologies for future aircraft systems, which primarily focuses on high-level conceptual design, often neglecting system-level and component-level details important for feasibility and design considerations. This follows traditional aircraft design methodology, where aircraft-level design precedes system-level design, which further precedes item-level design. While aircraft design is iterative, many infeasible architectures could be eliminated earlier by integrating critical systems sooner in the design process, reducing development time and cost, and allowing for more integrated system designs. Moreover, studies on AEA and HEPA architectures that apply conventional assumptions to cryogenic applications risk inaccurately estimating TMS size, weight, and performance.

It is becoming evident that TMS design must be considered during early development phases due to its impact on aircraft performance [7] . This necessitates early design methods that can be integrated into MDAO frameworks to accurately estimate the weight, volume, cost, and performance impact of HXs on novel aircraft designs. Furthermore, there is a need to develop integrated TMSs that utilize all available heat sources, transportation opportunities, and thermal sinks to minimize system performance impact.

Regarding HX design and sizing, several well-established numerical design methods exist, including the Log-Mean Temperature Difference (LMTD) and ε-NTU approaches. These methods are thoroughly documented in the literature by Kays and London [51], [58], Ranganayakulu and Seetharamu [59], Hesselgreaves et al. [33], Shah and Sekulic [60], Shah et al. [61], and Lee [62], among others. Modern design approaches employ higher fidelity techniques, such as the Nellis et al. [47] ε-NTU FDM or the Finite Element Method (FEM) and CFD approaches described by Ranganayakulu and Seetharamu [59].

The literature review indicates that contemporary HX design research predominantly focuses on developing optimization frameworks based on established numerical methods, such as the ε-NTU approach, to identify optimal solutions for specific applications.

Finally, the proposed methodology in this thesis addresses the following gaps:

- develop a HX sizing method for early aircraft design;

- develop a parametric HX sizing method to address both conventional and cryogenic applications;

- develop a framework-flexible HX sizing method to accommodate various variable input design parameters, allowing for any aircraft HX to be sized; and

- develop a HX sizing method for use in an aircraft MDAO framework for TMS design.

20

Chapter 3

Methodology

$\mathbf{T}$HIS chapter presents the HX design methodology developed to address the gaps identified in Section 2.4 while incorporating the nuances of designing for cryogenic applications detailed in Chapter 1. Section 3.1 provides an overview of the framework and methodology, followed by a discussion of relevant aviation rules, regulations, and recommendations. Section 3.2 explains the HX design methodology's assumptions and constraints, then breaks down the design process into three functional parts[1]: scoping process, sizing process, and performance evaluation.

3.1 Overview

The governing equations for HX design are based primarily on fluid dynamics and heat transfer principles, specifically, the Navier-Stokes equations and the First Law of Thermodynamics. With these principles, along with geometric properties and surrogate surface correlations, engineers can solve HX problems numerically without needing to entirely solve the Navier-Stokes equations through some form of thermal CFD analysis or Finite Element Analysis (FEA).

The design framework requires input parameters such as heat transfer capacity (Q) or heat transfer rate ($\dot{Q}$), mass flow rates ($\dot{m}$), and a certain number of inlet and outlet fluid properties. Other specifications, such as the weight and size, system pressure limitations, and pressure drop requirements, can be defined as constraints. Figure 3.1 presents a flowchart diagram illustrating an overview of the suggested process's different steps.

Multiple methodological approaches are required to accommodate varying numbers of input parameters. Such a methodological flexibility facilitates comprehensive design space exploration, enabling identification of optimal configurations based on the TMS architecture's specific interface conditions.

The methodology consists of seven sequential stages: requirements capture, type selection, flow selection, flow scoping, sizing and dimensional evaluation, and performance evaluation. Given that this thesis research focuses on HX sizing for alternative propulsion systems, including superconducting, the flowchart requirements specified are for the most limiting case of a hydrogen FC architecture.

Additionally, the Corrugated Plate Heat Exchanger (CPHE) is selected as the baseline because it represents a conservative assumption and requires fewer input parameters, making it the quickest

---

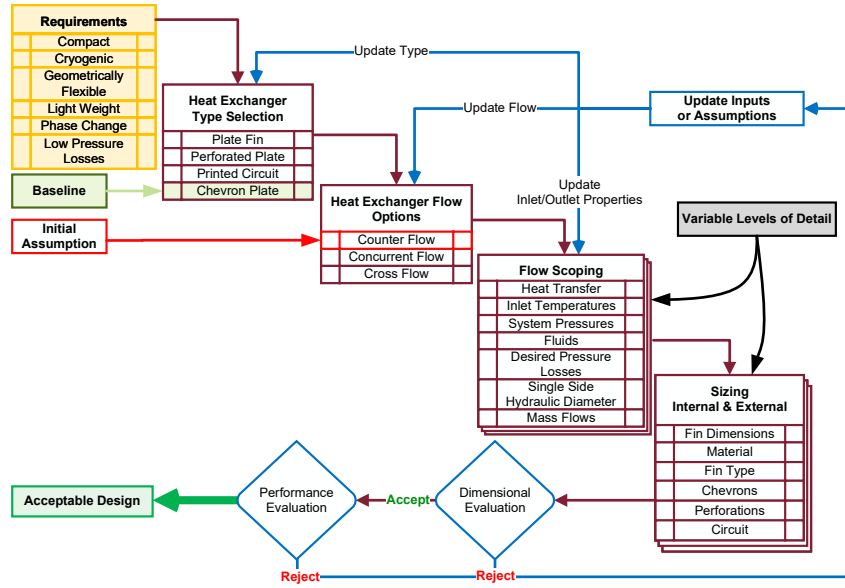[1]A methodology adapted from Hesselgreaves et al. [33]

21

Figure 3.1: HX sizing process.

PHE to computationally size for. In the same manner, a counterflow initial assumption is used as it will typically give the most economic design [33].

3.2 Heat Exchanger Design

The methodology developed is intended to explore the design space for both conventional and cryogenic HXs at an early design phase level of detail. The desired outputs are the weight, physical dimensions, system losses, and energy requirements. Section 3.2.1 will first detail the parametric specifications, assumptions, and constraints concepts, followed by an explanation of the three design steps: scoping, sizing, and performance evaluation in Sections 3.2.2, 3.2.3, and 3.2.4, respectively.

3.2.1 Parametric Specifications, Assumptions & Constraints

For this methodology, parametric specifications, assumptions, and constraints are classified into two distinct categories: framework-based and problem-based. In this context, "framework" refers to the systematic approach through which the methodology addresses a specific problem, while "problem" refers to the actual sizing task with its various inputs.

Framework-based specifications are computational tool-related elements that enable the HX sizing process to communicate with other sizing tools, as mentioned in Section 1.2. For instance, an MDAO framework might utilize the Common Parametric Aircraft Configuration Schema (CPACS) data definition, as implemented in the EAP project, to facilitate information exchange between tools. These specifications, assumptions, and constraints also define how the HX sizing process addresses a given problem, since multiple solution approaches exist depending on available parametric inputs. They also establish initial conditions for the iterative design process, incorporating standardized engineering parameters from established design tables and relationships.

Similarly, figure 3.2 shows the different parametric problem-based inputs, outputs, specifications, assumptions, and constraints. The problem-based specifications, assumptions, and constraints define key operational parameters, such as temperature gradients between fluid streams, system operating pressures, maximum allowable pressure drops, heat transfer coefficients, and geometric constraints governing HX configurations. Once again, standard engineering design references such as Kays and London [34] and Hesselgreaves [33] provide validated baseline values for designer-specified assumptions.
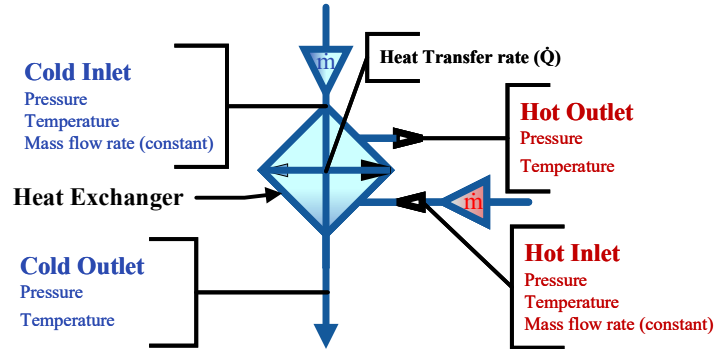

Figure 3.2: HX sizing parametric inputs, outputs, specifications, assumptions, and constraints.

Finally, the assumptions must encompass the maximum feasible range to enable comprehensive design space exploration, while constraints maintain solution viability. When solutions prove infeasible or fail to meet specified requirements, two remediation approaches are available: (1) constraint relaxation, or (2) assumption boundary expansion. These methodological modifications facilitate iterative refinement of the solution space until viable designs emerge. Initial broad input spaces typically yield feasible solutions; however, in cases where no solution exists, analysis of the obtained solution space relative to the objective space guides the designer toward necessary trade-offs for achieving acceptable, though non-optimal, solutions.

3.2.2 Scoping Process

The flow scoping analysis assumes the use of a thermophysical property library such as Cool-Prop [19] or the National Institute for Standards and Technology (NIST) database for evaluating the thermodynamic and transport properties of pure, pseudo-pure, and multicomponent fluid mixtures. The process is shown in an eXtended Design Structure Matrix (XDSM) diagram in figure 3.3, which illustrates that the system receives inputs from three distinct sources: system design specifications, optimizer variables, and solver feedback variables.

The counter-flow configuration serves as the initial assumption due to its analytical simplicity and superior thermal effectiveness, as noted in Section 3.1 and supported by [51]. For plate geometries, this arrangement delivers optimal compactness in terms of heat transfer surface area per unit volume. While cross-flow configurations offer reduced pressure penalties, this advantage is negated by the larger axial dimensions needed to achieve comparable thermal performance.

The scoping process applies the First Law of Thermodynamics to analyze each working fluid stream. It applies to both hot and cold sides of the HX, with equation (1) describing the energy balance for the cold stream. In this equation, the heat transfer rate ($\dot{Q}$) is calculated using the mass flow ($\dot{m}$), the specific heat (c_p) and the inlet and outlet temperature variation ($T_{c,in}$ and $T_{c,out}$). The
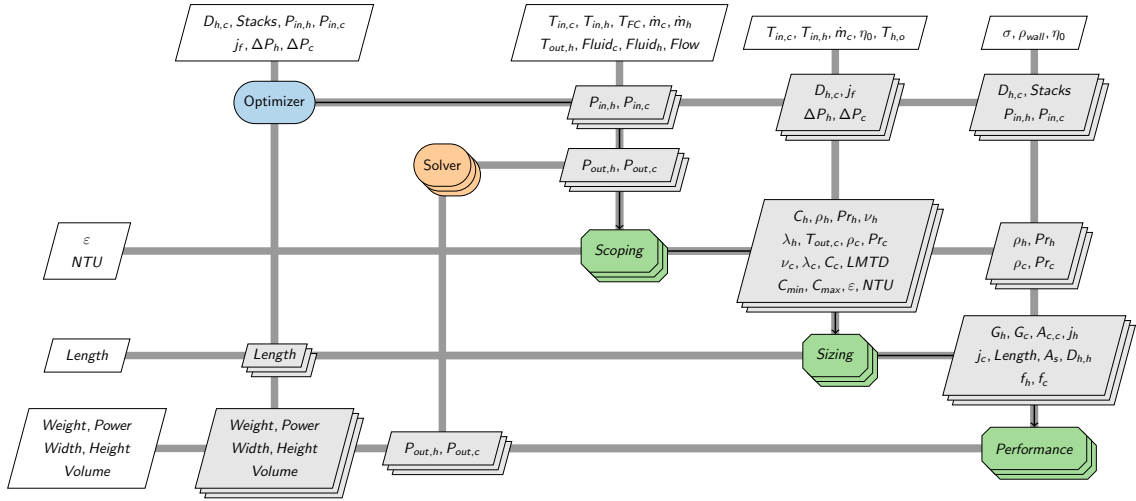
Figure 3.3: High-level XDSM diagram of the design process.

same equation can also be used with heat capacity rates (C) instead of mass flow and specific heat, which can be calculated using equation (2).

$$\dot{Q} = \dot{m}_c\, c_{p,c}\, \left(T_{c,out} - T_{c,in}\right) \tag{1}$$

$$C_c = \dot{m}_c\, c_{p,c} \tag{2}$$

For the hot side of the HX, an analogous equation applies with inverted temperature differentials, as presented in equation (3), and the heat capacity rate is calculated the same way as shown in equation (4).

$$\dot{Q} = \dot{m}_h c_{p,h}\left(T_{h,in} - T_{h,out}\right) \tag{3}$$

$$C_h = \dot{m}_h\, c_{p,h} \tag{4}$$

The ε-NTU method requires determining the minimum heat capacity rate C_{min}. Then, using it to find the maximum heat transfer rate $\dot{Q}_{max}$ and applying it to equation (6), the HX effectiveness[2] can be calculated.

$$\dot{Q}_{max} = C_{min}\left(T_{h,in} - T_{c,in}\right) \tag{5}$$

$$\varepsilon = \frac{\dot{Q}}{\dot{Q}_{max}} = \frac{C_h\left(T_{h,in} - T_{h,out}\right)}{C_{min}\left(T_{h,in} - T_{c,in}\right)} = \frac{C_c\left(T_{c,out} - T_{c,in}\right)}{C_{min}\left(T_{h,in} - T_{c,in}\right)} \tag{6}$$

The effectiveness calculation enables the determination of the Number of Transfer Units (NTU), as shown in equation (7), based on the selected flow configuration and the ratio of stream capacity rates. This ratio, denoted as C_R or C^*, is calculated according to equation (8). NTU is also related to the HX's heat transfer conductance, which is the product of overall heat transfer coefficient (α) and surface area (A), and C_{min}, allowing for the sizing of the HX as shown in equation (9); a

---

[2]Equation 6 is a common definition of effectiveness that is similarly defined in the SAE ARP 147E [35].

relationship derived from the heat exchange equation (10), where α is the heat transfer coefficient and η_0 is the surface effectiveness.

$$NTU = \begin{cases} \dfrac{1}{C^* - 1} \ln\left(\dfrac{\varepsilon - 1}{C^* \cdot \varepsilon - 1}\right) & \text{for counter flow} \\[2ex] \dfrac{\varepsilon}{1 - \varepsilon} & \text{for } C^* = 1 \text{ \& counter flow} \\[2ex] \dfrac{-\ln\left[1 - \varepsilon \cdot (1 + C^*)\right]}{1 + C^*} & \text{for parallel flow} \\[2ex] -\ln\left[1 + \dfrac{1}{C^*} \cdot \ln(1 - C^* \varepsilon)\right] & \text{for cross flow with } C_{max} \text{ mixed, } C_{min} \text{ unmixed} \\[2ex] -\dfrac{1}{C^*} \cdot \ln\left[1 + \ln(1 - \varepsilon)\right] & \text{for cross flow with } C_{max} \text{ unmixed, } C_{min} \text{ mixed} \\[2ex] -\ln(1 - \varepsilon) & \text{for all cases where } C^* = 0 \end{cases}$$

(7)

$$C^* = C_R = \frac{C_{min}}{C_{max}} \tag{8}$$

$$NTU = \frac{\alpha A}{C_{min}} \tag{9}$$

Alternatively, the LMTD method can also be used. It assumes that heat transfer coefficients remain constant along both sides of the HX, which may not always reflect reality depending on the design. However, for conceptual evaluation purposes, this simplification is adequate. The relationship for calculating it is shown in equation (11), where ΔT_A and ΔT_B are flow-dependent and are calculated according to figure 3.4.

$$\dot{Q} = (\eta_0 \alpha A) \Delta \overline{T} \tag{10}$$

$$\overline{\Delta T} = \frac{\Delta T_A - \Delta T_B}{\ln\left(\frac{\Delta T_A}{\Delta T_B}\right)} = \frac{\Delta T_A - \Delta T_B}{\ln \Delta T_A - \ln \Delta T_B} \tag{11}$$
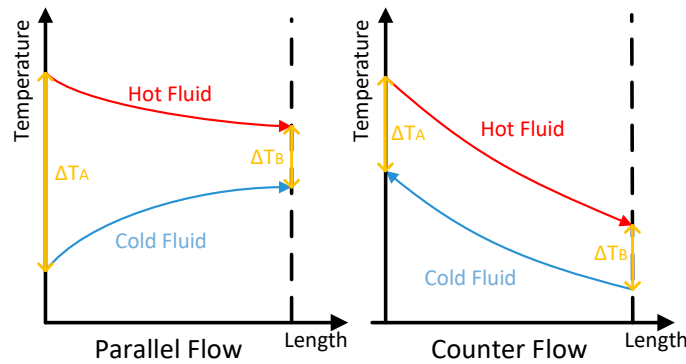

Figure 3.4: How to calculate ΔT_A and ΔT_B according to flow.

The scoping phase concludes when all variables highlighted in figure 3.2 are quantified, allowing the sizing process to begin based on the fluid and flow properties.

3.2.3 Sizing Process

The sizing process commences with identifying the critical side of the HX. The dimensionless thermal length (N) is first estimated using equation (12). In cases where the LMTD is indeterminate and direct calculation of N is not feasible, it is approximated according to established methods from [33]: 2NTU for a balanced HX, or 1.1NTU for the gas side of a liquid-gas HX, and 10C^* for the liquid side. The analysis proceeds by first determining core mass velocity (G) for each side according to equation (13).

$$N = \frac{\eta_o \alpha A}{\dot{m} c_p} = \frac{T_2 - T_1}{\overline{\Delta T}} \tag{12}$$

$$G = \sqrt{\frac{2\rho \Delta P \left(j_{factor} \right)}{Pr^{2/3} N}} \tag{13}$$

Subsequently, the cross-sectional area (A_{cs}) is derived from the relationship presented in equation (14).

$$A_{cs} = \frac{\dot{m}}{G} \tag{14}$$

The hydraulic diameter (d_h) is selected based on compactness requirements and serves as an initial input to calculate the Reynolds number (Re) for each flow stream using equation (16). Appendix B's Figure B provides a valuable reference for determining an appropriate hydraulic diameter during the sizing process. The Colburn factors (j) are then determined using equation (17), incorporating both Re and chevron angle (β) for a CPHE, which subsequently enables the calculation of HX length (L) through equation (18).

$$j_{factor} = \frac{j}{f_f} \tag{15}$$

$$Re = \frac{G d_h}{\mu} \tag{16}$$

$$j_{cphe} = 0.1 Re^{-1/3} \left(1 + 0.8 \left(\beta - 30 \right) / 30 \right) \tag{17}$$

$$L = \frac{d_h Pr^{2/3} N}{4j} \tag{18}$$

The heat transfer surface area (A_{sf}) is estimated using the standard hydraulic diameter definition as shown in equation (19). Although different heat transfer surface areas could be used for each side, there is no advantage in the initial design phase to pursue a more detailed approach or optimize each side individually, as this methodology focuses on early design phase exploration; both sides' heat transfer surface areas are therefore assumed to be identical, yielding conservative results.

$$d_h = \frac{4 A_{cs} L}{A_{sf}} \tag{19}$$

26

Since the sizing process occurs sequentially, starting with the most critical side, after determining the exchanger length, we can apply the same relationships to calculate the missing dimensions of the opposite side.

Using the fluid density (ρ), we can then calculate the flow velocity (U) as in equation (20).

$$U = \frac{G}{\rho} \tag{20}$$

Similar to the Colburn factor, the CPHE friction factors are estimated using the Reynolds numbers and established surrogate mathematical models. Martin's models from [63], [64], which incorporate the generalized Lévêque equation for heat-transfer coefficient prediction, are used as suggested by [33] and [60]. The resulting equations (21)[3], (22), and (23) determine the Fanning friction factor (f_f), which differs from the Darcy-Weisbach friction factor (f_D) presented in Martin's 1996 analysis. These semi-empirical models demonstrate accurate predictive capabilities for chevron angles between 10 and 80 degrees.

$$f_0 = \begin{cases} \dfrac{16}{Re}, & \text{for } Re < 2000 \text{ (Martin's original)} \\[2ex] \dfrac{20}{Re}, & \text{for } Re < 2000 \text{ (Hesselgreaves fully-developed laminar flow)} \\[2ex] (1.56 \ln Re - 3)^{-2}, & \text{otherwise} \end{cases} \tag{21}$$

$$f_1 = \begin{cases} \dfrac{149}{Re} + 0.9625, & \text{for } Re < 2000 \\[2ex] \dfrac{9.75}{Re^{0.289}}, & \text{otherwise} \end{cases} \tag{22}$$

$$\frac{1}{\sqrt{f_f}} = \frac{\cos \phi}{\sqrt{0.045 \tan \phi + 0.09 \sin \phi + f_0 / \cos \phi}} + \frac{1 - \cos \phi}{\sqrt{3.8 f_1}} \tag{23}$$

In contrast, the PFHE Colburn and friction factors require more details about the fins. The basic geometry for a plate-fin surface is shown in figure 3.5, and the different dimensions are defined in table 3.1. Using these dimensions, it is possible to use equation (24) for the Colburn factor and equation (25) for the friction factor. It is also possible to use a more "geometric" approach, as termed by [33], by using equations (26) and (27), which requires the ratio of fin area (A_{fin}) to total area (A_{tot}) and the fin thickness (t_{fin}).

$$j_{pfhe} = 0.6522 Re^{-0.5403} \alpha_{fin}^{-0.1541} \delta_{fin}^{-0.1409} \gamma_{fin}^{-0.0678} (1 + 5.269E{-}5 \cdot Re^{1.34} \alpha_{fin}^{0.504} \delta_{fin}^{0.456} \gamma_{fin}^{-1.055})^{0.1} \tag{24}$$

$$f_{f,pfhe} = 9.6243 Re^{-0.7422} \alpha_{fin}^{-0.1856} \delta_{fin}^{0.3053} \gamma_{fin}^{-0.2659} (1 + 7.669E{-}8 \cdot Re^{4.429} \alpha_{fin}^{0.92} \delta_{fin}^{3.767} \gamma_{fin}^{0.236})^{0.1} \tag{25}$$

$$j_{pfhe} = 0.664 Re^{-1/2} (d_h/l)^{1/2} (1 - 0.5(1 - A_{fin}/A_{tot})) \tag{26}$$

---

[3]Both the original equation from Martin [63] and the suggested by Hesselgreaves [33] for the fully-developed laminar flow conditions are shown in the equation.
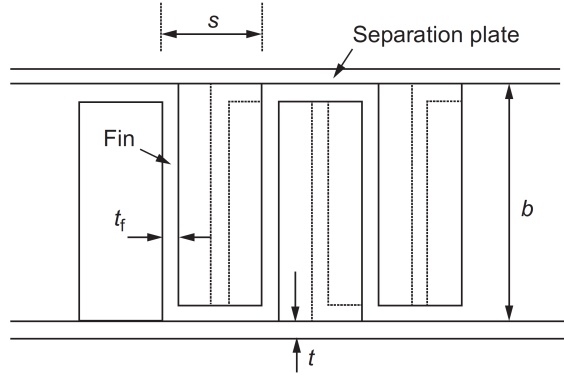
Figure 3.5: Basic geometry schematic of rectangular PFHE surface with Offset-Strip Fin (OSF) shown in dashed lines [33].

Table 3.1: OSF geometric definitions as defined in [33].

Dimensions	Symbol	Dimensionless Ratios
Fin thickness	t_{fin}	$\alpha_{fin} = s/h$
Separation plate thickness	t	$\delta_{fin} = t_{fin}/l$
Hydraulic diameter	d_h	$\gamma_{fin} = t_{fin}/s$
Plate-gap (= distance between plate surfaces)	b_{fin}	
Passage height ($= b_{fin} - tf$)	h	
Splitter plate thickness (if used)	t_s	
Fin spacing	s	
Fin (strip) length	l	

$$f_{f,pfhe} = Re^{-1/2}(d_h/l)^{1/2}(1.328 + 2(t_{fin}/l)^{1/2}) + \frac{18}{Re} \tag{27}$$

The sizing process then evaluates the flow area goodness factor with the newly obtained Colburn and friction factors according to equation (15). Then the process is iterated upon, starting from equation 13 until convergence or a set number of iterations. For the first sizing process, since fluid properties do not account for pressure losses that can impact results, it is possible to use a looser initial convergence tolerance or fewer iterations to reduce processing time.

3.2.4 Performance Evaluation

The HX design process concludes with a performance evaluation based on dimensional properties, weight, and pressure losses. While pressure losses typically serve as inputs, the non-critical side requires calculation. The evaluation sequence begins with the Nusselt number calculation, for CPHEs, the Sekulic and Shah's [60] experimental correlations shown in equation (28) are used.

$$Nu_{cphe} = 0.724(\beta/30)^{0.646}Re^{0.583}Pr^{1/3} \tag{28}$$

For PFHEs, the Nusselt number calculation is flow-dependent, and therefore equation (29) must be used with the help of the geometric relationship shown in figure 3.6 for the value of α.

$$Nu = \begin{cases} 8.235(1 - a\alpha + b\alpha^2 - c\alpha^3 + d\alpha^4 - e\alpha^5), & \text{for laminar flow} \\ \quad \text{where,} \quad a = 2.0421 \quad b = 3.0853 \quad c = 2.4765 \\ \quad\quad\quad\quad\quad d = 1.0578 \quad e = 0.1861 \quad \alpha = 2b/2a \\ \\ \dfrac{0.5 f_{f,pfhe}(Re - 1000)Pr}{1 + 12.7(0.5 f_{f,pfhe})^{1/2}(Pr^{2/3} - 1)}, & \text{for } 2300 \le Re \le 5e6, 0.5 \le Pr \le 2000 \\ \\ 0.024 Re^{0.8} Pr^{0.4}, & \text{for heating turbulent flow} \\ 0.026 Re^{0.8} Pr^{0.3}, & \text{for cooling turbulent flow} \end{cases} \tag{29}$$
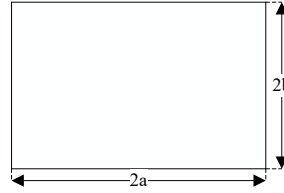

Figure 3.6: Geometric relationship to calculate the Nusselt number for rectangular ducts.

The calculation proceeds with determining actual thermal lengths using flow properties, superseding previous temperature-based estimations from equation (13) solved for N. The non-critical side's thermal length is expected to exhibit some variance from the previous estimates as the exchanger is optimized for the critical side's flow. Pressure drop calculations validate input parameters or provide values when unspecified, following equation (30). The final geometric dimensions for volume and weight proceed using equations (31) and (32), which account for the estimated exchanger porosity (σ) usually in the range of $0.7 - 0.85$ for CHEs [33]. For PFHEs, the porosity can be calculated using equation (33) based on the dimensions from table 3.1.

$$\Delta P = \frac{2G^2 L f_f}{\rho d_h} = \frac{1}{2}\rho U^2 \frac{L}{d_h} f_D \tag{30}$$

$$V = \frac{L A_{cs}}{\sigma} \tag{31}$$

$$W = \rho_w V (1 - \sigma) \tag{32}$$

$$\sigma_{pfhe} = \frac{sh}{(s - t_{fin})(b_{fin} + t)} = \frac{s(b_{fin} - t_{fin})}{(s - t_{fin})(b_{fin} + t)} \tag{33}$$

$$d_{h,pfhe} = \frac{4shl}{2(sl + hl + t_f h) + t_f s} \tag{34}$$

System pressures represent an important design parameter subject to optimization. These pressures determine the mean thermophysical fluid properties based on the inlet and outlet temperatures during heat transfer processes. Although pressure losses occur within HXs, the constant pressure assumption for fluid properties can provide acceptable accuracy for low heat transfer rates. For high heat transfer rate applications, such as those in aircraft propulsion systems, an iterative analytical

approach becomes necessary. Additionally, for future hydrogen-fueled aircraft, cryogenic hydrogen exhibits high compressibility in both gaseous and liquid states, resulting in large variations of thermophysical properties between the HX inlet and outlet conditions. The described methodology employs an iterative approach that begins with a constant pressure analysis and progressively incorporates estimated pressure losses into subsequent iterations until computational convergence is achieved.

Chapter 4

Implementation

S INCE the methodology aims to explore the design space for both conventional and cryogenic HXs at a component conceptual design level while being compatible with MDAO frameworks, the implementation incorporates several layers of flexibility:

(1) Multi-level of precision.

(2) Multi-framework compatibility.

(3) Modular functions.

This flexibility enables designers to implement the appropriate level of precision for each task. For example, as shown in figure 3.3, the sizing process requires a feedback loop to iteratively determine outlet pressures, which are initially undefined. For fluids with minimal variations in thermophysical properties during heat transfer, using the average properties between the inlet and outlet is sufficient. Hence, the sizing tool can be adjusted accordingly to save computational time.

For academic purposes and to ensure accessibility, the tool is developed in Python with exclusively open-source modules and libraries. The implementation leverages Coolprop [19] and Cantera [65] for calculating material transfer properties.

Thus, this section is organized into two subsections: Subsection 4.1 examines the necessary functions, and Subsection 4.2 compares the advantages and limitations of two mathematical equation solving approaches and explains the implementation for the optimization algorithm.

4.1 Required Functions

The system integrates with the EAP project's MDAO framework at its highest level. As illustrated in figure 4.1, the tool connects to the framework through a high-level run script using the CPACS[1]standard, more specifically, the open source TiXI XML Python library. Then, the HX design wrapper integrates the sizing problem received from the framework with the necessary local configuration, class libraries, default assumptions, and parameters. This subsection explores the essential functions, their specific purposes, and their implementation.

---

[1]CPACS is a data definition for the air transportation system and enables information exchange between different tools. It is meant to be used as a driver for multi-disciplinary and multi-fidelity design in distributed environments [66].
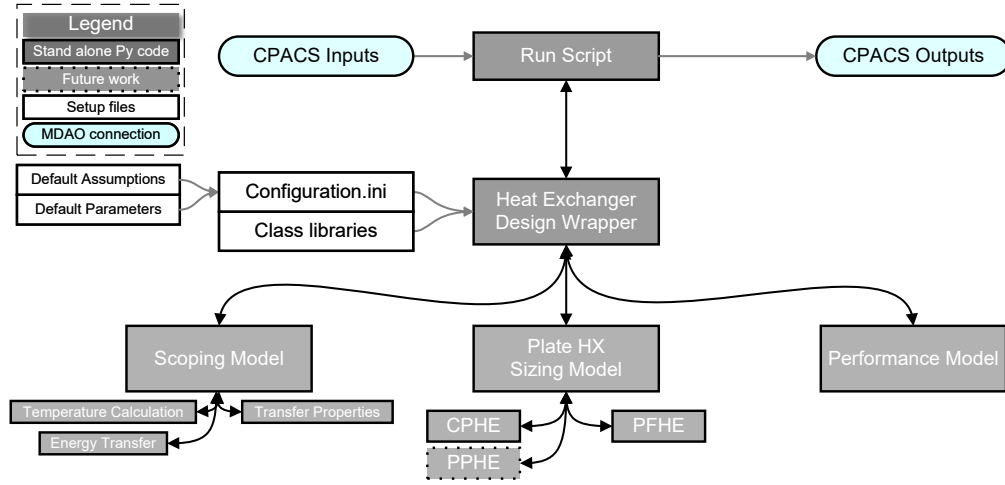
Figure 4.1: High-level architecture of the HX design script.

4.1.1 Configuration

The configuration file stores different local case studies that function like example problems with known solutions, ensuring consistent results across any setup. It also contains default assumptions and parameters for running incomplete sizing problems. For example, when sizing a HX that requires a hydraulic diameter range, the system will apply default values for CHEs if no specific range is provided.

When working within a shared MDAO framework using CPACS, the tool will instead use the information from the XML file it's directed to.

4.1.2 Class Libraries

The classes and libraries are maintained separately to enhance modularity and enable easier updates, allowing for more straightforward implementation of future work. The implementation primarily uses the open-source OpenMDAO [67] and Pymoo [68] with PyMOODE [69] libraries, which provide numerous classes for iteratively solving sizing problems, as explained in further detail in Section 4.2.

4.1.3 Temperature Calculation

A key function in sizing PHEs is calculating a fluid's outlet temperature based on mass flow and energy transfer using the convection equation, as shown in equations (1) and (3), or more generally in equation (35).

$$
\dot{Q} = \begin{cases} \dot{m}c_p(T_{in} - T_{out}), & \text{for cooling} \\ \dot{m}c_p(T_{out} - T_{in}), & \text{for heating} \\ \dot{m}c_p\Delta T, & \text{general form} \end{cases} \tag{35}
$$

With a known mass flow and heat transfer rate, we can calculate the outlet temperature by rearranging equation (35) to solve for temperature, as shown in equation (36).

$$T_{out} = \begin{cases} T_{in} - \dfrac{\dot{Q}}{\dot{m}c_p}, & \text{for cooling} \\[2ex] \dfrac{\dot{Q}}{\dot{m}c_p} + T_{in}, & \text{for heating} \end{cases} \tag{36}$$

This calculation is straightforward and requires only a few parameters. However, as discussed in Chapter 1, cryogenic applications cannot use simple average specific heat values for these calculations. Therefore, the chosen implementation uses a discrete numerical method instead, as shown in algorithm 1 for heating without phase change. Since specific heat values vary with temperature at each calculation step, a "while" loop continues until the desired heat transfer is achieved using increments that ensure accurate application of equation (35). The precision can be adjusted based on both the region of interest and the desired accuracy level by modifying the parameter n.

Algorithm 1 Outlet temperature algorithm for heating without phase change

---

Require: $\dot{m} > 0$

Require: $\dot{Q}_{final} > 0$

Ensure: $n \geq 1$

   $\dot{m} \leftarrow \dot{m}$ ▷ *Mass flow rate*

   $T_1 \leftarrow T_{in}$ ▷ *Cold side inlet temperature*

   $P_1 \leftarrow P_{in}$ ▷ *Cold side inlet pressure*

   $N \leftarrow n$ ▷ *Number of steps per degree*

   $\dot{Q}_0 \leftarrow 0$ ▷ *Initialize $\dot{Q}_0$ for **While** loop*

   $dT \leftarrow 1/N$ ▷ *Calculate steps dT*

   while $\dot{Q}_0 \leq \dot{Q}_{final}$ **do**   ▷ *Ends when $\dot{Q}_0 \geq \dot{Q}_{final}$*

      $T_2 \leftarrow T_1 + dT$

      $c_p \leftarrow (c_{p,1} + c_{p,2})/2$ ▷ *Average specific heat between T_1 and T_2 at P_1*

      $\dot{Q}_0 \leftarrow \dot{Q} + \dot{m}c_p(T_2 - T_1)$

      if $\dot{Q}_0 \leq \dot{Q}_{final}$ **then**   ▷ *Ensures $\dot{Q}_{out} \leq \dot{Q}_{final}$ for T_{out}*

         $\dot{Q}_{out} \leftarrow \dot{Q}_0$

         $T_{out} \leftarrow T_2$

      $T_1 \leftarrow T_2$

   return $[T_{out}, \dot{Q}_{out}]$

The described method offers an advantage over equation (36) by enabling a simple conditional check before calculations begin. In contrast, the alternative approach would require verifying phase changes after calculations are complete, which would increase computational time for a single sizing process and more so for an optimization process when the code runs multiple times. Figure 4.2 illustrates the logical process for phase change verification. Two scenarios are possible: full phase change or partial phase change. For partial phase changes, conventional methods are applied, and an additional parameter, the quality of the saturated liquid, is determined.

For cooling, the principles remain the same, with only minor changes to the code needed to account for the sign difference when calculating the temperature variation (ΔT) in equation (35).
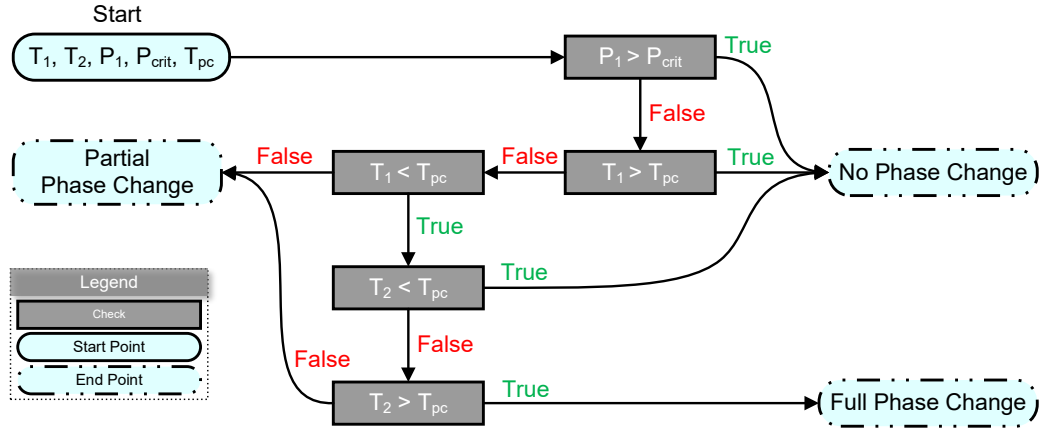
Figure 4.2: Logical process to verify if there is a change of phase during heating.

4.1.4 Heat Transfer Rate

Another key function calculates the heat transfer rate based on mass flow and temperature change for cases where these parameters are fixed. Advantageously, the logic and implementation from the temperature calculation can be repurposed, as the heat transfer rate ($\dot{Q}$) is already produced as an output parameter of that function, as evidenced in the returned array from algorithm 1. The updated implementation primarily adds new conditions to the "while" and "if" statements, as shown in algorithm 2, which highlights only the modifications.

This enhancement provides several advantages:

- minimizes code duplication;

- allows the algorithm to work with both the desired heat transfer rate and temperature limit; and

- ensures the sizing process can prevent solidification for cooling applications.

4.1.5 Mass Flow

The mass flow calculation function adopts a similar approach to the heat transfer calculation, adding new conditions to existing algorithms for better computational efficiency. It should be noted that for any sizing problem, as long as two of the three parameters (outlet temperature, heat transfer rate, and mass flow) are known, and assuming initial conditions are established, this method can scope any flow based on the discretization approach utilized.

Algorithm 2 Heat transfer rate algorithm for heating without phase change

---

Require: $\dot{m} > 0$

Require: $\dot{Q}_{final} > 0$ **or** $T_{target} > 0$ *▷ Add a T_{target} goal*

Ensure: $n \geq 1$

   $\dot{m} \leftarrow \dot{m}$

   $T_1 \leftarrow T_{in}$

   $P_1 \leftarrow P_{in}$

   $N \leftarrow n$

   $\dot{Q}_0 \leftarrow 0$

   $T_2 \leftarrow T_1$ *▷ Initialize T_2 for **While** loop*

   $dT \leftarrow 1/N$

   while $(\dot{Q}_0 \leq \dot{Q}_{final}$ **and** $\dot{Q}_{final} \neq 0)$ **or** $(T_2 \leq T_{target}$ **and** $T_{target} \neq 0)$ **do**

      $T_2 \leftarrow T_1 + dt$ *▷ Ends as before or when $T_2 \geq T_{target}$ is reached*

      $c_p \leftarrow (c_{p,1} + c_{p,2})/2$

      $\dot{Q}_0 \leftarrow Q + \dot{m}c_p(T_2 - T_1)$

      if $(\dot{Q}_0 \leq \dot{Q}_{final}$ **and** $\dot{Q}_{final} \neq 0)$ **or** $(T_2 \leq T_{target}$ **and** $T_{target} \neq 0)$ **then**

         $\dot{Q}_{out} \leftarrow \dot{Q}_0$ *▷ Now also ensures $T_{out} \leq T_{target}$ for $\dot{Q}_{out}$*

         $T_{out} \leftarrow T_2$

      $T_1 \leftarrow T_2$

   return $[T_{out}, \dot{Q}_{out}]$

4.1.6 Thermodynamic Transfer Properties

The determination of thermodynamic transfer properties constitutes a critical function that enables the aforementioned calculations. Various libraries are available for this purpose, including prominent commercial solutions such as the Reference Fluid Thermodynamic and Transport Properties Database (REFPROP) developed by NIST and the Engineering Equation Solver (EES) by F-Chart Software. While these commercial options provide comprehensive databases, an open-source alternative was selected for this implementation. The methodology, therefore, utilizes the CoolProp thermophysical property library [19]. All fluids in CoolProp use Helmholtz-energy explicit Equations of State (EOS) to calculate thermodynamic properties. In the selection of the library, two fluids were a deciding factor in choosing CoolProp: parahydrogen and helium.

Accurate calculation of fluid transfer properties is essential for the methodology; however, determining appropriate discretization presents a challenge. The process illustrated in Figure 4.3 functions as a structured approach to establishing optimal problem discretization by quantifying the number of discrete points required to achieve the specified precision threshold. Error tolerances can be established at multiple levels: property calculations, temperature determination, heat transfer rates, and mass flow rates. Additionally, the implementation leverages modern computational capabilities through multiprocessing techniques, enabling researchers and designers alike to optimize computational efficiency based on available hardware resources.
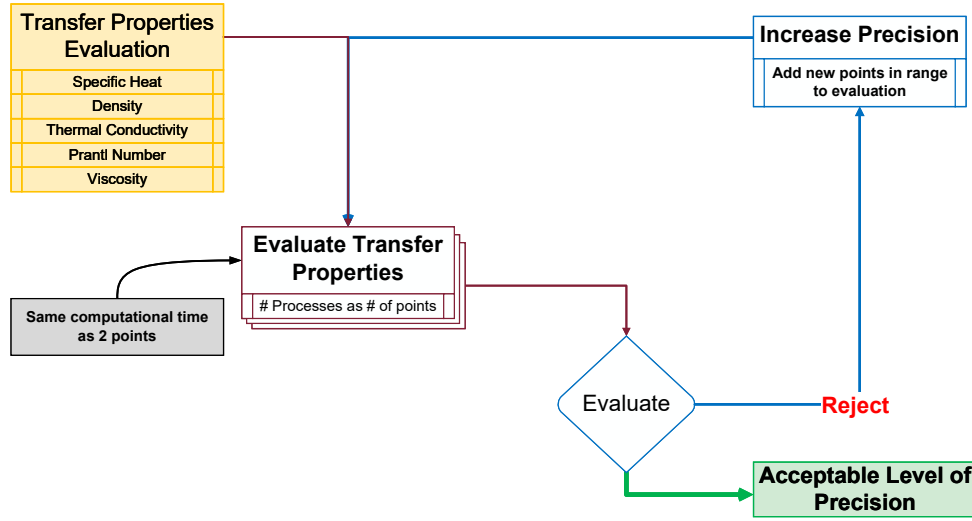
Figure 4.3: Process to determine required discretization.

4.2 Solvers and Optimization

The selection of solvers and optimization algorithms represents a critical consideration in developing a sizing methodology. As discussed in Section 3.2, the sizing process involves an equation system containing linear, non-linear, and discrete equations that requires an appropriate solving technique. Computational frameworks solve equation systems using two principal categories: direct and iterative methods, as illustrated in figure 4.4 [70]. These approaches exhibit fundamental differences in their mathematical foundations, computational efficiency characteristics, and practical applications within engineering contexts.
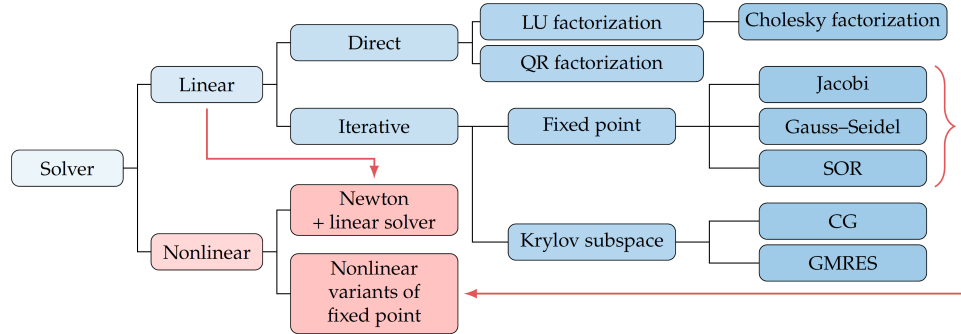
Figure 4.4: Overview of solution methods for linear and nonlinear systems as taken from Martins and Ning [70].

The implementation developed employs the Python programming language, which provides access to numerous solvers and optimization packages. Open-source packages OpenMDAO [67] and Pymoo [68] are selected specifically for their robust computational frameworks and optimization algorithms. OpenMDAO serves as the primary framework for HX sizing processes, while both

OpenMDAO and Pymoo are implemented through a wrapper for optimization tasks. Each framework provides specific advantages for different computational scenarios, enabling the designer to efficiently find solutions to complex thermophysical problems.

4.2.1 Solver Selection

The Python OpenMDAO computational framework offers numerous solver options across both direct and iterative categories. Distinguishing between these options becomes essential for selecting the appropriate solver based on the specific characteristics of the problem under consideration.

Direct solvers produce a final solution at the conclusion of a predetermined process, while iterative solvers begin with an initial approximation and progressively refine it through successive iterations. Although direct solvers come standard in most programming language libraries, they often become computationally prohibitive when dealing with large, sparse systems, making iterative methods the more practical choice.

Iterative approaches offer additional benefits, including efficient balancing of computational resources against solution precision, ensuring more reliable convergence when handling the varying thermophysical properties inherent in cryogenic applications. This flexibility in trading computational cost for precision is particularly valuable in optimization contexts where the model may be solved thousands of times.

Thus, when Newtonian direct solvers prove inadequate, an iterative approach is implemented using the Nonlinear Block Gauss-Seidel (NLBGS) solver for its:

- capacity to efficiently balance computational resources and precision for large systems, thereby enabling appropriate precision levels for each computational task;

- superior convergence rate compared to Jacobi methods through utilization of the most recently calculated values within each iteration, whereas Jacobi methods rely solely on values from previous iterations;

- reduced memory requirements for large systems compared to Newton's method, which necessitates storage of Jacobian matrices, particularly valuable when working with discretized HX models that may have thousands of variables; and

- enhanced convergence performance over Newton's method for systems demonstrating strong diagonal dominance, where each variable's update is predominantly influenced by its corresponding equation with minimal impact from other equations.

4.2.2 OpenMDAO Implementation

The Python OpenMDAO computational framework provides a good platform for HX sizing due to its specialized architecture designed for multidisciplinary analysis and optimization. For the presented HX implementation, OpenMDAO provides:

- a component-based modeling approach that aligns perfectly with the modular nature of HX design, allowing individual physics (heat transfer, fluid flow, pressure drop) to be encapsulated in separate components;

- options for handling both linear and nonlinear systems, crucial for the coupled thermal-hydraulic relationships in HXs; and

- scalable parallel computing[2] for computationally intensive simulations involving complex fluid property calculations.

The NLBGS solver within OpenMDAO is particularly valuable as it can easily incorporate Aitken relaxation, which provides several critical advantages:

- adaptive convergence acceleration that dynamically adjusts relaxation factors during iterations, significantly improving convergence rates for the temperature-dependent fluid property calculations common in HX design;

- robust performance when dealing with the highly nonlinear behavior of cryogenic fluids, where property variations with temperature can be extreme; and

- enhanced stability for systems with strong coupling between heat transfer and pressure drop calculations, preventing oscillatory behavior that often occurs in fixed-step methods.

Furthermore, the described implementation allows the HX sizing methodology to reliably converge even when dealing with challenging conditions such as phase changes, wide temperature ranges, and varying thermophysical properties across the HX domain.

4.2.3 Optimization Implementation

The optimization methodology requires careful algorithm selection to address computational challenges. For HX design specifically, algorithms must be strategically chosen to balance convergence speed, solution diversity, and overall performance. Therefore, a genetic algorithm is selected as the optimization approach.

Genetic algorithms represent an effective optimization strategy for HX design as they excel at exploring complex multi-modal design spaces without requiring gradient information. These types of problems typically involve multiple competing objectives, for example, minimizing pressure drop while maximizing heat transfer, numerous constraints, and discrete variables, including fin configurations or tube arrangements.

Genetic algorithms can efficiently navigate these complex design spaces by working with populations of potential solutions that evolve through selection, crossover, and mutation operations. They are particularly valuable when the design space contains discontinuities or when analytical derivatives are unavailable. The population-based approach also allows genetic algorithms to identify multiple near-optimal solutions in a single optimization run, giving designers a range of viable options to consider based on manufacturing constraints or other practical considerations that may be difficult to formulate mathematically.

Two frameworks for evolutionary optimization are used:

(1) OpenMDAO's SimpleGADriver provides a natural baseline for comparison since OpenMDAO is already utilized for iterative solving capabilities and is readily available.

(2) Pymoo, with its PyMOODE extension, offers multi-objective optimization capabilities through specialized algorithms, specifically designed for exploring and maintaining diverse Pareto-optimal solutions in complex non-linear design spaces.

---

[2]While OpenMDAO supports scalable parallel computing, this functionality presents implementation challenges for Windows users due to its Linux-oriented design. Consequently, there is a steep learning curve to effectively utilize and implement this feature across different systems.

When comparing the genetic algorithm implementations in OpenMDAO and Pymoo with Py-MOODE extensions, several key differences emerge in their approach.

Algorithm Architecture

OpenMDAO's SimpleGADriver implements a simplified genetic algorithm using binary encoding with configurable bit resolution for continuous variables, treating unspecified variables as integers by default. While offering straightforward implementation, it primarily focuses on single-objective optimization with limited multi-objective capabilities through weighted aggregation or Pareto front approximation.

In contrast, Pymoo with PyMOODE provides a comprehensive, modular framework designed explicitly for multi-objective optimization, implementing mixed-variable handling natively (supporting continuous, integer, binary, and categorical variables simultaneously), and featuring specialized algorithms for many-objective problems (more than three objectives). The PyMOODE extension enhances Pymoo with advanced diversity preservation through its M-Nearest Neighbors (MNN) rank and crowding survival strategy [71].

Selection and Survival Strategies

OpenMDAO's SimpleGADriver implements basic tournament selection with minimal elitism preservation, offers limited multi-objective capabilities through its "compute_pareto" option, and relies on fixed penalty parameters for constraint handling.

On the other hand, Pymoo with PyMOODE MNN delivers a Pareto-based ranking system with specialized crowding metrics that calculate distances to multiple neighbors rather than just adjacent solutions. This approach demonstrates particular efficacy for many-objective problems where traditional crowding distance metrics become ineffective, significantly enhances diversity preservation in high-dimensional objective spaces, and provides advanced constraint handling mechanisms specifically optimized for multi-objective problems [71]. These distinctions directly influence algorithm performance in the complex, non-linear design spaces characteristic of HX optimization problems, where maintaining solution diversity becomes critical for identifying truly optimal designs.

Performance and Scaling Characteristics

OpenMDAO's SimpleGADriver offers integration advantages through straightforward parallelization via the "run_parallel" option, distributed evaluation capabilities with the "procs_per_model" parameter, population sizing heuristics, and seamless integration with OpenMDAO's multidisciplinary analysis framework.

Conversely, Pymoo with PyMOODE MNN implementation provides computational advantages through advanced genetic operators optimized for performance, albeit with algorithmic complexity of $O(M \times N^2)$ where N represents population size and M denotes objective count. The framework's multiple crowding implementation variants offer different performance characteristics for specific problem classes. Its specialized algorithms for large-scale problems enhance efficiency when dealing with extensive design spaces characteristic of complex heat exchanger optimization scenarios. Additionally, Pymoo also provides efficient multiprocessing capabilities through its parallelization interface.

Algorithm Selection Considerations

OpenMDAO's SimpleGADriver demonstrates superior performance for integration-focused scenarios with computationally expensive models, particularly within existing OpenMDAO workflows addressing single-objective or simplified multi-objective problems.

By comparison, Pymoo with PyMOODE MNN extension exhibits enhanced capabilities for complex multi-objective and many-objective optimization scenarios, especially those involving high-dimensional objective spaces requiring specialized diversity preservation, advanced visualization tools, detailed algorithm behavior analysis, and heterogeneous variable types.

4.3 Summary

In summary, by leveraging existing temperature and heat transfer logic, the algorithm eliminates redundant code while accommodating both heating and cooling scenarios through appropriate sign conventions. The functional implementation demonstrates robust handling of thermodynamic complexities, including phase changes and varying thermophysical properties, which is particularly crucial for cryogenic applications. Furthermore, the algorithm incorporates essential physical constraints that prevent computationally possible but physically impossible flow conditions. Through the strategic implementation of three fundamental functions (temperature calculation, heat transfer rate determination, and mass flow calculation), the methodology establishes a comprehensive framework for heat exchanger flow scoping applicable across conventional and cryogenic TMSs, thereby addressing the computational challenges highlighted in the preceding discussion of solver selection and optimization frameworks.

In addition, the implementation combines OpenMDAO's robust iterative solving capabilities with Pymoo's advanced genetic optimization algorithms to create an effective framework for heat exchanger design. The OpenMDAO component leverages the NLBGS solver with Aitken relaxation to efficiently handle the coupled thermal-hydraulic calculations inherent in heat exchanger sizing. This iterative approach provides superior stability and convergence characteristics when dealing with the highly nonlinear behavior of cryogenic fluids. Complementing this, the Pymoo framework with PyMOODE MNN extension delivers sophisticated multi-objective optimization capabilities through its specialized genetic algorithm implementation. The PyMOODE MNN approach enhances diversity preservation in high-dimensional objective spaces by calculating distances to multiple neighbors rather than just adjacent solutions, making it particularly effective for complex heat exchanger optimization problems with competing objectives such as minimizing pressure drop while maximizing heat transfer. This hybrid implementation balances computational efficiency with solution quality, enabling comprehensive exploration of the design space to identify optimal heat exchanger configurations for advanced aircraft TMSs.

Chapter 5

Validation

T HIS section presents a validation of the HX sizing methodology through comparative analysis against two distinct reference cases. The validation approach employs multiple benchmarks to demonstrate the model's versatility across conventional and cryogenic applications. The first validation case examines a Bell & Gossett brazed plate HX operating under standard conditions, while the second investigates a 2 K helium HX designed for extreme cryogenic environments. These cases establish the robustness of the methodology across diverse operating regimes and provide a quantitative assessment of the algorithm's accuracy in predicting HX performance. The validation process incorporates both dimensional analysis and performance metrics to verify the computational approach against established industry standards and published research.

5.1   Bell & Gossett Brazed Heat Exchanger

The first validation study for the HX sizing model is done through comparative analysis against the Bell & Gossett BP400-40 HX, utilizing specifications obtained from manufacturer documentation presented in table 5.1. The BP400-40 is selected as a validation example due to its industry-standard design parameters and comprehensive documentation from a reputable manufacturer with established expertise in hydronic systems.

Although the HX is well documented, certain critical parameters, such as the chevron specifications, are unavailable in the manufacturer's documentation. However, through analysis of multiple photographic references of the HX , it was possible to estimate these values with reasonable accuracy.

The parameters, serving as input variables for validation, and their assumptions are summarized in Table 5.2. Figure 5.2 demonstrates the successful positioning of the Bell & Gossett BP400-40 within the design space, denoted by a green indicator line and a red dot marking the closest found result. The chevron angle parameter varies from 10° to 80° in the analysis. This methodological approach addresses the inherent challenges in the precise determination of critical HX properties, particularly chevron angle and hydraulic diameter.

Table 5.1: Bell & Gosset HX specifications.

BP400-40 (3/4" MPT)	
Heat Transfer Rate	
BTU/Hr	kW
350000	103
Design Pressure	
PSI	bar
435	30
Weight	
Lbs	kg
6.7	3.04
Surface Area	
ft^2	m^2
5.2	0.483
Length	
in	mm
6.77	172

Boiler Side							
Flow		Pressure Drop		Supply Temperature		Return Temperature	
GPM	kg/s	PSI	kPa	$°F$	K	$°F$	K
14.4	0.909	3.4	23.4	180	355	130	328

Domestic Water Side							
Flow		Pressure Drop		Supply Temperature		Return Temperature	
GPM	kg/s	PSI	kPa	$°F$	K	$°F$	K
7.8	0.492	1	6.9	50	283	140	333

Figure 5.1: Image of Bell & Gossett BP400 heat exchanger [72].

Table 5.2: Input parameters and assumptions.

Inputs	Assumptions	Units
$d_{h,cold}$	$2 \rightarrow 4$	mm
β	$10 \rightarrow 80$	$degrees$
$flow$	$counterflow$	
σ	0.8	
η_0	0.8	
j_{factor}	0.25	
ρ_{wall}	7.97	g/cm^3

The cold side hydraulic diameter serves as a primary input parameter and has a large influence on the three validation metrics: length, heat transfer surface area, and weight. Operating conditions include a design pressure of 30 bar, with pressure losses conforming to domestic heating specifications. The visually determined chevron angle was estimated at approximately 70°, which aligns with the results shown in figure 5.2. In the same vein, figure 5.3 shows the objective space, with
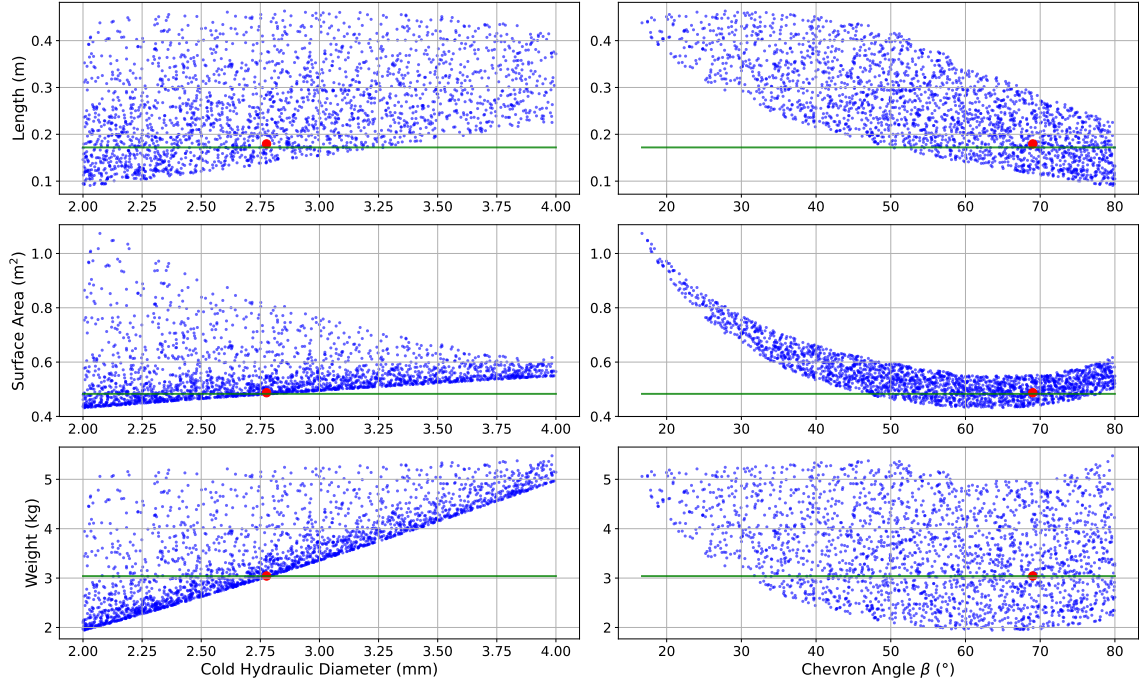
Figure 5.2: Design space for the Design of Experiments (DOE) analysis conducted on the Bell & Gossett BP400-40 HX specifications for validation. A total of 2160 points are used.

the actual validation case dimensions displayed in green and the nearest computed value shown in red—the two nearly overlap. Although exact replication of the reference case was not the primary goal of this DOE, the results confirm that the solution falls within the defined objective space, thereby validating the methodology.

5.2 2 K Helium Heat Exchanger

Building upon the Bell & Gossett brazed HX validation, a secondary validation case addresses cryogenic HX applications through analysis of a 2 K helium PFHE based on the work by Zhu et al. [54]. This validation examines an advanced superconducting accelerator component operating with a helium flow rate between 5 and 12.5 g/s. The reference study employed a distributed parameter method for design calculations, which divided the HX into small segments to accurately model temperature and pressure variations at cryogenic conditions. The researchers utilized the NSGA-II optimization algorithm to generate Pareto front solutions targeting optimal outlet temperature and pressure drop performance.

Their experimental results validated the computational approach, showing outlet temperatures within 6% of design calculations and achieving 82.4% heat transfer efficiency. This case study provides an excellent validation benchmark for cryogenic applications where helium's large property variations at extreme low temperatures present unique thermal management challenges.

Due to the differences in methodologies, adjustments were necessary, beginning with the search parameters highlighted in table 5.3. The implementation, as discussed in Section 3.2.3, primarily uses the non-dimensional parameters α_{fin}, δ_{fin}, and γ_{fin} as defined in table 3.1. Consequently, the
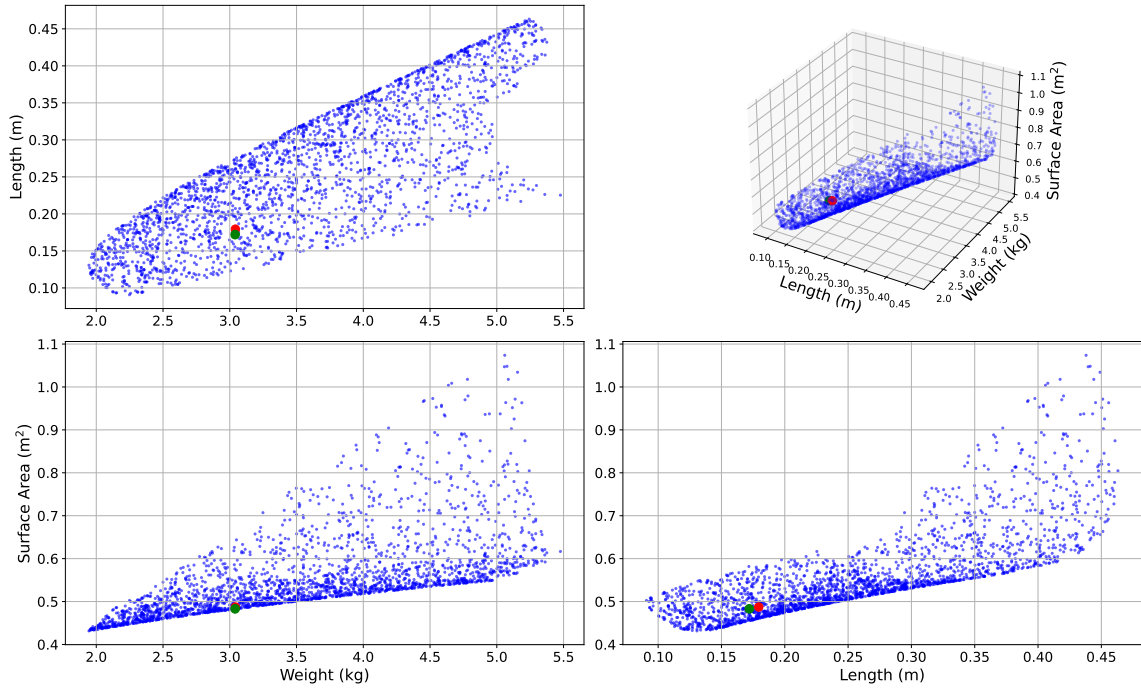
Figure 5.3: Objective space for the DOE analysis conducted on the Bell & Gossett BP400-40 HX specifications for validation.

given parameters were first converted into their non-dimensional equivalents, shown in table 5.4, and then applied as constraints.

For the helium properties at extremely low temperatures, specialized functions were required. Missing data points from CoolProp were interpolated from graphs provided in [54] since the original data was not openly available. Aluminum material properties were obtained from NIST standardized equations [73].

In reality, the design space for the discussed implementation is broader since it aims to identify the most optimal design rather than working with a specific PFHE cross-section. This approach aligns with the aerospace industry's philosophy of designing HX s for specific requirements, as discussed in Section 2.2.

Table 5.3: Validation case search parameters [54].

Inputs	
Variable	**Range**
Fin thickness (t_f)	0.4 mm
Mass flow ($\dot{m}$)	5 to 12.5 g/s
Cold Pressure (P_c)	3.1 kPa
Hot Pressure (P_h)	300 kPa
Constraints	
Variable	**Range**
Cold pressure loss (ΔP_c)	$\leq$250 kPa
Hot pressure loss (ΔP_c)	$\leq$4000 kPa
Fin height (b)	2 to 10 mm
Fin space (s)	2 to 20 mm
Hot channel layers	1 to 20
Heat exchanger flow width	100 to 500 mm
Length (L)	0.1 to 1.5 m

Table 5.4: Converted search parameters for discussed methodology.

Inputs		
Variable	**Range**	**Equation**
α_{fin}	0.05 to 15	s/h
δ_{fin}	$2e-4$ to $4.5e-4$	t_{fin}/l
γ_{fin}	0.001 to 0.5	t_{fin}/s

For validation, the implementation necessitates ten distinct constraints for the parameters highlighted in table 5.3. The identification of an exact solution with a 0.4 mm fin thickness requires preliminary calculations based on the dimensionless parameters. To initialize the algorithm efficiently, the fin thickness (t_f), length[1] (L), fin height (h), and fin spacing (s) parameters are calculated according to the equations in table 5.4 and subsequently utilized to determine the hydraulic diameter (d_h) according to equation (34).

Figure 5.4 displays the validation results. The slight difference in Pareto front trends may be attributed to the fact that their results were extracted from a figure rather than raw data and the unknown baseline surface effectiveness (η_0). Additionally, the thesis methodology employs correlations specific to plain rectangular fins, whereas the validation case utilizes perforated rectangular fins; therefore, a 20% penalty is applied to the calculation of the friction factors as suggested by [33].

In order to truly compare the results, the selected HX by the case study was calculated using the sizing tool. The results showed that for the same HX size, the tool obtains 28.7 Pa of pressure drop compared to the 26.7 Pa from the validation case, which amounts to an error percentage of 7.5%.

Table 5.5: 2K validation case selected point comparison.

	Results Obtained	**Validation Case**	**Units**	**Error (%)**
Fin height (h)	4.5	4.5	mm	-
Fin spacing (s)	8.5	8.5	mm	-
Width (w)	146.5	147	mm	0.34
Length (L)	470	470	mm	-
Pressure loss (P)	24.9	26.7	Pa	6.7
Hot temperature out (T_h)	2.85	2.85	K	-

---

[1]In equation (34) the symbol for length is l, which is the fin length for the OSFs. In this case, there is only a single strip, hence the length of the HX (L) is used.
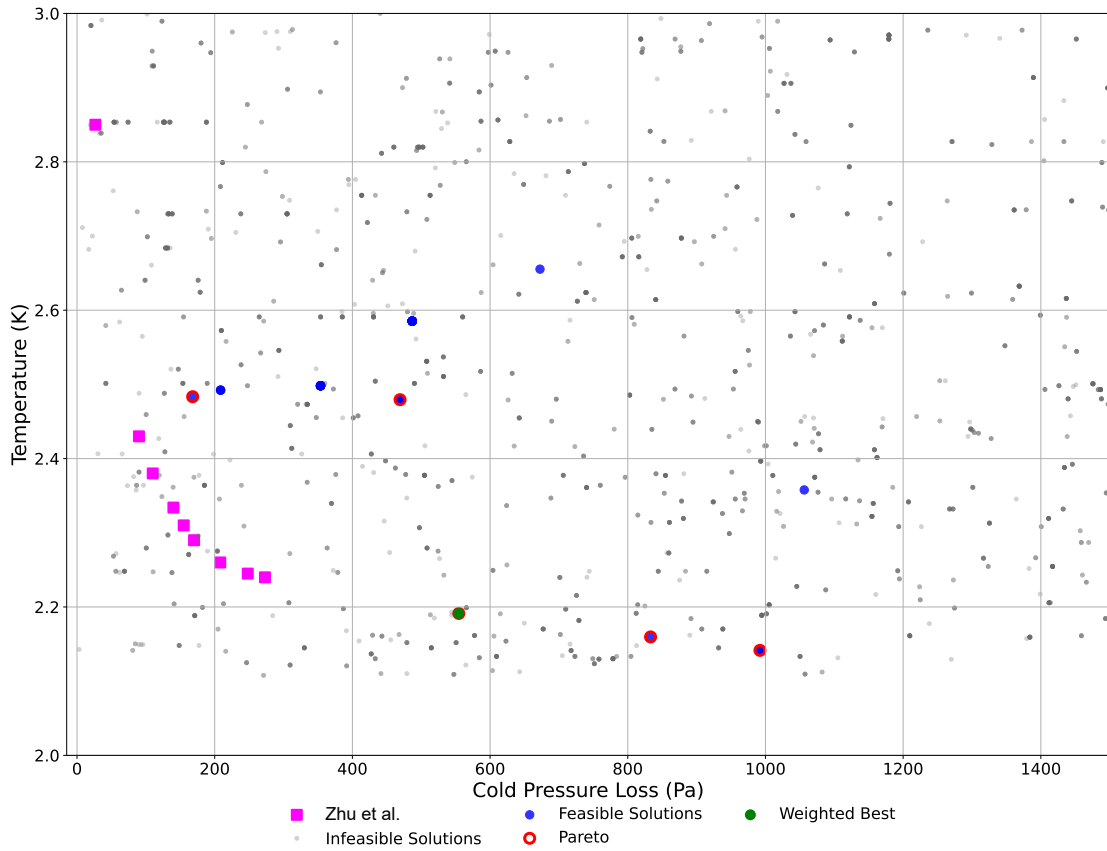
Figure 5.4: Cryogenic PFHE validation results with comparison to Zhu et al. [54].

It is necessary to acknowledge that the divergence between the two methodologies stems partially from the absence of banking factor and layering effects in the current methodology, stemming from differences in their intended applications. While the validation methodology aims to closely approximate exact results for a specific design, the implemented approach focuses on preliminary design assessment.

The methodology is designed for aircraft scoping applications, prioritizing early design feasibility assessment over detailed engineering specifications. Consequently, the algorithm generates conservative results that provide a reliable foundation for subsequent detailed engineering analysis.

5.3 Conclusion

The experimental results demonstrate the efficacy of the developed methodology, validating its capacity to accurately model and optimize HX performance across diverse operating conditions. The validation studies indicate that the computational approach successfully predicts thermal-hydraulic behavior in both conventional and cryogenic applications with notable precision. For the Bell & Gossett validation case, the methodology accurately positions the commercial HX within the predicted design space, confirming the robustness of the dimensional analysis approach. Similarly, for the 2 K helium HX validation, the methodology demonstrates convergence to solutions comparable to those reported in the literature, with performance metrics having less than 6.7% error. These

validation outcomes provide evidence that the developed approach offers reliable predictive capabilities for HX design optimization across conventional temperature regimes and extreme cryogenic conditions. The methodology's ability to accommodate large property variations at low temperatures while maintaining computational stability represents an advancement in thermal management system design for next-generation aerospace applications.

Chapter 6

Fuel Cell Propulsion System Case Studies

T HIS chapter applies the HX sizing methodology and computational tool developed in previous chapters to conceptual case studies relevant to novel aircraft propulsion systems. The case studies selected demonstrate the practical application and versatility of the parametric sizing approach across different operational scenarios and design requirements.

The chapter examines multiple applications with varying thermal loads, fluid properties, and design constraints. Each case study follows a structured approach: first defining the specific thermal management challenge, then applying the parametric sizing methodology to develop potential solutions, and finally analyzing the results to extract design insights.

The case studies specifically address critical thermal interfaces in electric and hydrogen-based propulsion architectures, including:

- Cryogenic HX applications for liquid hydrogen fuel systems.

- Thermal management solutions for fuel cell exhaust heat recovery.

- Integration challenges in hybrid-electric propulsion thermal systems.

- Comparative analysis of different HX geometries for specific aircraft applications.

Through these examples, the chapter illustrates how the developed methodology addresses the key challenges identified in the literature review, particularly those related to variable material properties at cryogenic temperatures, design parameter sensitivity, and integration with broader aircraft TMS. The case studies provide valuable insights for aerospace engineers and system designers working on novel propulsion architectures, while demonstrating the practical utility of the developed computational tool in early-stage aircraft design.

The analysis begins with an overview of design parameters, assumptions, and the cryogenic propulsion thermal management architecture derived from the Hartmann et al. [14] case and established component temperature requirements, followed by an evaluation of the H_2 fuel heating pathway. Subsequently, the analysis concludes with HX sizing calculations that conform to business jet aircraft dimensional constraints.

6.1 Overview

The TMS sizing investigation considers a business jet aircraft with a maximum power requirement specification of 7.6 MW [74], corresponding to performance characteristics similar to those of the Bombardier Challenger 300 aircraft [75], as shown in table 6.1.

Table 6.1: Case study inputs and assumptions.

Aircraft Performance	
Propulsion System	
Engine	Honeywell HTF 7000
Power	$7.6\ MW$
Takeoff Thrust	$30.9\ kN$
Max Airspeed	$476\ knots$

The architecture under investigation, shown in figure 6.1 and highlighted earlier in figure 1.7, consists of a PEMFC, HTSC, a DC/AC converter, a SCM, a gearbox, and a propeller. Component losses are treated as heat losses and are calculated using equation (37), where $P_{downstream}$ represents the power required downstream from each component and η denotes the component efficiency.

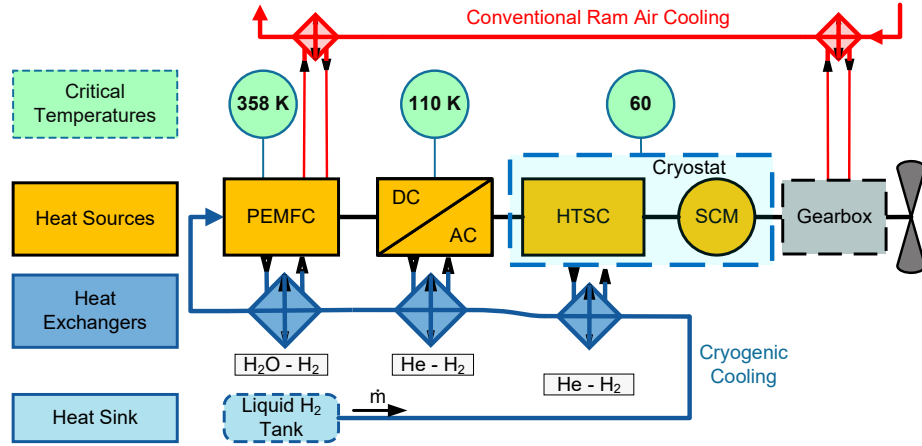$$\dot{Q} = P_{downstream}\left(\frac{1}{\eta} - 1\right) \tag{37}$$

Figure 6.1: H_2 heating path and component critical temperatures.

The propulsion system efficiencies derive from established ranges as documented by Hartmann et al. [14] and presented in table 6.2. A significant architectural modification in the case study involves the elimination of the DC/DC converter in favor of a single DC/AC converter implementation. This modification enhances system efficiency through reduced weight, decreased complexity, and optimized component spacing. Quantitative analysis of the system, considering the maximum power requirement of 7.6 MW, the established component efficiencies, and the reaction losses, indicates that the total required H_2 energy amounts to 21.6 MW. Therefore, the mass flow calculations for H_2 are based on this number.

Table 6.2: Component efficiencies at maximum power.

Component Efficiencies				
PEMFC	HTSC	DC/AC Converter	SCM	Gearbox
40%	99.95%	99%	99%	99%
Component Heat Loss				
11.7 MW	3.9 kW	78.3 kW	77.5 kW	77 kW

Figure 6.2 presents the distribution of heat losses across components based on their respective efficiencies. As the FC's cooling requirements exceed the H_2's cooling capacity, and the H_2 cooling potential is dependent on fluid properties and operating conditions, it is necessary to specify the initial H_2 storage conditions before determining the total H_2 heating required. The system requires thermal energy to elevate the H_2 temperature to the FC inlet condition of 358K, while excess thermal energy transfers to a conventional ram air HX along with the gearbox heat losses.
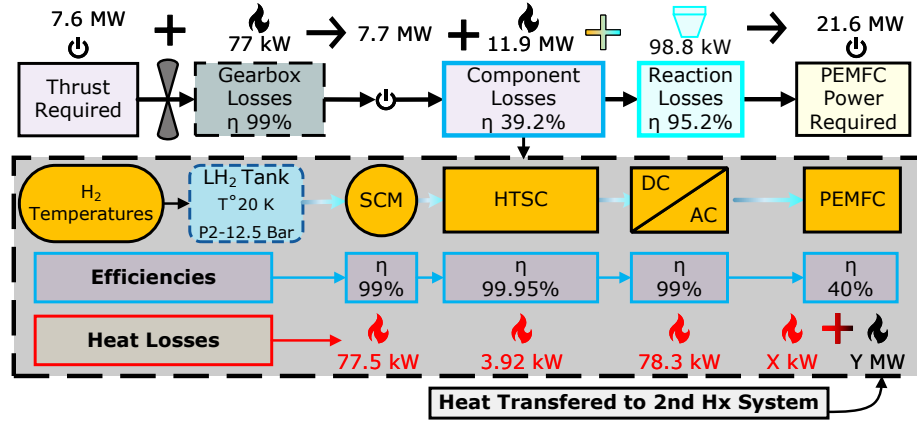

Figure 6.2: Superconducting propulsion system heat loss summary.

6.2 Hydrogen Heating Path

The utilization of H_2 fuel as a cryogenic coolant requires careful consideration of the fluid's thermal pathway in relation to the critical temperature thresholds of each propulsion system component, as illustrated in figure 6.1. The heat transfer sequence starts at the SCM and HTSC cryostat, then the DC/AC converter, and concludes at the PEMFC, thereby achieving the requisite reaction temperature and pressure for optimal system performance. Given the high variability of H_2 properties at cryogenic temperatures in both the liquid and gaseous states, a fuel heating curve must be calculated for each set of conditions inside the tank. Figure 6.3 presents four cases examining tank temperatures of 20 K across pressures ranging from 1.5 to 20 bar. The analysis demonstrates that latent heat decreases at higher pressures due to proximity to H_2's critical pressure point of 12.9 bar. While the constant-temperature characteristic of latent heat during phase change offers advantages in HX size reduction through two-phase fluid behavior, system-level benefits may favor higher pressures to utilize expansion cooling potential. This study implements an isothermal expansion device to focus on demonstrating the need for parametric sizing models for TMS rather than expansion device optimization.
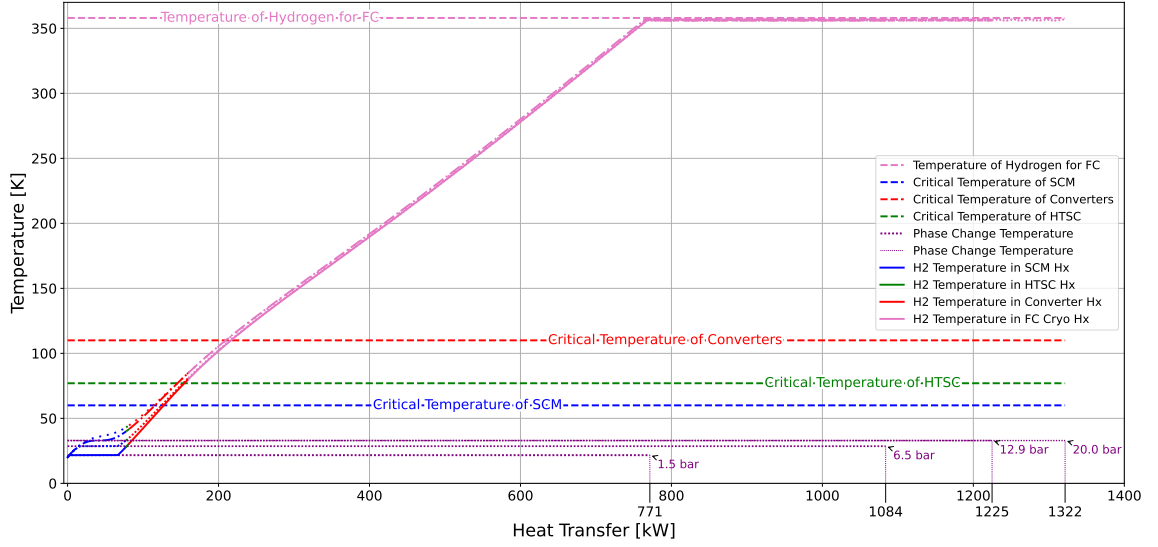
Figure 6.3: H_2 heating curve for pressures of 1.5 bar, 6.5 bar, and 12.9 bar.

The H_2 heating curve analysis presented in figure 6.3 neglects pressure losses across HXs. This simplified analysis demonstrates the critical significance of heating path characterization and validates the necessity of parametric sizing tools in accurately modeling these TMS. While this idealization facilitates initial system characterization, practical applications necessitate incorporating these losses to achieve sufficiently accurate performance predictions.

6.3 Heat Exchanger Sizing

The investigation employs a multi-objective optimization framework across the HX network to simultaneously minimize system mass, Helium (He)-side inlet pressure, and H_2-side pressure losses. Table 6.3 presents the common initial assumptions employed in this analysis. Additionally, to keep the focus on the HXs, all the pumps, lines, and expansion devices are modeled with no losses.

Table 6.3: Case study input parameters and assumptions.

Input Parameter	Assumption	Units
$d_{h,cold}$	$2 \rightarrow 8$	mm
β	$10 \rightarrow 80$	$degrees$
$Stacks$	$1 \rightarrow 250$	
$flow$	$counterflow$	
σ	0.8	
η_0	0.8	
j_{factor}	0.25	
ρ_{wall}	2.7	g/cm^3

6.3.1 Powertrain Interfacing Heat Exchanger

The first sizing process addresses specific requirements for the SCM and HTSC cryostat environment. Figure 6.4 presents the interfacing components and corresponding sizing specifications. The hot side operates on a dependent cryogenic loop, with specifications provided by the electric motor design team from the EPA project. The hot side working fluid, mass flow rate, outlet conditions, and inlet temperature are fixed parameters, while the inlet pressure serves as a design variable. The cold-side operating conditions are governed by the initial storage conditions for fluid temperature, with an ideal pump facilitating the required pressure increase. The H_2 mass flow rate is fixed according to the PEMFC's maximum power demand. The design space encompasses six more design variables: H_2 inlet pressure, hydraulic diameter, number of plates, pressure loss ratios for both fluid streams, and chevron angle.
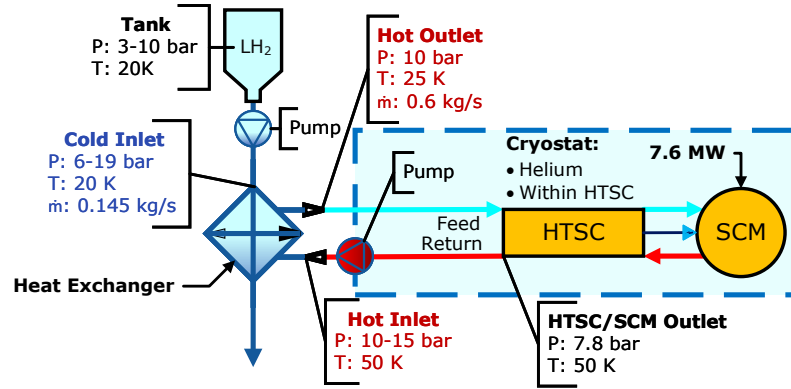

Figure 6.4: SCM & HTSC HX sizing details.

6.3.2 Electric Converter Heat Exchanger

The second sizing process is shown in figure 6.5 and focuses on the cryogenic electric converter. In the absence of a dedicated design team providing hot side flow requirements, the component's critical temperature is used to determine the hot inlet temperature. Additionally, the same working fluid and a similar inlet pressure range are used, given the similarity in heat transfer rates between the first and second HXs. The cold side fluid properties are determined by the outlet conditions of the previous HX, while the mass flow rate remains constant. Likewise, the model employs the hydraulic diameter, number of plates, pressure loss ratios for both fluid streams, and chevron angle as design variables.
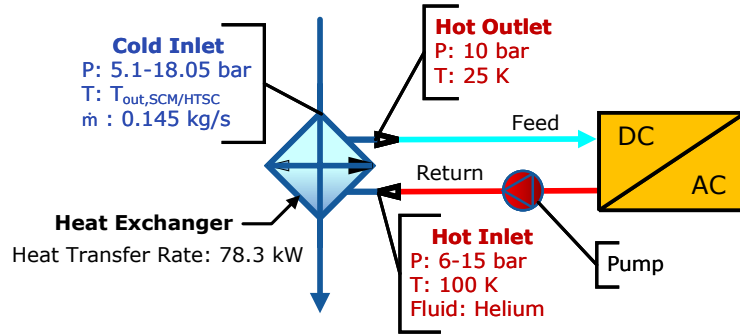
Figure 6.5: Superconducting DC/AC converter HX sizing details.

6.3.3 Fuel Cell Heat Exchangers

The third sizing process, depicted in figure 6.6, analyzes H_2 heating requirements to achieve PEMFC inlet specifications. The HX employs the FC coolant stream, in this case water, as the hot-side working fluid to demonstrate the methodology's constraints. Hot-side inlet properties are governed by FC operating parameters. The cold-side thermal analysis adheres to previous HX methodologies while incorporating an additional outlet temperature constraint specification.
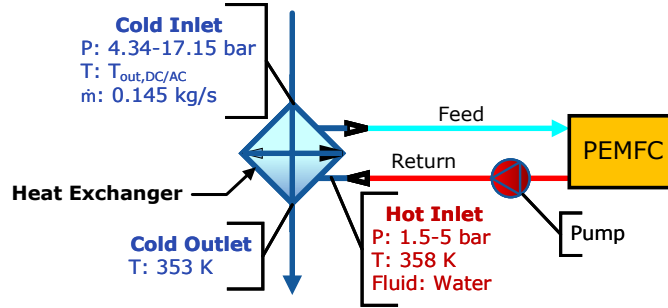

Figure 6.6: First FC HX sizing details.

Recalling the conclusions from Figure 6.3 and running some sensitivity analyses, it is found that the H_2 inlet pressure exceeds the FC operating requirements when initial pressures are sufficiently above the FC working pressure, necessitating an expansion process, which, for simplicity, is assumed to be under ideal conditions (a reversible and adiabatic process). Therefore, the system architecture requires both an expansion device and a supplementary FC HX to achieve optimal operating conditions.

The H_2 undergoes cooling through an isentropic expansion process, characteristic of various expansion devices (which can function as power generators). A fourth HX sizing process, operating under conditions similar to the first FC exchanger, incorporates two modifications: (1) the expansion device reduces gas pressure to 2 bars which will be take as the inlet pressure; and (2) the HX pressure loss accounts for the differential at the specified sizing point bringing the final pressure to the desired value. Figure 6.7 graphically shows the assumptions, while table 6.4 presents a comprehensive summary of these assumptions.
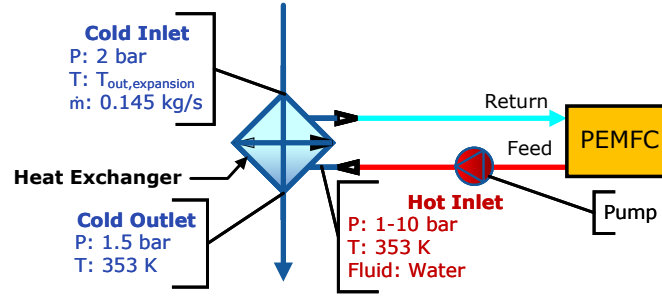
Figure 6.7: Second FC HX sizing details.

6.4 Discussion and Results

As demonstrated in Section 6.3, the analysis requires three distinct input sets to determine a solution for the fuel TMS design problem. The framework development necessitated at least one of the following variables for HX sizing: heat transfer rate ($\dot{Q}$), cold-side outlet temperature (T_{co}), or hot-side outlet temperature (T_{ho}). The analysis reveals that utilizing only $\dot{Q}$ generates the largest design space, presenting both advantages and challenges for optimization potential while increasing computational requirements.

The optimization configuration was initialized with a population size of 480 individuals using the Latin hypercube sampling method. Each subsequent generation was of a smaller population size of 120 individuals, and a period of 5 generations was used to calculate and compare the following tolerances: $xtol = 1e^{-3}$, $cvtol = 1e^{-4}$, $ftol = 0.01$.

Figure 6.8 presents the Pareto-optimal solutions, highlighted by blue dots circled in red, as the blue dots alone represent the feasible solutions. The final design point selection employs a pseudo-weight vector approach from [76], prioritizing the minimization of system weight, followed by starting pressure, and finally system pressure losses. The selected point is located in the bottom left quadrant and represented by a green dot over a red Pareto-optimal point. In this case, the solution has a total weight of 6.6 kg, a total pressure loss of 338.9 kPa, and a starting pressure of 13.7 bar. It is also important to note that the results shown have been truncated to the area of interest in terms of weight ($\leq$50 kg), with all those outside of the region not displayed.

Despite utilizing high-performance computing resources, the computational analysis requires around 20 minutes of processing time due to its iterative nature, potential absence of solutions within given constraints, and convergence challenges near boundary conditions. While designers can mitigate these computational demands by constraining the design space prior to analysis, the framework implementation prioritizes accessibility by enabling comprehensive design feasibility evaluation, particularly beneficial for designers with varying levels of expertise.

Analysis of the fuel heating path reveals comparative results across three scenarios presented in figure 6.9: ideal HXs without pressure losses and ideal expansion, non-ideal HXs incorporating pressure losses with ideal expansion, and HXs with pressure losses and single-stage expansion. The experimental data demonstrate that pressure losses diminish the LH$_2$'s cooling potential by 60 kW, while the implementation of single-stage expansion further reduces this capacity by 38 kW, resulting in a cumulative reduction of approximately 100 kW. These findings indicate that idealized assumptions may overestimate the system's cooling potential by as much as 10%.

54

Table 6.4: Case study HX specifications.

Sizing for Maximum Power Conditions at 7.6 MW						
Superconducting Motor and High Temperature Superconducting Cables Heat Exchanger						
Critical Temperature	60 K					
Heat Transfer Rate	78.6 kW					
Cold Side						
Fluid	Flow	Inlet Pressure	Pressure Drop	Outlet Pressure	Inlet Temperature	Outlet Temperature
	kg/s	bar	$\%InletPressure$	bar	K	K
$Hydrogen$	0.145	$6 \rightarrow 19$	$5 \rightarrow 15$	$5.1 \rightarrow 18.05$	20	$-$
Hot Side						
Fluid	Flow	Inlet Pressure	Pressure Drop	Outlet Pressure	Inlet Temperature	Outlet Temperature
	kg/s	bar	$\%InletPressure$	bar	K	K
$Helium$	0.6	$10 \rightarrow 15$	$5 \rightarrow 15$	10	50	25
DC/AC Converter Heat Exchanger						
Critical Temperature	110 K					
Heat Transfer Rate	78.3 kW					
Cold Side						
Fluid	Flow	Inlet Pressure	Pressure Drop	Outlet Pressure	Inlet Temperature	Outlet Temperature
	kg/s	bar	$\%InletPressure$	bar	K	K
$Hydrogen$	0.145	$5.1 \rightarrow 18.05$	$5 \rightarrow 15$	$4.34 \rightarrow 17.15$	*from SCM/HTSC Hx*	$30 \rightarrow 90$
Hot Side						
Fluid	Flow	Inlet Pressure	Pressure Drop	Outlet Pressure	Inlet Temperature	Outlet Temperature
	kg/s	bar	$\%InletPressure$	bar	K	K
$Helium$	$-$	$6 \rightarrow 15$	$5 \rightarrow 15$	$-$	100	$30 \rightarrow 75$
First Fuel Cell Heat Exchanger						
Fuel Cell Operating Temperature	358 K					
Fuel Cell Operating Pressure	1.5 bar					
Heat Transfer Rate	$-$					
Cold Side						
Fluid	Flow	Inlet Pressure	Pressure Drop	Outlet Pressure	Inlet Temperature	Outlet Temperature
	kg/s	bar	$\%InletPressure$	bar	K	K
$Hydrogen$	0.145	$4.34 \rightarrow 17.15$	$5 \rightarrow 15$	$3.7 \rightarrow 16.3$	*from DC/AC Hx*	353
Hot Side						
Fluid	Flow	Inlet Pressure	Pressure Drop	Outlet Pressure	Inlet Temperature	Outlet Temperature
	kg/s	bar	$\%InletPressure$	bar	K	K
$Water$	1.24	$1 \rightarrow 3$	$5 \rightarrow 15$	$-$	358	$-$
Second Fuel Cell Heat Exchanger						
Fuel Cell Operating Temperature	358 K					
Fuel Cell Operating Pressure	1.5 bar					
Heat Transfer Rate	$-$					
Cold Side						
Fluid	Flow	Inlet Pressure	Pressure Drop	Outlet Pressure	Inlet Temperature	Outlet Temperature
	kg/s	bar	bar	bar	K	K
$Hydrogen$	0.145	2	0.5	1.5	*from expansion*	348
Hot Side						
Fluid	Flow	Inlet Pressure	Pressure Drop	Outlet Pressure	Inlet Temperature	Outlet Temperature
	kg/s	bar	$\%InletPressure$	bar	K	K
$Water$	$-$	$1 \rightarrow 10$	$5 \rightarrow 15$	$0.85 \rightarrow 9.5$	353	$273.15 \rightarrow 350$

The analysis reveals that actual heat availability, while lower than theoretical predictions, remains sufficient for H_2 heating requirements. Furthermore, the analysis demonstrates that HX sizing is primarily constrained by volumetric rather than mass considerations, aligning with previous research on plate-fin HXs and microchannel HXs.
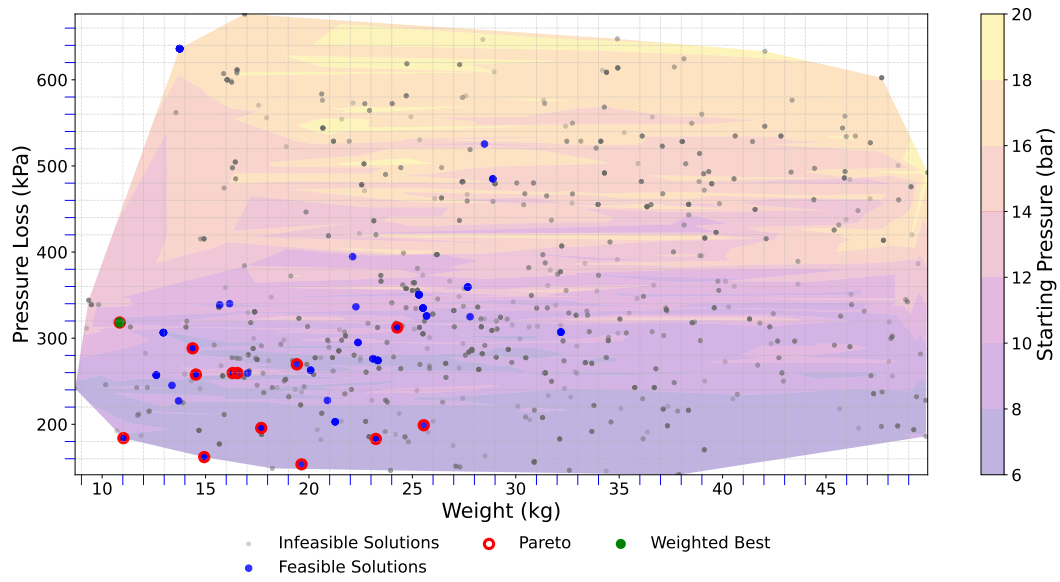
Figure 6.8: Case study sizing results showing the objective space for the pressure loss, weight, and system inlet pressure.
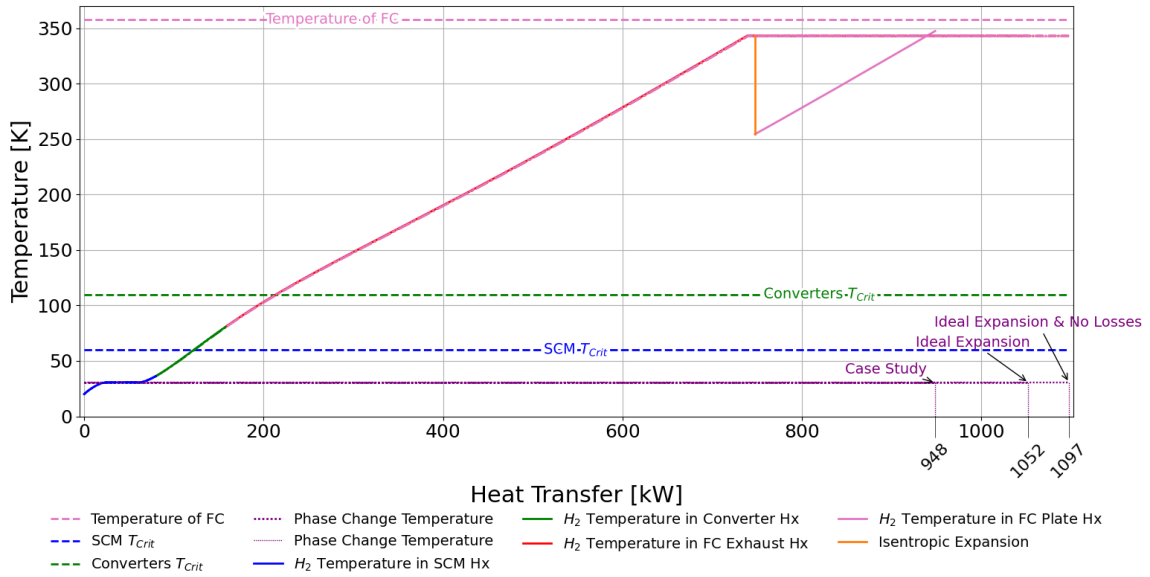

Figure 6.9: Case study fuel heating path comparing ideal expansion with and without pressure losses to single stage expansion with pressure loss.

6.5   Multidisciplinary Design Analysis and Optimization

The MDAO framework is implemented using Remote Component Environment (RCE) [77], an open source application that integrates disciplinary tools to define dependencies between them via a
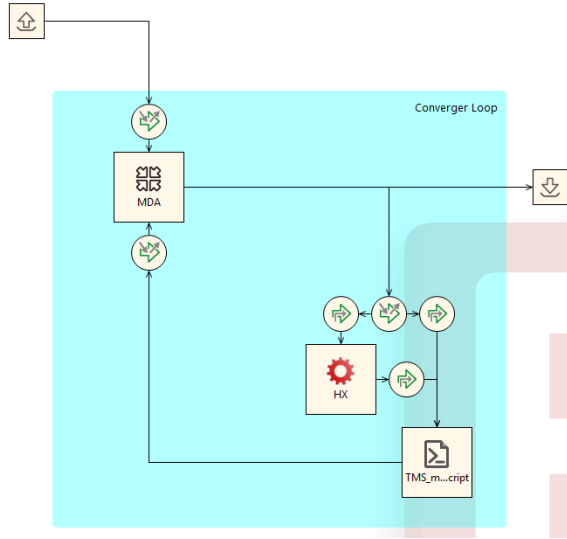
Figure 6.10: HX sizing tool RCE implementation.

graphical interface, as shown in figure 6.10. The framework was successfully tested locally[1] using the powertrain HX case from Section 6.3.1. The input parameters were loaded from the CPACS input XML file, and the results were saved into an output XML file that was readily available for the connecting tools. As is seen in 6.3.1, there is an RCE convergence loop which can be used as an outer optimization or as the main optimization algorithm, allowing for a flexible architecture exploration. It is possible to run the same FC propulsion system case studies entirely using the RCE framework and CPACS data definition by connecting the HX sizing tool as a component, hence leveraging the graphical interface advantages.

6.6 Summary

In conclusion, the investigation demonstrates the computational framework's capability to generate viable thermal management solutions while managing intersecting constraints across multiple components. The case study results indicate that the parametric sizing approach produces realistic system designs with quantifiable performance characteristics. Furthermore, idealized assumptions overestimate hydrogen cooling potential by approximately 10%, necessitating the incorporation of pressure losses and expansion effects in system modeling. HX sizing for hydrogen propulsion systems faces volumetric rather than mass constraints, consistent with findings in plate-fin and microchannel HX research [78]. The computational implementation balances solution accuracy with processing time requirements, enabling designers to evaluate design feasibility across a broad parameter space. This approach facilitates optimization at both component and system levels, providing a foundation for TMS design in advanced propulsion architectures. The methodology established here transfers to various aerospace thermal management applications where parametric exploration of design spaces offers advantages over conventional sizing methods.

---

[1]The RCE test was conducted on the Concordia University local network

Chapter 7

Conclusion and Next Steps

T HIS thesis proposes a parametric HX sizing methodology for cryogenic applications, addressing the thermal management challenges in H$_2$-FC EPA systems, while also being applicable to conventional design approaches.

It addresses the existing gaps in aircraft TMS HX design for alternative propulsion architectures by establishing an approach that accommodates the unique and intersecting constraints present in aerospace applications and cryogenic environments. Existing studies predominantly focus on conventional HX designs or resort to scaling methods without addressing the unique constraints imposed by novel aircraft applications. While researchers have established fundamental thermodynamic relationships for HX performance, there remains insufficient parameterization of these relationships for aerospace-specific implementation. Furthermore, the literature lacks systematic approaches for balancing thermal performance with pressure drop considerations in cryogenic environments.

This research addresses these gaps by developing a sizing methodology with a flexible discretization scheme that incorporates aerospace constraints while establishing relationships between fluid properties, heat transfer dynamics, and pressure effects that determine optimal HX configurations. Through a case study in Chapter 6, it was demonstrated that this methodology can accommodate multiple frameworks, enabling the sizing of a HX network for a H$_2$-FC based propulsion system. Additionally, within the same case study and through the two validation cases, the methodology successfully sized cryogenic and conventional HXs. By using a constrained optimization algorithm, this methodology allows HXs to be sized according to interfacing system requirements, as shown in Section 6.3.1. Furthermore, as shown in figure 6.9 from Section 6.4, when assuming no pressure losses within a cryogenic HX network, the total amount of cooling potential is overestimated, which could allow infeasible aircraft TMS architectures to proceed to later design phases. Furthermore, the methodology developed in this research is designed for integration with MDAO frameworks, enabling system-level analysis and optimization of cryogenicHXs as part of an aircraft-level analysis.

Finally, the proposed methodology in this thesis addresses the following gaps:

- develop a HX sizing method for early aircraft design;

- develop a parametric HX sizing method to address both conventional and cryogenic applications;

- develop a framework-flexible HX sizing method to accommodate various variable input design parameters, allowing for any aircraft HX to be sized; and

- develop a HX sizing method for use in an aircraft MDAO framework for TMS design.

7.1 Contributions

The key contributions of this thesis include:

- The investigation and identification of appropriate cryogenic HX technologies for aerospace applications.

- The development of a parametric HX sizing methodology with a flexible discretization scheme suitable for integration into a MDAO framework.

- The establishment of an analytical approach that accounts for the inter-dependencies between thermodynamic parameters and HX dimensions.

- The development of a flexible computational tool that supports variations in design parameters and fluid properties.

7.2 Limitations & Future Work

The HX sizing methodology developed in this thesis provides a foundation for further enhancements and integration into broader aircraft design frameworks. While the current methodology offers valuable capabilities, it has a few limitations:

- Based on the need for a compact cryogenic HX sizing tool for aerospace applications, the methodology described is designed specifically to size PHEs and would need some changes to make it applicable to other types of HXs.

- As headers are not within the scope of this thesis, the HX sizing process does not account for their impact on pressure losses and weight, which has a larger impact for smaller HXs.

The thermal management challenges in alternative propulsion systems are significantly more complex due to their unique characteristics. These include strict power density constraints, extensive thermal dissipation requirements, and specialized cooling needs for components like batteries, fuel cells, and power electronics. As the industry moves toward more electric, hydrogen-based, or cryogenic propulsion solutions, effective thermal management becomes a critical factor in ensuring system efficiency, reliability, and safety. Therefore, TMSs must be incorporated into the conceptual design phase to guarantee viable aircraft architectures.

Future work will include integrating this sizing methodology into a multidisciplinary design optimization environment, which would represent an advancement in novel aircraft propulsion systems research. This integration would enable system-level trade studies of thermal, propulsive, and structural component inter-dependencies during early design phases. By incorporating thermal management models into MDAO frameworks, researchers could perform parametric analysis across various conditions and configurations. The resulting integrated analysis capabilities would provide aircraft designers with quantitative insights regarding the impact of thermal management requirements on overall system performance, weight, and complexity during early design phases.

Additional research should explore the need for this methodology to address other HX types and configurations. A critical area for investigation is determining the appropriate level of model

fidelity required at different design stages, balancing computational efficiency with accuracy to ensure practical applicability in time-constrained design environments. Therefore, determining the optimal range of geometric configurations, material selections, and operating conditions is crucial.

These improvements would enhance the capability of the methodology to support the development of next-generation aircraft propulsion systems, ultimately contributing to the aviation industry's transition toward more sustainable technologies and reduced environmental impact.

References

[1] "Agenda item 14(e). methodological issues under the convention: Emissions from fuel used for international aviation and maritime transport," International Civil Aviation Organization, Montreal, Canada, Submission SBSTA57, 2022. [Online]. Available: https://www.icao.int/environmental-protection/Documents/SBSTA57_ICAO%20Submission_Final.pdf.

[2] M. Bracha, "Liquid hydrogen – status and trends as potential aviation fuel," in *Fuel Cell and Hydrogen Technologies in Aviation*, C. O. Colpan and A. Kovač, Eds., Cham: Springer International Publishing, 2022, pp. 23–53, ISBN: 978-3-030-99018-3. DOI: 10.1007/978-3-030-99018-3_2. [Online]. Available: https://doi.org/10.1007/978-3-030-99018-3_2.

[3] Air Transport Action Group. "Waypoint 2050," Waypoint 2050. (2021), [Online]. Available: https://aviationbenefits.org/environmental-efficiency/climate-action/waypoint-2050/.

[4] Air Transport Action Group, "Aviation: Benefits beyond borders 2024," Switzerland, Industry High Level Group Report, Dec. 2024. [Online]. Available: https://aviationbenefits.org/media/e5ynn4x0/abbb2024_full_report.pdf.

[5] "Consortium for research and innovation in aerospace in quebec (CRIAQ)," Home - CRIAQ. (2025), [Online]. Available: https://www.criaq.aero/en/.

[6] "Projects - EAP: Exploration and modeling of alternative propulsion technologies for business jets," Projects - CRIAQ. (2025), [Online]. Available: https://www.criaq.aero/en/projects/.

[7] A. Van Heerden, D. Judt, S. Jafari, C. Lawson, T. Nikolaidis, and D. Bosak, "Aircraft thermal management: Practices, technology, system architectures, future challenges, and opportunities," *Progress in Aerospace Sciences*, vol. 128, 2022, ISSN: 0376-0421. DOI: 10.1016/j.paerosci.2021.100767.

[8] ZeroAvia. "Hydrogen-electric powertrains," zeroavia.com. (2025), [Online]. Available: https://zeroavia.com/powertrains/.

[9] I. Moir and A. G. Seabridge, *Aircraft systems: mechanical, electrical, and avionics subsystems integration* (Aerospace series), 3rd ed. Chichester, West Sussex, England ; Hoboken, NJ: Wiley, 2008, 504 pp., OCLC: ocn190786124, ISBN: 978-0-470-05996-8.

[10] H. Kellermann, S. Fuhrmann, M. Shamiyeh, and M. Hornung, "Design of a battery cooling system for hybrid electric aircraft," *Journal of Propulsion and Power*, vol. 38, no. 5, pp. 736–751, Sep. 2022, _eprint: https://doi.org/10.2514/1.B38695. DOI: 10.2514/1.B38695. [Online]. Available: https://doi.org/10.2514/1.B38695.

[11] M. A. Rendón, C. D. Sánchez R., J. Gallo M., and A. H. Anzai, "Aircraft hybrid-electric propulsion: Development trends, challenges and opportunities," *Journal of Control, Automation and Electrical Systems*, vol. 32, no. 5, pp. 1244–1268, Oct. 1, 2021, ISSN: 2195-3899. DOI: 10.1007/s40313-021-00740-x. [Online]. Available: https://doi.org/10.1007/s40313-021-00740-x.

[12] National Aeronautics and Space Administration. "EAP frequently asked questions." Section: Aeronautics. (2025), [Online]. Available: https://www.nasa.gov/eap-faqs/.

[13] N. Gray, S. McDonagh, R. O'Shea, B. Smyth, and J. D. Murphy, "Decarbonising ships, planes and trucks: An analysis of suitable low-carbon fuels for the maritime, aviation and haulage sectors," vol. 1, 2021. DOI: 10.1016/j.adapen.2021.100008. [Online]. Available: http://dx.doi.org/10.1016/j.adapen.2021.100008.

[14] C. Hartmann, J. K. Nøland, R. Nilssen, and R. Mellerud, "Dual use of liquid hydrogen in a next-generation PEMFC-powered regional aircraft with superconducting propulsion," *IEEE Transactions on Transportation Electrification*, vol. 8, no. 4, pp. 4760–4778, Dec. 2022, Conference Name: IEEE Transactions on Transportation Electrification, ISSN: 2332-7782. DOI: 10.1109/TTE.2022.3170827.

[15] S. Hall, *Rules of thumb for chemical engineers*, Sixth edition. Amsterdam, Netherlands: Elsevier, 2018, ISBN: 978-0-12-811038-6 0-12-811038-4 978-0-12-811037-9 0-12-811037-6. [Online]. Available: http://uclibs.org/PID/301267.

[16] S. Gudmundsson, *General aviation aircraft design : applied methods and procedures*, Second edition. Oxford, United Kingdom: Elsevier, 2022, ISBN: 978-0-12-822647-6 0-12-822647-1. [Online]. Available: https://search.ebscohost.com/login.aspx?direct=true&scope=site&db=nlebk&db=nlabk&AN=2464466.

[17] "Innovative benchmark technology for aircraft engineering design and efficient design phase optimisation — FP7," CORDIS — European Commission. (Jun. 2024), [Online]. Available: https://cordis.europa.eu/project/id/605396/reporting.

[18] R. F. Barron and G. F. Nellis, *Cryogenic Heat Transfer*, 2nd ed. Boca Raton: CRC Press, Taylor & Francis Group, 2016, 704 pp., ISBN: 978-1-4822-2745-1 1-4822-2745-2. DOI: 10.1201/b20225. [Online]. Available: https://doi.org/10.1201/b20225.

[19] I. H. Bell, J. Wronski, S. Quoilin, and V. Lemort, "Pure and pseudo-pure fluid thermophysical property evaluation and the open-source thermophysical property library CoolProp," *Industrial & Engineering Chemistry Research*, vol. 53, no. 6, pp. 2498–2508, Feb. 12, 2014, Publisher: American Chemical Society, ISSN: 0888-5885. DOI: 10.1021/ie4033999. [Online]. Available: https://doi.org/10.1021/ie4033999.

[20] Z. Ouyang, T. Nikolaidis, and S. Jafari, "Integrated power and thermal management systems for civil aircraft: Review, challenges, and future opportunities," *Applied Sciences*, vol. 14, no. 9, p. 3689, Apr. 26, 2024, ISSN: 2076-3417. DOI: 10.3390/app14093689. [Online]. Available: https://www.mdpi.com/2076-3417/14/9/3689.

[21] J. Kim, K. Kwon, S. Roy, E. Garcia, and D. N. Mavris, "Megawatt-class turboelectric distributed propulsion, power, and thermal systems for aircraft," in *2018 AIAA Aerospace Sciences Meeting*, Kissimmee, Florida: American Institute of Aeronautics and Astronautics, Jan. 8, 2018, ISBN: 978-1-62410-524-1. DOI: 10.2514/6.2018-2024. [Online]. Available: https://arc.aiaa.org/doi/10.2514/6.2018-2024.

[22] M. Coutinho *et al.*, "A review on the recent developments in thermal management systems for hybrid-electric aircraft," *Applied Thermal Engineering*, vol. 227, p. 120 427, Jun. 5, 2023, ISSN: 1359-4311. DOI: 10.1016/j.applthermaleng.2023.120427. [Online]. Available: https://www.sciencedirect.com/science/article/pii/S1359431123004568.

[23] T. Yu, Y. Huangfu, H. Bai, Y. Liu, W. Shi, and Z. Zhang, "An energy management strategy based on equivalent consumption minimum for hybrid-electric aircraft with battery cooling system," in *2022 IEEE 5th International Conference on Electronics Technology (ICET)*, ISSN: 2768-6515, May 2022, pp. 280–284. DOI: 10.1109/ICET55676.2022.9824153.

[24] B. Tarhan, O. Yetik, and T. H. Karakoc, "Hybrid battery management system design for electric aircraft," *Energy*, vol. 234, p. 121 227, Nov. 1, 2021, ISSN: 0360-5442. DOI: 10.1016/j.energy.2021.121227. [Online]. Available: https://www.sciencedirect.com/science/article/pii/S0360544221014754.

[25] Thomas Imre Cyrille Buidin and Florin Mariasiu, "Battery thermal management systems: Current status and design approach of cooling technologies," *Energies*, vol. 14, no. 4879, p. 4879, 2021, ISSN: 1996-1073. DOI: 10.3390/en14164879.

[26] R. Jansen, C. Bowman, A. Jankovsky, R. Dyson, and J. Felder, "Overview of NASA electrified aircraft propulsion (EAP) research for large subsonic transports," in *53rd AIAA/SAE/ASEE Joint Propulsion Conference*, ser. AIAA Propulsion and Energy Forum, American Institute of Aeronautics and Astronautics, Jul. 7, 2017. DOI: 10.2514/6.2017-4701. [Online]. Available: https://doi.org/10.2514/6.2017-4701.

[27] J. M. Rheaume and C. E. Lentsii, "Design and simulation of a commercial hybrid electric aircraft thermal management system," in *2018 AIAA/IEEE Electric Aircraft Technologies Symposium (EATS)*, Jul. 2018, pp. 1–9. [Online]. Available: https://ieeexplore.ieee.org/document/8552766.

[28] J. M. Rheaume, M. Macdonald, and C. E. Lents, "Commercial hybrid electric aircraft thermal management system design, simulation, and operation improvements," in *2019 AIAA/IEEE Electric Aircraft Technologies Symposium (EATS)*, Aug. 2019, pp. 1–23. DOI: 10.2514/6.2019-4492.

[29] M. Sumption, J. Murphy, M. Susner, and T. Haugan, "Performance metrics of electrical conductors for aerospace cryogenic motors, generators, and transmission cables," *Cryogenics*, vol. 111, p. 103 171, Oct. 1, 2020, ISSN: 0011-2275. DOI: 10.1016/j.cryogenics.2020.103171. [Online]. Available: https://www.sciencedirect.com/science/article/pii/S0011227520301739.

[30] G. Licheva and S. Liscouët-Hanke, "CRYOGENIC TANK SIZING MODEL FOR THE CONCEPTUAL DESIGN OF HYDROGEN-POWERED AIRCRAFT," in *Aircraft Design and Integrated System*, Florence, Italy: International Council of the Aeronautical Sciences, 2024. [Online]. Available: https://www.icas.org/icas_archive/icas2024/data/papers/icas2024_0193_paper.pdf.

[31] H. Nakagawa, Y. Miseki, and M. Akoshima, "Gas adsorption, thermal and structural properties of sinters made of fine silver powder for ultra-low-temperature heat exchangers," *Cryogenics*, vol. 102, pp. 1–8, Sep. 2019, ISSN: 00112275. DOI: 10.1016/j.cryogenics.2019.07.001. [Online]. Available: https://linkinghub.elsevier.com/retrieve/pii/S001122751930061X (visited on 08/10/2025).

[32] B. Sundén and J. Fu, *Heat transfer in aerospace applications*, 1 online resource (xv, 255 pages) vols. London: Academic Press, 2017, ISBN: 978-0-12-809761-8. [Online]. Available: http://www.books24x7.com/marc.asp?bookid=120113 (visited on 07/31/2023).

[33] J. E. HESSELGREAVES, R. LAW, and D. A. REAY, *Compact heat exchangers : selection, design, and operation*. Amsterdam: Pergamon, 2001, ISBN: 9780080529547; 0080529542; 1281072044; 9781281072047; 9786611072049; 6611072047. [Online]. Available: http://site.ebrary.com/id/10206373.

[34] W. M. Kays, *Compact Heat Exchangers (3rd Edition)*, in collab. with A. L. London. Erscheinungsort nicht ermittelbar: Scientific International, 2018, ISBN: 978-93-87938-03-8 978-1-5231-2179-3.

[35] "*NOMENCLATURE, AIRCRAFT AIR CONDITIONING EQUIPMENT*," SAE ARP 147, version E, SAE International, Oct. 2024, Reaffirmed.

[36] "*Engine Bleed Air Systems for Aircraft*," SAE ARP 1796, version B, SAE International, May 2020, Reaffirmed.

[37] D. Popov *et al.*, "Cryogenic heat exchangers for process cooling and renewable energy storage: A review," *Applied Thermal Engineering*, vol. 153, pp. 275–290, May 2019, ISSN: 13594311. DOI: 10.1016/j.applthermaleng.2019.02.106. [Online]. Available: https://linkinghub.elsevier.com/retrieve/pii/S1359431118336007.

[38] M. Weikl, K. Braun, and J. Weiss, "Coil-wound heat exchangers for molten salt applications," *Energy Procedia*, vol. 49, pp. 1054–1060, 2014, ISSN: 18766102. DOI: 10.1016/j.egypro.2014.03.113. [Online]. Available: https://linkinghub.elsevier.com/retrieve/pii/S1876610214005670 (visited on 12/16/2023).

[39] M. A. Tomić, S. K. Ayed, Ž. Ž. Stevanović, P. S. ekić, P. M. Živković, and M. V. Vukić, "Perforated plate convective heat transfer analysis," *International Journal of Thermal Sciences*, vol. 124, pp. 300–306, 2018, ISSN: 1290-0729. DOI: 10.1016/j.ijthermalsci.2017.10.021.

[40] Massachusetts Institute of Technology. "Printed-circuit heat exchanger (PCHE)," MIT ASE. (2025), [Online]. Available: https://ase.mit.edu/projects/printed-circuit-heat-exchanger-pche/ (visited on 12/04/2023).

[41] "*Air Conditioning Systems for Subsonic Airplanes*," ARP85, version G, SAE International, Oct. 2024, Reaffirmed.

[42] H. Strumpf and Z. Mirza, "Development of a microchannel heat exchanger for aerospace applications," in *ASME*, American Society of Mechanical Engineers Digital Collection, Jul. 22, 2013, pp. 459–467. DOI: 10.1115/ICNMM2012-73043. [Online]. Available: https://asmedigitalcollection.asme.org/ICNMM/proceedings-abstract/ICNMM2012/44793/459/246238.

[43] O. P. Arsenyeva, L. L. Tovazhnyansky, P. O. Kapustenko, and G. L. Khavin, "Optimal design of plate-and-frame heat exchangers for efficient heat recovery in process industries," *Energy*, vol. 36, no. 8, pp. 4588–4598, 2011, 4588. DOI: 10.1016/j.energy.2011.03.022. [Online]. Available: http://dx.doi.org/10.1016/j.energy.2011.03.022.

[44] K. Xu and R. Smith, "Design and optimization of plate heat exchanger networks," in *Computer Aided Chemical Engineering*, vol. 44, Elsevier, 2018, pp. 451–456, ISBN: 978-0-444-64241-7. DOI: 10.1016/B978-0-444-64241-7.50070-7. [Online]. Available: https://linkinghub.elsevier.com/retrieve/pii/B9780444642417500707.

[45] "GAMS - cutting edge modeling." (2025), [Online]. Available: https://www.gams.com/.

[46] M. White, G. Nellis, S. Kelin, W. Zhu, and Y. Gianchandani, "An experimentally validated numerical modeling technique for perforated plate heat exchangers," *Journal of heat transfer*, vol. 132, pp. 1–9, Nov. 1, 2010. DOI: 10.1115/1.4000673.

[47] G. Nellis, "A heat exchanger model that includes axial conduction, parasitic heat loads, and property variations," *Cryogenics*, vol. 43, no. 9, pp. 523–538, 2003, 523. DOI: 10.1016/S0011-2275(03)00132-2. [Online]. Available: http://dx.doi.org/10.1016/S0011-2275(03)00132-2.

[48] A. Allahyarzadeh-Bidgoli, M. Mehrpooya, and J. I. Yanagihara, "Geometric optimization of thermo-hydraulic performance of multistream plate fin heat exchangers in two-stage condensation cycle: Thermodynamic and operating cost analyses," *Process Safety and Environmental Protection*, vol. 162, pp. 631–648, Jun. 2022, ISSN: 09575820. DOI: 10.1016/j.psep.2022.03.088. [Online]. Available: https://linkinghub.elsevier.com/retrieve/pii/S0957582022003032.

[49] H. Najafi, B. Najafi, and P. Hoseinpoori, "Energy and cost optimization of a plate and fin heat exchanger using genetic algorithm," *Applied Thermal Engineering*, vol. 31, no. 10, pp. 1839–1847, Jul. 2011, ISSN: 13594311. DOI: 10.1016/j.applthermaleng.2011.02.031. [Online]. Available: https://linkinghub.elsevier.com/retrieve/pii/S1359431111001128.

[50] M. Mehrpooya, M. M. M. Sharifzadeh, M. J. Zonouz, and M. A. Rosen, "Cost and economic potential analysis of a cascading power cycle with liquefied natural gas regasification," *Energy Conversion and Management*, vol. 156, pp. 68–83, Jan. 2018, ISSN: 01968904. DOI: 10.1016/j.enconman.2017.10.100. [Online]. Available: https://linkinghub.elsevier.com/retrieve/pii/S0196890417310324 (visited on 07/01/2025).

[51] W. M. Kays and A. L. London, *Compact heat exchangers* (McGraw-Hill series in mechanical engineering), 2d ed. New York: McGraw-Hill Book Co., 1998, xi, 272, Section: xi, 272 pages illustrations 24 cm., ISBN: 978-0-07-033391-8.

[52] K. Deb, A. Pratap, S. Agarwal, and T. Meyarivan, "A fast and elitist multiobjective genetic algorithm: NSGA-II," *IEEE Transactions on Evolutionary Computation*, vol. 6, no. 2, pp. 182–197, Apr. 2002, ISSN: 1089778X. DOI: 10.1109/4235.996017. [Online]. Available: http://ieeexplore.ieee.org/document/996017/.

[53] S. Wang, C. Liu, S. Zhang, Q. Li, and E. Huo, "Multi-objective optimization and fluid selection of organic rankine cycle (ORC) system based on economic-environmental-sustainable analysis," *Energy Conversion and Management*, vol. 254, 2022. DOI: 10.1016/j.enconman.2022.115238. [Online]. Available: http://dx.doi.org/10.1016/j.enconman.2022.115238.

[54] K. Zhu *et al.*, "Design, optimization and experimental testing of 2 k cryogenic plate-fin heat exchanger," *Applied Thermal Engineering*, vol. 223, p. 119 973, Mar. 2023, ISSN: 13594311. DOI: `10.1016/j.applthermaleng.2023.119973`. [Online]. Available: `https://linkinghub.elsevier.com/retrieve/pii/S1359431123000029` (visited on 06/02/2025).

[55] H. M. Müller-Steinhagen, "Fouling phenomena during boiling of cryogenic liquids," *Cryogenics*, vol. 28, no. 6, pp. 406–408, Jun. 1, 1988, ISSN: 0011-2275. DOI: `10.1016/0011-2275(88)90040-9`. [Online]. Available: `https://www.sciencedirect.com/science/article/pii/0011227588900409`.

[56] B. D. Raja, R. Jhala, and V. Patel, "Many-objective optimization of cross-flow plate-fin heat exchanger," *International Journal of Thermal Sciences*, vol. 118, pp. 320–339, Aug. 2017, ISSN: 12900729. DOI: `10.1016/j.ijthermalsci.2017.05.005`. [Online]. Available: `https://linkinghub.elsevier.com/retrieve/pii/S1290072916314661`.

[57] D. P. Raymer, *Aircraft design: a conceptual approach* (AIAA education series), Sixth edition. Reston, Virginia: American Institute of Aeronautics and Astronautics, Inc., 2018, xxx, 1062, Section: xxx, 1062 pages : illustrations ; 24 cm, ISBN: 978-1-62410-490-9.

[58] W. M. Kays and A. L. London, *Compact heat exchangers*, Repr. ed. 1998 with corrections. Malabar, Fla: Krieger Pub. Co, 1998, 335 pp., ISBN: 978-1-57524-060-2.

[59] C. Ranganayakulu and K. N. Seetharamu, *Compact Heat Exchangers: Analysis, Design and Optimization using FEM and CFD Approach*. ASME Press, May 20, 2018, ISBN: 978-1-119-42418-5. DOI: `10.1115/1.861CHE`. [Online]. Available: `https://asmedigitalcollection-asme-org.lib-ezproxy.concordia.ca/ebooks/book/45/Compact-Heat-Exchangers-Analysis-Design-and`.

[60] D. P. Sekulić and R. K. Shah, *Fundamentals of Heat Exchanger Design*, 1st ed. Wiley, Sep. 21, 2023, ISBN: 978-1-119-88326-5 978-1-119-88329-6. DOI: `10.1002/9781119883296`. [Online]. Available: `https://onlinelibrary.wiley.com/doi/book/10.1002/9781119883296` (visited on 08/11/2025).

[61] R. K. Shah, A. E. Bergles, F. Mayinger, and T. NATO Advanced Study Institute on "Heat Exchangers–Thermal-Hydraulic Fundamentals {and} Design" (1980 : Istanbul, *Heat exchangers: thermal-hydraulic fundamentals and design* (Advanced Study Institute book). Washington: Hemisphere Pub. Corp. ; 1981, xi, 1131, Section: xi, 1131 pages : illustrations ; 25 cm., ISBN: 978-0-07-033284-3.

[62] H. Lee, *Thermal design: heat sinks, thermoelectrics, heat pipes, compact heat exchangers, and solar cells*, Second edition. Hoboken, NJ, USA: John Wiley & Sons, Inc., 2022, ISBN: 978-1-119-68604-0 978-1-119-68601-9 978-1-119-68603-3 978-1-119-68597-5. [Online]. Available: `https://concordiauniversity.on.worldcat.org/search/detail/1305501326?queryString=Thermal%20Design%20lee&databaseList=&clusterResults=true&groupVariantRecords=false`.

[63] H. Martin, "A theoretical approach to predict the performance of chevron-type plate heat exchangers," *Chemical Engineering and Processing: Process Intensification*, vol. Volume 35, no. 4, 1996, ISSN: 0255-2701. DOI: `10.1016/0255-2701(95)04129-X`. [Online]. Available: `https://doi.org/10.1016/0255-2701(95)04129-X`.

[64] H. Martin, "Economic optimization of compact heat exchangers," in *Proceedings of the EF-Conference on Compact Heat Exchangers and Enhancement Technology for the Process Industries*, Banff, AB, Canada., 1999.

[65] D. G. Goodwin, H. K. Moffat, I. Schoegl, R. L. Speth, and B. W. Weber, *Cantera: An object-oriented software toolkit for chemical kinetics, thermodynamics, and transport processes*, version 3.1.0, Dec. 14, 2024. DOI: 10.5281/zenodo.14455267. [Online]. Available: https://zenodo.org/records/14455267 (visited on 04/14/2025).

[66] M. Alder, E. Moerland, J. Jepsen, and B. Nagel, "RECENT ADVANCES IN ESTABLISHING a COMMON LANGUAGE FOR AIRCRAFT DESIGN WITH CPACS," presented at the Aerospace Europe Conference, Bordeaux, France, 2020.

[67] J. S. Gray, J. T. Hwang, J. R. R. A. Martins, K. T. Moore, and B. A. Naylor, "OpenMDAO: An open-source framework for multidisciplinary design, analysis, and optimization," *Structural and Multidisciplinary Optimization*, vol. 59, no. 4, pp. 1075–1104, Apr. 2019, ISSN: 1615-147X, 1615-1488. DOI: 10.1007/s00158-019-02211-z. [Online]. Available: http://link.springer.com/10.1007/s00158-019-02211-z (visited on 05/04/2025).

[68] J. Blank and K. Deb, "Pymoo: Multi-objective optimization in python," *IEEE Access*, vol. 8, pp. 89 497–89 509, 2020, ISSN: 2169-3536. DOI: 10.1109/ACCESS.2020.2990567. [Online]. Available: https://ieeexplore.ieee.org/document/9078759/ (visited on 05/20/2025).

[69] B. Leite, A. O. S. D. Costa, and E. F. D. Costa Junior, "Multi-objective optimization of adiabatic styrene reactors using generalized differential evolution 3 (GDE3)," *Chemical Engineering Science*, vol. 265, p. 118 196, Jan. 2023, ISSN: 00092509. DOI: 10.1016/j.ces.2022.118196. [Online]. Available: https://linkinghub.elsevier.com/retrieve/pii/S0009250922007801 (visited on 05/20/2025).

[70] J. R. R. A. Martins and A. Ning, *Engineering Design Optimization*, 1st ed. Cambridge University Press, Nov. 18, 2021, ISBN: 978-1-108-98064-7 978-1-108-83341-7. DOI: 10.1017/9781108980647. [Online]. Available: https://www.cambridge.org/core/product/identifier/9781108980647/type/book (visited on 05/24/2024).

[71] S. Kukkonen and K. Deb, "A fast and effective method for pruning of non-dominated solutions in many-objective problems," in *Parallel Problem Solving from Nature - PPSN IX*, T. P. Runarsson, H.-G. Beyer, E. Burke, J. J. Merelo-Guervós, L. D. Whitley, and X. Yao, Eds., vol. 4193, Series Title: Lecture Notes in Computer Science, Berlin, Heidelberg: Springer Berlin Heidelberg, 2006, pp. 553–562, ISBN: 978-3-540-38990-3 978-3-540-38991-0. DOI: 10.1007/11844297_56. [Online]. Available: https://link.springer.com/10.1007/11844297_56 (visited on 05/20/2025).

[72] "Bell & Gossett BP400-40 - Brazed Plate Heat Exchanger." en. (), [Online]. Available: https://www.statesupply.com/bh4215 (visited on 11/18/2024).

[73] "Aluminum 6061-T6 (UNS AA96061)." en, NIST. (), [Online]. Available: https://www.nist.gov/mml/acmd/aluminum-6061-t6-uns-aa96061 (visited on 06/29/2025).

[74] "HTF7000 turbofan engine," Honeywell. (2025), [Online]. Available: https://aerospace.honeywell.com/us/en/products-and-services/product/hardware-and-systems/engines/htf7000-turbofan-engine (visited on 05/23/2024).

[75] "Bombardier challenger 300," Elevate Aviation Group. (2025), [Online]. Available: https://eag.aero/best-private-jets/super-midsize-private-jets/bombardier-challenger-300/ (visited on 04/14/2025).

[76] T. Takagi, K. Takadama, and H. Sato, "Incremental lattice design of weight vector set," in *Proceedings of the 2020 Genetic and Evolutionary Computation Conference Companion*, ser. GECCO '20, New York, NY, USA: Association for Computing Machinery, Jul. 8, 2020, pp. 1486–1494, ISBN: 978-1-4503-7127-8. DOI: 10.1145/3377929.3398082. [Online]. Available: https://dl.acm.org/doi/10.1145/3377929.3398082 (visited on 05/20/2025).

[77] B. Boden *et al.*, "RCE: An integration environment for engineering and science," *SoftwareX*, vol. 15, p. 100 759, Jul. 2021, ISSN: 23527110. DOI: 10.1016/j.softx.2021.100759. [Online]. Available: https://linkinghub.elsevier.com/retrieve/pii/S2352711021000820 (visited on 08/21/2025).

[78] H. Strumpf and Z. Mirza, "Development of a Microchannel Heat Exchanger for Aerospace Applications," en, in *ASME*, American Society of Mechanical Engineers Digital Collection, Jul. 22, 2013, pp. 459–467. DOI: 10.1115/ICNMM2012-73043.

[79] P. Zhang *et al.*, "Thermal cycling behavior of selective laser-remelted thermal barrier coatings with different laser dot distances," *Journal of Thermal Spray Technology*, vol. 30, no. 4, pp. 1038–1048, Apr. 2021, ISSN: 1059-9630, 1544-1016. DOI: 10.1007/s11666-021-01173-3. [Online]. Available: https://link.springer.com/10.1007/s11666-021-01173-3.

[80] C. Wang, X. Lin, L. Wang, S. Zhang, and W. Huang, "Cryogenic mechanical properties of 316l stainless steel fabricated by selective laser melting," *Materials Science and Engineering: A*, vol. 815, p. 141 317, May 2021, ISSN: 09215093. DOI: 10.1016/j.msea.2021.141317. [Online]. Available: https://linkinghub.elsevier.com/retrieve/pii/S0921509321005864.

Appendix A

Cryogenic Heat Transfer

This appendix examines heat exchanger design challenges, addressing the intersecting factors of variable material properties, thermal insulation requirements, near-critical-point convection phenomena, and radiation heat transfer mechanisms.

A.0.1 Specific heat

Specific heat (c_p) significantly influences heat transfer as it varies based on material state (solid, liquid, or gaseous). Each state exhibits different dominant heat transfer mechanisms. As the amount of heat energy required to raise one gram of a substance by one degree Kelvin, specific heat can substantially affect thermal management system performance.

These storage mechanisms can be translational, rotational, and vibrational kinetic energy in gases; vibrational kinetic and potential energy in liquids; vibrational kinetic and potential energy of atoms plus electron kinetic energy in electrically conductive solids; and specialized energy storage in materials such as paramagnetic solids [18].

Referring back to figure 1.5, it illustrates a notable characteristic where H_2 in a supercritical liquid or compressed liquid state transitions to a supercritical fluid state without displaying a distinct phase change. This behavior is depicted with greater clarity in the H_2 phase diagram shown in figure A.1, which represents the thermodynamic states of H_2.

A.0.2 Thermal Conductivity

Heat conduction can be defined as the transfer of thermal energy between entities or within a medium resulting from a temperature gradient and occurring in the absence of any mass flow [18]. Thermal conductivity (k_t), by contrast, is a material property that quantifies how effectively it conducts heat on a microscopic level, essentially measuring the material's ability to transfer energy through thermal conduction.

It is most often a function of material temperature and pressure. Nevertheless, for ideal gases at low pressure, incompressible fluids, and most solids, thermal conductivity remains mostly independent of pressure. Thermal conduction mechanisms differ by state in the same manner as for the specific heat storage mechanisms.

Thermal conduction is proportional to the product of the number density of microscopic energy carriers of the material (n), their thermal mass (c_{th}), average molecular velocity ($\overline{v}$), and distance between collisions (L_{cd}), as shown in equation (38).
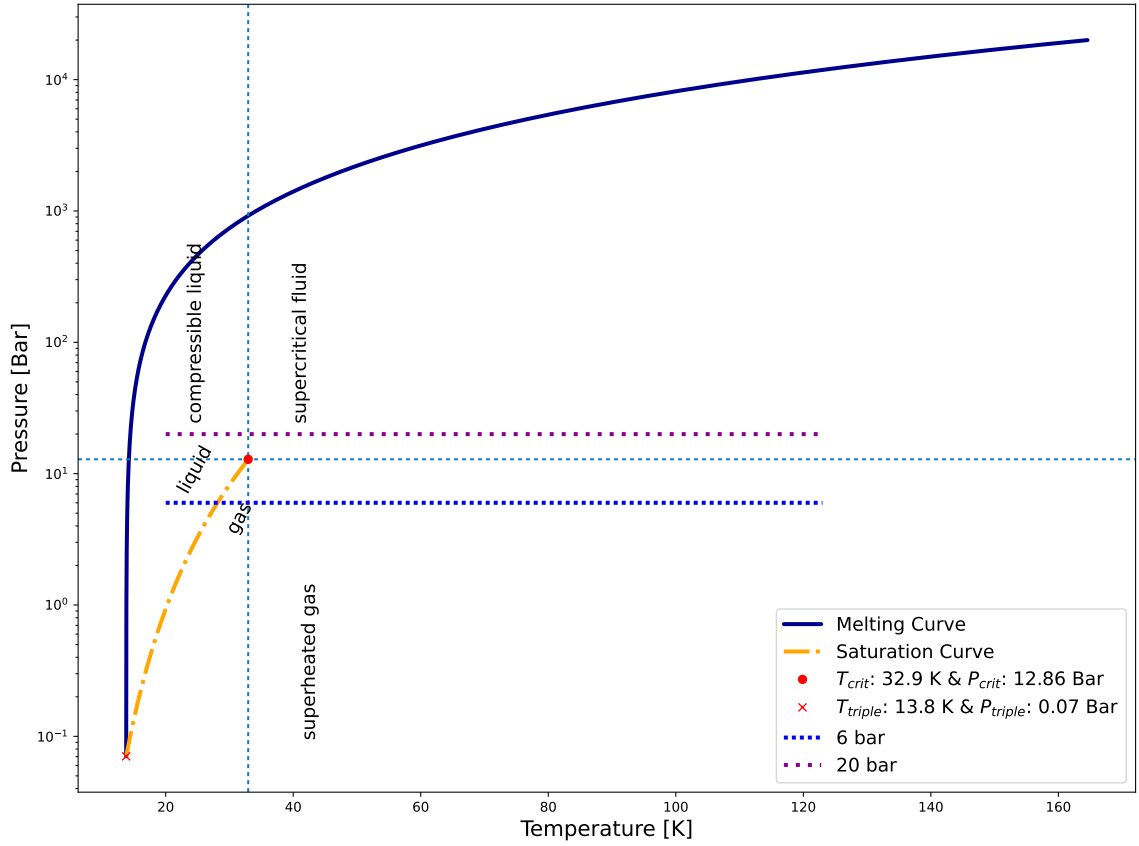
Figure A.1: Hydrogen phase plot highlighting the cases shown in figure 1.5 using Coolprop [19] for fluid transfer properties.

$$k_t \propto n c_{th} \overline{v} L_{cd} \qquad (38)$$

The rate of heat transfer through the material by conduction can be defined by Fourier's Law of heat conduction, as shown in equation (39), where q is the heat flux, and ∇T is the temperature gradient.

$$q = -k_t \nabla T \qquad (39)$$

The thermal conductivity of gases at atmospheric pressure (P_{atm}) in the cryogenic temperature (T_{cryo}) range decreases as the temperature drops. Using the equations for the internal energy at a molecular level of a substance in tandem with the ideal gas law[1], it can be found that the temperature dependence of the thermal conductivity for a gas should be the same as that for the gas viscosity, which varies proportionally to the $1/2$ power of the absolute temperature (T_{abs}), as shown in the equation (40), but in reality the exponent generally falls between 0.6 and 0.9.

---

[1]See [18] Section 1.3.3.1 (p.24) for the full mathematical breakdown.

$$k_T \propto T_{abs}^{1/2} \tag{40}$$

For real gases, the Eucken relation provides a better approximation ($<10\%$ error) by correlating gas thermal conduction (k_t) with specific heat ratio (γ), viscosity (μ), and constant volume specific heat capacity (c_v), as shown in equation (41).

$$k_t = \frac{1}{4}(9\gamma - 5)\mu c_v \tag{41}$$

For liquids, no simple theoretical model exists for predicting thermal conductivity; consequently, tables or material property software packages must be used. For cryogenic liquids, the thermal conductivity of the saturated liquid generally increases as the temperature decreases. LH$_2$ and liquid He I are the only two exceptions to this trend—the thermal conductivity of their saturated liquid states decreases with lower temperatures.

For solids, where thermal conduction depends on vibrations moving through the material, the chemical structure significantly influences behavior at cryogenic temperatures. This occurs because thermal energy transport relies on two independent mechanisms: phonon (or lattice vibrational) energy transfer and electron energy transport. The thermal conductivity is the sum of these two mechanisms, as shown in equation (42).

$$k_t = k_{ph} + k_{el} \tag{42}$$

For electrical insulators (dielectric solids), phonon conduction is the predominant conduction mechanism. The density and average molecular velocity for the material are weak functions of temperature, causing the thermal conductivity of dielectric materials to vary proportionally to $1/T$ at room temperature and above, and proportionally to T^3 at low temperatures.

For metals that are good electrical conductors with a large number of "free" electrons, the electron contribution generally represents the larger component of heat conduction at ambient temperature. Since phonon and electron conduction are approximately equivalent at these temperatures, these materials also vary proportionally to $1/T$.

$$k_{ph} = k_{el} = constant \tag{43}$$

At cryogenic temperatures, electron energy transport is affected by two key factors: phonon interference and lattice imperfections (dislocations, grain boundaries, impurity atoms) with resistances that operate in series as shown in equation (44).

$$\frac{1}{k_{el}} = \frac{1}{k_{el,ph}} + \frac{1}{k_{el,im}} \tag{44}$$

Impurity atoms and dislocations remain temperature-independent. Electron specific heat is proportional to absolute temperature, while density and velocity stay constant. Since the mean free path for impurity interference is also constant, the impurity contribution to thermal conductivity is proportional to the temperature (T). The resistance to electron motion due to phonon interactions at low temperatures is proportional to T^2, making the conductivity inversely proportional to T^2.

Therefore, for pure metals, thermal conductivity initially increases proportionally to their temperature from absolute zero to an intermediate temperature where it peaks. Beyond this point, it

decreases proportionally to $1/T^2$ until approaching ambient temperatures, where it stabilizes and becomes nearly constant.

A.0.3 Near-Critical-Point Heat Transfer Properties

The thermodynamic critical pressure for many cryogenic fluids is much lower than that of most conventional fluids. Consequently, convective heat transfer at near-critical and supercritical conditions occurs more frequently in cryogenic systems than in systems operating at ambient or elevated temperatures.

Correlating heat transfer and pressure drop data in the near-critical region presents significant challenges due to the rapid variation of thermodynamic and transport properties. At the thermodynamic critical point itself, both specific heat capacity and thermal expansion coefficient become infinitely large. Similarly, most other fluid properties undergo substantial changes as temperature and pressure vary around the critical point. These transfer property changes are shown for Parahydrogen (p-H$_2$) in figure A.2 and Nitrogen (N$_2$) in figure A.3, highlighting their impact for different pressures.

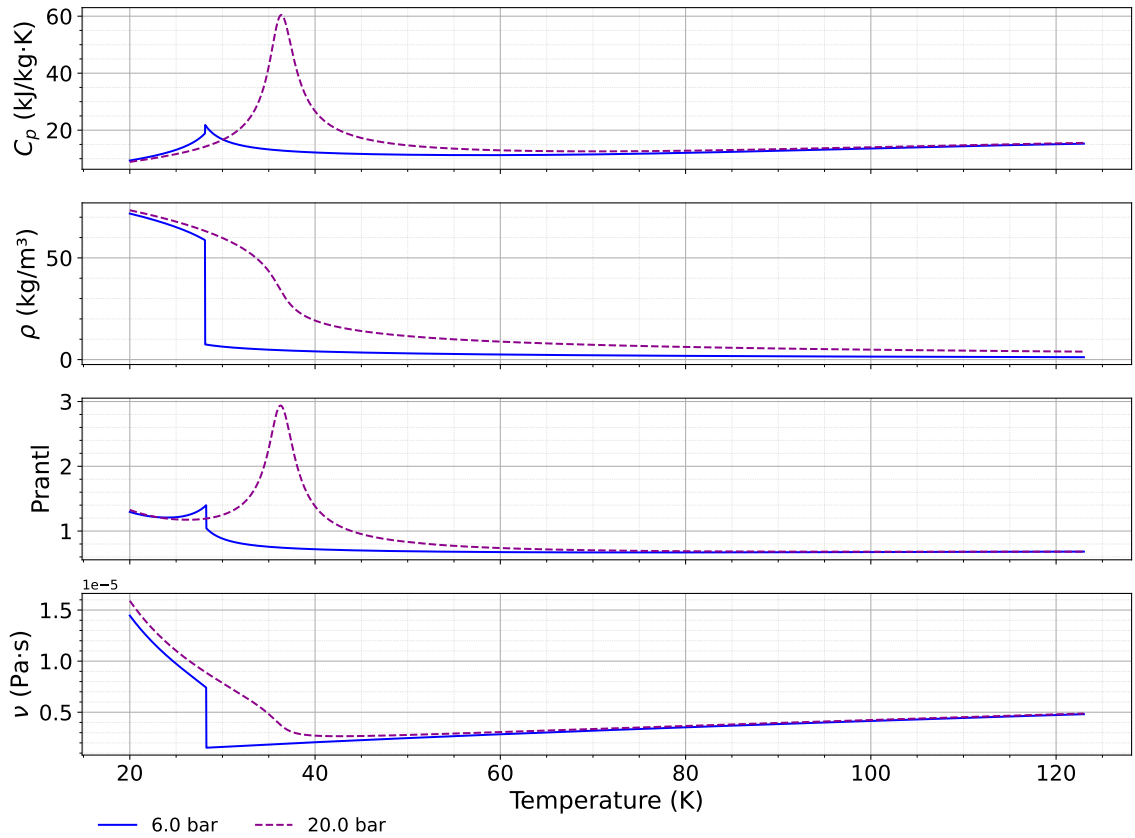Figure A.2: Cryogenic p-H$_2$ transfer property changes at constant pressures of 6 and 20 bar calculated using Coolprop [19].
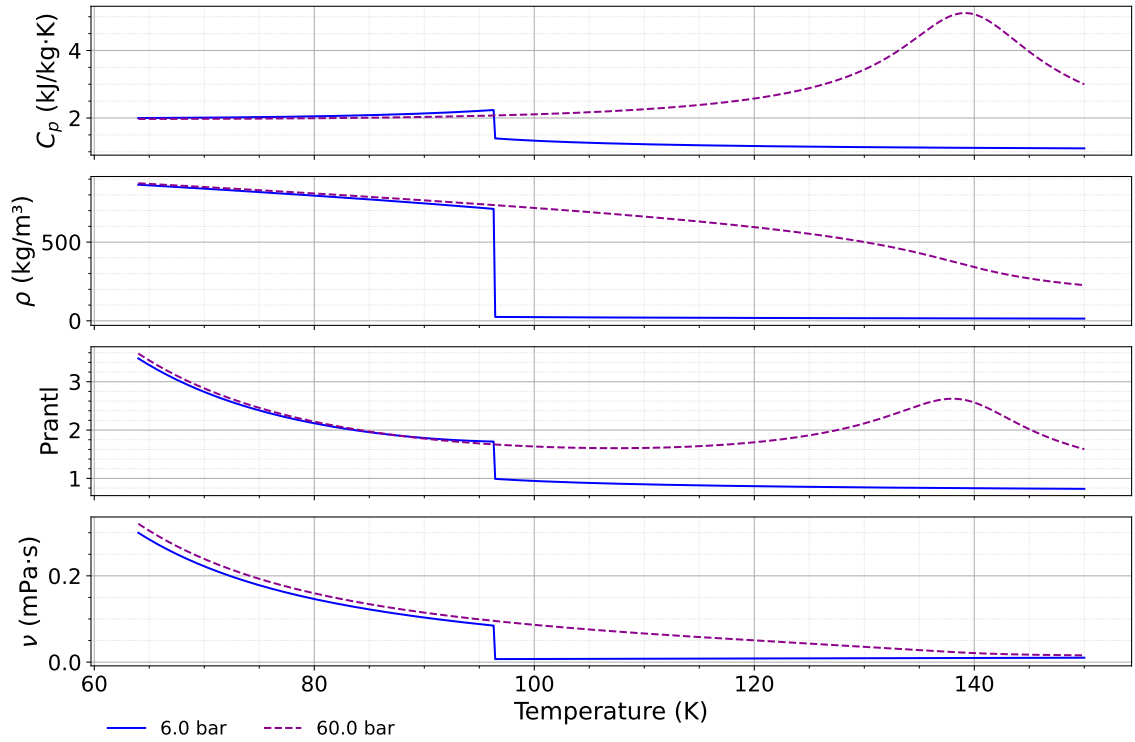
Figure A.3: Cryogenic N_2 transfer property changes at constant pressures of 6 and 60 bar calculated using Coolprop [19].

A.0.4 Addressing Variable Material Properties

Once again, conventional approaches to HX design assume near-constant material properties for small changes in pressures and temperatures, or that these properties exhibit near-linear relationships. Consequently, the mean transfer properties between inlet and outlet conditions can generally be used with minimal error. However, as was previously discussed, in cryogenic applications, the assumption of constant or linearly varying properties becomes invalid due to the dramatic property changes that occur within the cryogenic temperature range. Thus, as mentioned in Section **??**, a segmented or discrete approach to design is necessary.

A.0.5 Thermal Insulation Solutions

Cryogenic liquids have relatively small heats of vaporization. For example, liquid N_2's heat of vaporization is only 199.3 kJ/kg at 1 atm, while water's is 2257 kJ/kg at the same pressure. Due to high liquefaction costs, safety concerns, and this low heat of vaporization, specialized high-performance insulations are necessary to minimize evaporation rates in cryogenic liquid storage vessels. They are also critical in cryogenic HX design due to the extreme temperature differentials between the cryogenic fluid and the ambient environment. Conventional insulation materials used at room temperature often perform poorly in cryogenic applications due to thermal contraction issues, moisture condensation, and air infiltration.

Multi-Layer Insulation (MLI)s used in cryogenic systems have thermal conductivity approximately 1000 times lower than the fiberglass insulation commonly used in residential buildings.

These systems, consisting of alternating layers of highly reflective material (typically aluminized Mylar) and low-conductivity spacer material, provide superior performance by minimizing heat transfer through all three mechanisms: conduction, convection, and radiation. Vacuum-jacketed designs further enhance insulation effectiveness by eliminating gas conduction and convection pathways.

Additionally, specialized foam insulations like aerogels or polyimide foams maintain their thermal resistance properties at cryogenic temperatures while accommodating thermal cycling without significant degradation. Beyond those highlighted, there are several types of insulation, such as expanded closed-cell foams, gas-filled powders and fibrous materials, vacuum alone, evacuated powders and fibrous materials, opacified powders, and microsphere insulation.

The system must also be meticulously engineered with careful attention to thermal bridges at supports, instrumentation penetrations, and other necessary discontinuities that could otherwise compromise the overall thermal performance of the cryogenic HX.

Furthermore, insulation must be designed to protect cryogenic materials from radiation. According to Wien's law[2], shown in equation (45), the wavelength (λ) at which peak radiant intensity occurs for blackbody radiation is inversely proportional to the absolute temperature (T_{abs}). For example, at 1 K the peak occurs at a wavelength of 2.9 mm. Most metallic shields used to reduce radiation heat transfer in cryogenic systems have thicknesses comparable to or less than this value. Consequently, the treatment of radiation problems at cryogenic temperatures differs significantly from those near room temperature, where the wavelength peak occurs at approximately 0.01 mm.

$$\lambda_{pk} = \frac{b}{T_{abs}} \tag{45}$$

A.0.6 Material Selection

Material selection becomes crucial as conventional materials may become brittle or lose their structural integrity at extremely low temperatures, while specialized materials like austenitic stainless steels, aluminum alloys, and certain copper alloys maintain their mechanical properties and remain viable options for cryogenic HX construction.

These specialized materials must also withstand repeated thermal cycling, which introduces additional mechanical stresses due to differential thermal expansion and contraction rates that can lead to fatigue failure. To address this, it is possible to include expansion joints or bellows to accommodate dimensional changes, design with uniform cross-sections to ensure even temperature distribution, select materials with matched thermal expansion coefficients for joined components, employ finite element analysis to identify potential stress concentration points, and incorporate strain-relieving features that allow controlled deformation without compromising structural integrity.

Several manufacturing techniques can address thermal cycling challenges, including controlled cooling rates during fabrication, stress-relief heat treatments [79], specialized brazing procedures (such as cryogenic treatments), and strategic welding sequences that minimize residual stresses in cryogenic components. Modern additive manufacturing methods, like Selective Laser Melting

---

[2]b is Wien's displacement constant ($\approx 2.898e{-}3\ mK$)

[2]The properties shown in the figure are for parahydrogen (p-H_2) for specific heat capacity (c_p) and density (ρ), while the Prandtl number and kinematic viscosity (ν) values are for standard H_2.

(SLM) [80], offer additional solutions by enabling the creation of complex geometries with optimized thermal performance that would be impossible to achieve using conventional fabrication techniques. In some instances, these processes can even improve material properties.

A.1   Summary

As discussed, the design challenges for cryogenic heat exchangers stem mainly from material transfer properties being more volatile and/or nonlinear in the cryogenic temperature region. While fundamental heat transfer relationships still apply, it is necessary to modify the common assumptions made for conventional heat exchanger design.

These challenges can be addressed through segmented analysis methods, advanced insulation systems like MLI and vacuum-jacketed designs, careful selection of specialized alloys, and appropriate manufacturing techniques.

Comprehensive modeling techniques need to be developed for cryogenic applications, especially near critical regions. New manufacturing methods like SLM create interesting opportunities for optimized geometries that can improve heat exchanger performance while maintaining or improving material properties, as shown in [80]

Appendix B

Hydraulic Diameter Ranges Based on Compactness

Figure B.1 from [60] provides a critical reference for establishing appropriate hydraulic diameter ranges during the sizing process. The figure presents typical values applicable to cryogenic heat exchangers and similar applications.

Although micro-channel heat exchangers offer theoretical advantages in many scenarios, their implementation introduces potential complications related to fouling and maintenance accessibility. This reference enables designers to select hydraulic diameter values that optimize performance while accounting for specific application constraints and operational requirements.
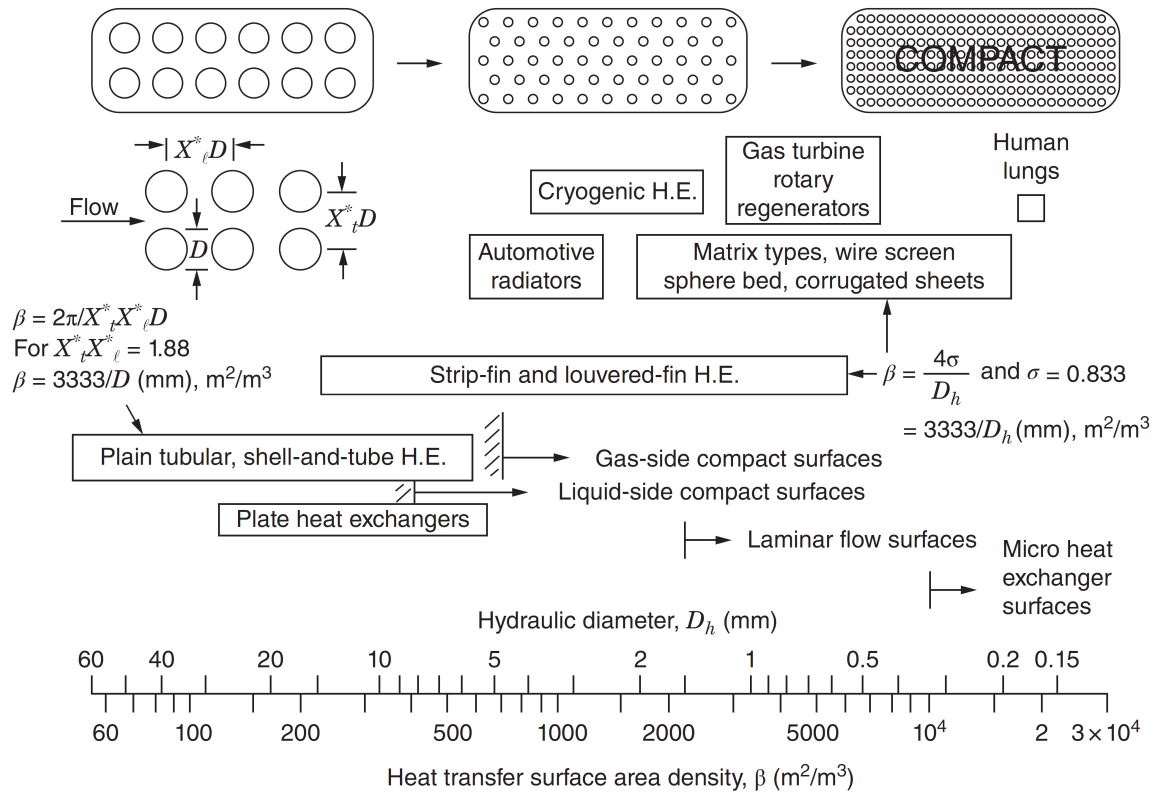
Figure B.1: Heat transfer surface area density spectrum of exchanger surfaces [60].